

https://dspace.org/

Synthesis and functionalization of gallium nitride nanostructures for gas sensing and catalyst support

Kente, Thobeka

2014-01-10
http://hdl.handle.net10539/13431

Downloaded from a DSpace repository. https://dspace.org/

Synthesis and Functionalization of Gallium Nitride Nanostructures for Gas Sensing and Catalyst Support

by

Thobeka Kente

(Student Number: 0504744G)

A thesis submitted to the Faculty of Science, University of the Witwatersrand, Johannesburg, in fulfilment of the requirements for the degree of Doctor of Philosophy.

October 2013

Johannesburg, South Africa

Declaration

I declare that this thesis is my own original work under the supervision of Dr S.D. Mhlanga and Prof. N.J. Coville. It is being submitted for the degree of Doctor of Philosophy to the University of the Witwatersrand, Johannesburg, South Africa. It has not been submitted before for any degree or examination in any other University.

Signature of candidate ……

On this……day of……2013

Abstract

We report the role of a double step heat treatment process in the synthesis of novel GaN nanostructures (NSs) using a two stage furnace following a catalyst free vapour-solid growth mechanism. Morphological analysis revealed that GaN NSs were composed of rod-like structures with average diameter of 250 nm and accumulated particulates of GaN with diameter of ~ 12 – 16 nm providing enhanced surface area. The wurtzite phase of GaN nanorods of agglomerated nanoclusters was synthesized at temperatures as low as 750 °C. An X-ray photoelectron spectroscopic study confirmed formation of GaN. The surface areas of the GaN NSs were high at ~20 m^2/g with respect to that expected for solid nanorod structures. The GaN NSs were of high crystallinity and purity as revealed by structural studies. Raman spectral analysis showed stronger intensity of the A_1(LO) mode with respect to that for E_2(high) mode indicating the high electronic quality of the sample. A photoluminescence study revealed the dominant presence of a defect band around 1.7-2.1 eV corresponding to nitrogen di-vacancies. Subsequent annealing in NH_3 has demonstrated a compensation of the defect state and evolution of a band edge peak with possible hydrogen compensation of surface states.

We also report the role of activated carbon on Ga_2O_3 to make GaN/C nanostructure composites using a single stage furnace. TEM analysis showed that GaN/C nanostructures gave different morphologies with different ratios of GaN/C. The surface areas of these materials showed an increase as the ratio of activated carbon was increased. PXRD showed that a ratio of Ga_2O_3: C of 1:0.5 (w/w) was sufficient to form GaN. TGA revealed that the ratios of Ga_2O_3: C of 1:0.5 – 1:2 gave materials that were thermally stable. Raman spectra showed that the material had excellent electronic properties. The material with a Ga_2O_3/C 1:2 ratios showed a poor gas response due to the change in reference value of resistance with the variation of hydrogen concentration.

This study also provides the first investigation of GaN as a catalyst support in hydrogenation reactions. The GaN NSs were synthesized via chemical vapour deposition (CVD) in a double stage furnace (750 ºC) while nitrogen doped carbon spheres (NCSs) were made by CVD in a single stage furnace (950 ºC). TEM analysis revealed that the GaN NSs were rod-like with average diameters of 200 nm, while the NCSs were solid with smoother surfaces, and with diameters of 450 nm. Pd nanoparticles (1 and 3% loadings) were uniformly dispersed on acid functionalized GaN NSs and NCSs. The Pd nanoparticles had average diameters that were influenced by the type of support material used. The GaN NSs and NCSs were tested for the selective hydrogenation of cinnamaldehyde in isopropanol at 40 and 60 °C under atmospheric pressure. A comparative study of the activity of the nanostructured materials revealed that the order of catalyst activity was 3% Pd/GaN >3% Pd/NCSs > 1% Pd/NCSs > 1% Pd/GaN. However, 100% selectivity to hydrocinnamaldehyde (HCALD) was obtained with 1% Pd/GaN at reasonable conversion rates.

Dedications

I would like to dedicate this thesis to the following people:

- In memory of my parents.
- My family (sisters, brothers, nieces, nephews).
- My friends.

I thank you all for everything you have done for me, I am grateful. May the Lord bless you all.

Acknowledgements

I give thanks to you:

- Lord God Almighty for giving me strength.
- My supervisors. Dr S.D. Mhlanga and Prof. N.J. Coville for your advices, guidance, encouragements and being supportive.
- The Council for Scientific and Industrial Research (CSIR), Wits Postgraduate Merit Awards, Bradlow, and Local Merit Scholarship for funding my studies.
- Mr Basil Chassoulas and Tshepo Mashoene for technical support.
- Mr T. Dzara the glass blower for making the quartz tubes and boats available to me so that I can do my experiments.
- Mr D. Moloto and Mr A. Baloyi the store managers for providing me with chemicals, gas cylinders, etc.
- Prof. M. Witcomb and Prof. A. Ziegler for your help in Microscopy and Microanalysis Unit.
- Dr R. M. Erasmus for Raman analysis.
- Dr E. Coetsee (UFS) for XPS measurements.
- Siyasanga Mpelane (Mintek) for HRTEM analysis.
- CATOMMAT group for friendly environment and your help in many various ways.
- Dr S. Dhara and MSG group at IGCAR, India for their help on gas sensing measurements, Resonance Raman and PL analysis.
- Natsayi Chiwaye and Wilson Mogodi for their help on XRD analysis.
- Mbongiseni William Dlamini for proof reading this thesis.
- My family for believing in me and giving me the support.

"No one who achieves success does so without acknowledging the help of others. The wise acknowledge this help with gratitude" Unknown.

Publications

(a) Published Papers:

1. *T. Kente, S.M.A. Dube, N.J. Coville, S.D. Mhlanga, Application of Gallium Nitride Nanostructures and Nitrogen Doped Carbon Spheres as Supports for the Hydrogenation of Cinnamaldehyde. Journal of Nanoscience and Nanotechnology, Volume 13, Number 7, pp 4990-4995, 2013.*

(b) Submitted Papers:

2. *T. Kente, N.J. Coville, S.D. Mhlanga, H.C. Swart, R.M. Erasmus, S. Dhara, Catalyst free vapour-solid growth of novel GaN nanostructures at low temperature, Material Chemistry and Physics (under review), 2013.*

3. *T. Kente, A.K. Prisada, S. Dhara, S. D. Mhlanga, N.J. Coville, Synthesis and functionalization of carbon doped GaN NSs for hydrogen gas sensing, Sensors, 2013.*

4. *T. Kente, A. Pantsha, S. Dhara, N.J. Coville, S.D. Mhlanga, Gallium nitride nanostructures: a review, Acta Materialia, 2013.*

(c) Conference proceedings:

1. *T. Kente, N.J. Coville, S.D. Mhlanga, Synthesis and characterization of gallium nitride nanorods (GaN-NRs) for sensor and catalysis applications. IEEE (2011) 392-395. ICONSET2011, 28-30 Sept, 2011, Sathyabama University, Chennai, India, ISBN: 978-1-4673-0072-8; www.iconset2011.com/index.html*

Presentations

Conferences attended

(i) NanoAfrica 2012: The 4th International Conference on Nanoscience and Nanotechnology, University of the Free State, South Africa: Oral presentation.

(ii) SACI 2011: South African Chemical Institute, University of the Witwatersrand, Johannesburg, South Africa: Poster presentation.

(iii) NanoAfrica 2009: The 3rd International Conference on Nanoscience and Nanotechnology, CSIR, Pretoria, South Africa: Poster presentation.

Seminars and Workshops

(i) CATOMMAT group seminars (2010-2013): Oral

(ii) DST/NRF Center of Excellence in Strong Materials Workshop, Wits University, 2012: Poster

(iii) Wits University Cross Faculty Symposium 2012: Poster

(iv) Colloquium in the School of Chemistry 2011: Oral

(v) IBSA Workshop 2013: Oral

Table of contents

Declaration……ii

Abstract……. iii

Dedication……. v

Acknowledgement…… vi

Publications…….. vii

Presentations……. viii

Contents……. ix

List of figures…… xv

List of tables…….. xxi

Abbreviations…… xxii

Contents

Chapter 1……1

1.1 Introduction……..1

1.1.1 Background……1

1.2 Aims and Objectives……..3

1.3 Thesis outline……4

1.4 References……..6

Chapter 2……....10

Literature Review…….. 10

2.1 Introduction……..10

2.2 Crystalline structure of GaN…… 11

2.3 Synthesis of GaN nanostructures……15

2.4 GaN nanostructure morphologies and the growth processes……...27

2.4.1 GaN nanorods……... 27

2.4.2 GaN nanowires……..30

2.4.3 GaN nanotubes……. 33

2.5 Other Structures……... 35

2.5.1 GaN nanobelts……...35

2.5.2 GaN nanobelts with herringbone morphology……..36

2.5.3 GaN nano-flowers……37

2.5.4 Durian-like GaN……38

2.5.5 Dandelion-like GaN……..39

2.5.6 Triangular nanowires…… 41

2.5.7 Conical shape nanorods…… 42

2.5.8 Needle- like nanowire array……..43

2.5.9 GaN hollow spheres……..43

2.5.10 GaN nanochestnuts…… 46

2.6 Properties and Applications of GaN nanostructures……49

2.6.1 GaN Alloy nanostructures…… 50

2.7 Properties and Applications of GaN nanostructures in Sensors…….. 51

2.8 Catalyst support……... 53

2.9 References……54

Chapter 3……62

Experimental and characterization techniques……...62

3.1 Introduction……..62

3.2 Synthesis of GaN NSs and carbon coated GaN……...62

3.3 Functionalization of GaN NSs……64

3.4 Characterization techniques……65

3.4.1 Transmission and scanning electron microscopy (TEM and SEM)…. 65

3.3.2 Raman spectroscopy…… 66

3.3.3 Photoluminescence……... 67

3.3.4 Brunauer Emmett Teller (BET) surface area…… 67

3.3.5 Thermogravimetric analysis……..68

3.3.6 Electron Dispersive X-ray (EDX) analysis……...68

3.3.7 Powder X- ray diffraction (PXRD) analysis……68

3.3.8 X-ray photo-electron spectroscopy (XPS)……68

3.4. Gas measurement system……69

3.5 References……70

Chapter 4……72

Catalyst free vapour-solid growth of novel GaN nanostructures at low temperature……... 72

4.1 Introduction…… .72

4.2. Experimental details……74

4.2.1 Growth of GaN Nanostructures…… 74

4.2.2 Characterization of the GaN nanostructures……74

4.3. Results and discussion…… 75

4.3.1 Morphological analysis……75

4.3.2 PXRD analysis……...77

4.3.3 BET surface area analysis……79

4.3.4 X-ray photo-electron spectroscopy (XPS) analysis……..80

4.3.5 Raman spectroscopic analysis……...86

4.3.6 Photoluminescence (PL) analysis……89

4.4 Conclusion……... 91

4.5 References…….92

Chapter 5……94

Functionalization and characterization of carbon coated GaN nanostructures…….. 94

5.1 Introduction……..94

5.2 Experimental……95

5.2.1 Synthesis of carbon coated GaN (GaN/C)……95

5.2.2 Functionalisation of GaN/C……. 95

5.3 Results and discussion……96

5.3.1 HRTEM analysis……...96

5.3.4 TGA analysis…… 98

5.3.5 BET surface area analysis……104

5.3.6 Raman analysis……104

5.3.7 Photoluminescence (PL) analysis……105

5.4 Conclusions……..107

5.5 References……108

Chapter 6……109

Synthesis and functionalization of GaN/C nanostructured composites for hydrogen gas sensing……109

6.1 Introduction……..109

6.2 Experimental……110

6.2.1 Synthesis and functionalization of GaN/C NSs……110

6.2.2 Preparation of Pd/GaN catalysts……...111

6.3 Characterization of GaNNSs……112

6.4 Results and discussion……. 112

6.4.1 PXRD analysis……..112

6.4.2 Morphological studies……...114

6.4.3 BET Analysis…… 116

6.4.5 TGA analysis…… 117

6.4.7 Raman spectroscopic analysis……...119

6.4.8 Photoluminescence (PL) analysis……. 120

6.4.9 Morphological studies and elemental analysis after 3%Pd loaded on GaN NSs……121

6.5 Hydrogen gas sensing…….. 123

6.6. Conclusions……124

6.7. References……...126

Chapter 7…… 128

Application of GaN nanostructures and nitrogen doped carbon spheres as supports for the hydrogenation of cinnamaldehyde……. 128

7.1 Introduction……..128

7.2 Experimental……...131

7.2.1. Synthesis and Functionalization of GaN Nanostructures…… 131

7.2.2. Synthesis and Functionalization of NCSs……131

7.2.3 Preparation of Pd/GaN and Pd/NCS Catalysts……. 132

7.2.4 Characterization of the Supports and Catalysts…… 132

7.2.5 Hydrogenation of Cinnamaldehyde…….. 133

7.3 Results and Discussion…… 133

7.3.1 XRD and TEM analysis…… 133

7.3.2 BET Surface Area Analysis……..136

7.3.3 Comparison of Catalyst Activity: Cinnamaldehyde Hydrogenation… 137

7.4 Conclusions……..140

7.5 References…….142

Chapter 8…… 143

General Conclusion and Recommendations…….. 143

List of Figures

Fig. 2.1: Crystal structure of (a) Wurzite GaN and (b) Zinc-blende GaN……12

Fig. 2.2: (a) Low-magnification image of a GaN nanorod including its tip, (b) a high-magnification image of the interface of the tip and the nanorod……...28

Fig. 2.3: Schematic illustration of VLS process for GaN nanorod (GaN-NR) growth by a pyrolysis route……28

Fig. 2.4: Schematic illustration of the condensation growth mechanism for GaN nanorods. (Left) GaN nuclei responsible for the tripod, bunched and hyperbunched growth. (Right) Final GaN NR morphologies depending on the crystal symmetry of the nuclei……...30

Fig. 2.5: GaN nanowire growth on different substrates. (a, c) Si(100), (b, d) Si(111). In the case of (a) and (b), the flow rates were 50 sccm for NH_3 and 100 for Ar, and in the case of (c) and (d), the flow rates are 125 sccm for NH_3 and 25 sccm for Ar; (e) higher magnification image of the cones……31

Fig. 2.6: 45°-Tilted scanning electron microscopy (SEM) view of a typical non-catalytic MOVPE growth of self-assembled GaN single-crystal wires on a c-plane sapphire substrate. The growth is homogeneous on the whole 2 inch wafer surface……...32

Fig. 2.7: Growth mechanism of GaN nanowires by catalyst free MOVPE……32

Fig. 2.8: (a) TEM image of a GaN nanotube and (b) magnified view of (a) and (c) scanning electron micrograph of GaN nanotubes……33

Fig. 2.9: A schematic illustration of the formation process of GaN nanotubes: (a) substrate before growth; (b) formation of Au droplets upon heating to growth temperature; (c) initial growth of GaN nanotubes using an Au/Ga alloy as catalyst; (d) continuous growth of nanotubes using Ga droplets as catalyst; (e) cross-

sectional image of a nanotube illustrating the diffusion-limited growth process. The N concentration in the Ga droplet is schematically depicted by the gray scale (darker indicates higher N concentration)……..35

Fig. 2.10: (a) A SEM micrograph showing high-density GaN nanobelts grown on a large area of the silicon substrate. (b) A magnified view revealing the belt-like structure…….36

Fig. 2.11: Low-magnification TEM image of an individual GaN nanobelt and the inset shows corresponding high-magnification TEM image…….37

Fig. 2.12: SEM images of GaN nanostructures (a) and (b) grown on a silicon substrate at 1323 K/25 SCCM and 1323 K/50 SCCM (c) and (d) on GaN and AlN substrates respectively grown with 1323 K/25 SCCM……..38

Fig. 2.13: (a and b) Low magnification SEM images of durian-like GaN. (c) Medium magnification of durian-like GaN. (d) High magnification images of durian-like GaN having sharp tips…….39

Fig. 2.14: (a and b) shows the low magnification images and (c and d) shows high magnification of SEM images of dandelion-like GaN microstructures…….40

Fig. 2.15: The growth mechanism for the formation of dandelion-like GaN microstructures…. …….……41

Fig. 2.16: FESEM images of GaN nanowires grown on Si (100) at (a) low magnification and (b) high magnification. The inset shows the existence of the Au catalysts at the end of the nanowires……..41

Fig. 2.17: FESEM images of GaN nanorods prepared at 1100 °C (a) top view, (b) side view, (c) low magnification tilted view and (d) high magnification tilted view (inset is the tip angle)……..…42

Fig. 2.18: Low magnification and (b) high magnification SEM images for the needle-like GaN nanowires……...….43

Fig. 2.19: TEM images of GaN hollow spheres synthesized at (a) 700 °C and (b) 900 °C…….44

Fig. 2.20: Schematic mechanism for the formation of GaN hollow spheres using carbon spheres as templates……...45

Fig. 2.21: A schematic illustration of the formation process of hollow GaN spheres and hollow nanotubes: a) Generation of nanosized liquid Ga droplets; b) GaN nanocrystal nucleation and growth on the surface of Ga liquid droplets; c) the hollow GaN sphere is formed with small shell size; d, e) at high temperatures they formed hollow GaN spheres aggregate and hollow GaN nanotubes are formed by the coalescence of the nanosized hollow GaN spheres……45

Fig. 2.22: FE-SEM images of (a) a GaN nanorod chestnut, (b) a cross-sectional image of a nanorod chestnut, (c) a nanoneedle chestnut, and (d) a cross-sectional image of a nanoneedle chestnut……..……47

Fig. 2.23: Schematic diagram of a possible growth mechanism of GaN chestnut-like nanostructures…….47

Fig. 2.24: Various ternary and quaternary materials used for LEDs with the wavelength ranges indicated……..…51

Fig. 2.25: Schematic of Pt/GaN Schottky diode for hydrogen gas sensing……53

Fig. 2.26: SEM micrograph of completed device, showing bond wire attached (top) and photograph of device bonded into header……..53

Fig. 3.1: Single stage furnace for CVD experiments…….63

Fig. 3.2: Double stage furnace used in CVD experiments…….63

Fig. 3.3: Reaction setup used for hygrogenation reaction……..64

Fig. 3.4: FEI Tecnai G^2 Spirit electron microscope……...65

Fig. 3.5: JEOL 7500F scanning electron microscope……....66

Fig. 3.6: Schematic diagram of gas measurement system…….69

Fig. 4.1: SEM and TEM (inset) images of GaN nanostructures grown in the two stage furnace at (a) 750 °C, and (b) 800 °C, for 2 h; (c) 850 °C and (d) 900 °C for 1 h……..76

Fig. 4.2: TEM image shows the (a) agglomerated nanoparticles typically grown in the two stage furnace at 750 ^{o}C (b) morphology of the GaN materials at 1100 °C grown in single stage furnace……77

Fig. 4.3: PXRD pattern of GaN nanostructures synthesized using Ga_2O_3 and NH_3 at various growth conditions. Spectra are shifted vertically for clarity……..78

Fig. 4.4: Average grain sizes of the GaN nanostructures synthesized at different growth temperatures. The line acts as a guide to the eye……..79

Fig.4.5: Typical high resolution binding energy spectra of the N1s (a), $Ga2p_{3/2}$ (b) and O1s (c) observed in the GaN nanostructures synthesized at 800 °C in the two stage furnace……..82

Fig.4.6: Typical high resolution binding energy spectra of the N1s (a), $Ga2p_{3/2}$ (b) and O1s (c) observed in the GaN nanostructures synthesized at 850 °C in the two stage furnace……..83

Fig.4.7: Typical high resolution binding energy spectra of the N1s (a), $Ga2p_{3/2}$ (b) and O1s (c) observed in the GaN nanostructures synthesized at 900 °C in the two stage furnace……..84

Fig.4.8: Typical high resolution binding energy spectra of the N1s (a), $Ga2p_{3/2}$ (b) and O1s (c) observed in the GaN nanostructures synthesized at 1100 °C in the two stage furnace……..85

Fig. 4.9: a) Raman spectra of GaN nanostructures synthesized at different growth temperatures using 514.5 nm excitation. b) Resonance Raman spectra of GaN nanostructures synthesized at different growth temperatures using 325 nm excitation. Spectra are shifted vertically for clarity……...88

Fig. 4.10: Room temperature PL spectra a) for pristine GaN nanostructures synthesized at various growth temperatures showing broad and intense peak in the range of 1.7-2.1 eV. Inset shows the zoomed spectra for free-to-bound emission at around 3.25 eV, b) for post-annealed GaN nanostructures synthesized at various growth temperatures showing clear free-to-bound emission peak at around 3.25 eV……...90

Fig. 5.1: TEM images. (a) Dark field image and SAED pattern (inset) (b) bright field image of GaN/C…….....97

Fig. 5.2: (a) High magnification TEM images and SAED (inset) (b) TEM images of 30% fGaN/C. …….....97

Fig. 5.3: (a) High magnification TEM images and SAED (inset) (b) TEM images of 55% fGaN/C …….....98

Fig. 5.4: TGA profile and derivative of GaN/C at different temperatures……..100

Fig.5.5: (a) TGA profile and (b) the derivative of GaN/C as a function of time (T = 600 °C, flow rate = 50 mL/min)…….....101

Fig. 5.6: TGA profile of (a) the functionalized samples and as synthesized GaN/C and (b) their derivative curves……..103

Fig. 5.7: Raman spectra for as synthesized and fGaN/C samples....……....105

Fig. 5.8: Room temperature PL spectra for GaN/C and fGaN/C…….....106

Fig. 5.9: Room temperature PL spectra (zoom) for GaN/C and functionalized GaN/C……..106

Fig. 6.1: PXRD patterns showing the effect of synthesis time on GaN synthesis using a Ga_2O_3/C ratio (1:3) in NH_3 at 1100 °C……....113

Fig. 6.2: PXRD patterns showing the effect of Ga_2O_3/C ratio on the synthesis of GaN NSs. Synthesis was carried out at 1100 °C for 45min…….113

Fig. 6.3: SEM images of GaN synthesised with different ratio of Ga_2O_3 to activated carbon (a) 1:0.5 (b) 1:1 (c) 1.:2 (d) 1:3 (e) 1: 4 (f) 1: 5…….115

Fig. 6.4: TGA profiles of GaN NSs synthesized with and without activated carbon at 1100 °C…….118

Fig.6.5: Derivative weight loss of GaN-NSs with and without activated carbon at 1100 °C…….118

Fig. 6.6: (a) Raman spectra of GaN nanostructures with different ratios of Ga_2O_3/C using the 514.5 nm excitation. (b) Resonance Raman spectra of GaN nanostructures with different ratios of Ga_2O_3/C using 325 nm excitation……...120

Fig. 6.7: Room temperature PL spectra of the GaN nanostructures with different ratios of Ga_2O_3/C using the 325 nm excitation……121

Fig. 6.8: TEM images of 3%Pd /GaN/C……..122

Fig. 6.9: EDS spectrum of 3%Pd/ GaN/C……122

Fig. 6.10: Resistance and response curve (inset) of different concentration H_2 exposure at 200 °C……...124

Fig. 7.1: Reaction scheme proposed for the selective hydrogenation of cinnamaldehyde……130

Fig. 7.2: PXRD patterns of (a) as-synthesized GaN NSs (synthesis temp = 750 °C) and (b) as-synthesized NCSs……....134

Fig. 7.3: TEM images of (a) 1%Pd/GaN, (b) 3%Pd/GaN, (c) 1%Pd/NCSs and (d) 3%Pd/NCSs. The dark spots are Pd nanoparticles……...135

Fig. 7.4: Particle size distribution graphs of (a) 3 % Pd/GaN, (b) 1 % Pd/NCSs and (c) 3 % Pd/NCSs……136

Fig.7.5: Graphs showing CALD remaining as a function of time on stream at 40 and 60 ^oC for 1% Pd/GaN and 1% Pd/NCSs catalysts…….138

Fig. 7.6: Graphs showing (a) the product selectivity to HCALD and 3P1P (b) CALD remaining as a function of time on stream at 60^{o}C for 3%Pd/GaN and 3% Pd/NCSs catalysts……139

List of Tables

Table 2.1: Physical properties of GaN……...13

Table 2.2: Electronic properties of GaN……....14

Table 2.3: Synthetic parameters related to the synthesis of GaN nanostructures……....17

Table 4.1: Previous work on the synthesis of GaN in a double stage furnace…...73

Table 4.2: BET surface areas of the GaN NSs synthezised at different temperatures in a double stage furnace (synthesis time = 1 h for 850 ˚C and 900 ˚C and 2 h for 750˚C and 800 ˚C)……..80

Table 4.3: The binding energies of the GaN synthesized at various growth temperatures……...86

Table 5.1: BET surface area of carbon coated GaN and functionalised GaN/C..104

Table 6.1: BET surface areas showing the variation of surface area with and without carbon (synthesis time = 45 min, temperature = 1100 °C). The ratio refers to the Ga_2O_3: C mass ratio……...116

Table 7.1: BET surface areas and pore volumes of the supports and catalysts……137

Table 7.2: A summary of the % CALD conversions and selectivities of the Pd/GaN and Pd/NCSs catalysts using different Pd loadings and reaction temperatures……140

Abbreviations

1D	One dimensional
2DEG	Two dimensional electron gas
3D	Three dimensional
AlN	Aluminium nitride
Al_2O_3	Aluminium oxide
BET	Brunauer-Emmett-Teller
CVD	Chemical vapour deposition
EDX	Energy dispersive X-ray spectroscopy
F-B	Free to bound
GaCl	Gallium chloride
GaN	Gallium nitride
H_2	Hydrogen
HNO_3	Nitric acid
H_2SO_4	Sulphuric acid
HRTEM	High resolution transition electron microscopy
HVPE	Hydride vapour phase epitaxy
LO	Longitudinal optical
mL/min	millilitre per minute
MOVPE	Metal organic vapour phase epitaxy
NH_3	Ammonia

N_2	Nitrogen
Nm	nanometers
PL	Photoluminescence
PAMBE	Plasma assisted molecular beam epitaxy
RT	Room temperature
SAED	Selected area electron diffraction
SEM	Scanning electron microscopy
TEM	Transition electron microscopy
T	Temperature
T	time
TGA	Thermogravimetric analysis
TO	Transverse optical
UHV	Ultrahigh vaccum
UV	Ultra violet
VLS	Vapor-liquid-solid
WZ	Wurtzite
XPS	X-ray photoluminescence spectroscopy
YL	Yellow luminescence
ZB	Zone boundary

Chapter 1

1.1 Introduction

1.1.1 Background

There is much interest in the development of wide band gap semiconductors for use as gas and chemical sensors. Semiconductors such as gallium nitride (GaN) can be operated at higher temperatures than conventional semiconductors and sensors based on GaN can be operated at higher temperatures than conventional Si-based devices [1]. Hydrogen gas is used for the detection of fuel leaks in space craft, automobiles and gas emission in industries [2-3]. Developing highly sensitive hydrogen detectors for use in a wide range of conditions has become very important. These detectors allow monitoring gas concentrations continuously in a range of environments in a quantitative and selective way. Hence, hydrogen sensors form an integral part of many gas sensor systems [4].

GaN materials are used for H_2 gas sensing because of the sensitivity to surface charge. They are also stable over a wide temperature range [5-6]. GaN gas sensors have a unique advantage, in that they can be integrated with GaN-based optical devices or high-power, high-temparature electronic devices on the same chip [4]. GaN materials have also been used for the production of different devices such as high power microwave tubes, laser diodes, light emitting diodes, detectors, and field emitter arrays due to their field emission and photoluminescence properties [7].

Gallium nitride nanostructures (GaN NSs) have been synthesized using different synthetic methods that include chemical vapour deposition (CVD) [7-27], metal-

organic vapour phase epitaxy (MOVPE) [28], metal- organic chemical vapour deposition (MOCVD) [29], halide vapour phase epitaxy (HVPE) [30-31] and pyrolysis [32]. They have been synthesized with different morphologies: nanorods [8, 33], nanowires [22, 23, 28, 34], nanotubes [25, 29, 30], nanobelts [10], nanoflowers [11], durian–like [7], dandelion–like [16], grass-like [14], nanochestnuts [31], nanospindles [35], leaf-like [24] and hollow spheres [36].

One dimension nanomaterials such as nanowires, nanotubes, nanorods and nanobelts are excellent candidates for use as hydrogen gas sensors because of their high surface to volume ratios [37-40]. Generally the sensitivity of a detector is determined by the surface to volume ratio of the material [41]. There are a few studies that have reported on the use of GaN nanowires as H_2 gas based sensors. Many of the studies reported on gas sensors are based on ZnO nanorods [42], SnO_2 nanowires [39], carbon nanotubes [38] and they show excellent response and recovery characteristics.

Hydrogen detection sensitivity of a semi-conductor can be increased by using a catalytic metal coating or transition metal to dope the sensor material [43 - 44]. The catalytic metal method leads to catalytic dissociation of H_2 to atomic hydrogen, which generates a sensor response through binding to surface atoms and altering the surface potential [45]. Deposition of a catalytic metal on the surface of GaN nano-material is known to enhance its catalytic activity. Palladium (Pd) and platinum (Pt) have been used as the metals of choice for nitride and oxide based sensors in many applications [46-48].

In this thesis we report the catalyst free synthesis of novel GaN NSs, at low temperature (750 – 900 °C) by exploiting a two stage oven system. The first heating zone was used to preheat the nitrogen source (NH_3) to high temperature (1100 °C) and the second heating zone was used for the growth of GaN NSs at lower temperatures (750 – 900 °C). The growth of carbon doped GaN NSs at high temperature (1100 °C) in a single stage oven is also reported. In an attempt to lower the synthesis temperature and time, activated carbon was mixed with Ga_2O_3 during

the synthesis. The role of activated carbon was to reduce the Ga_2O_3. However, the processes using carbon still required high temperatures to obtain the GaN NSs. The material with carbon was used for palladium (Pd) deposition. Pd was used as a metal of choice for H_2 gas sensing. The synthesis of carbon coated pre-produced GaN NSs in a single stage oven at 600 °C and the functionalization of this material using different concentrations of acid (HNO_3) is also reported. High surface area in GaN makes it a good candidate for catalysis hence our choice is to exploit its ability to act as a support material for Pd catalysts. The new synthetic strategies that allow for the synthesis of nano shaped/sized semi-conductors thus opens up the possibility of using these materials as catalyst supports. We have also explored the use of GaN nanostructures as catalyst support for hydrogenation reactions. These studies thus complement the typical studies of semiconductors as sensors.

1.2 Aims and Objectives

The specific aims of this thesis are the following:

- To synthesize GaN NSs in a single stage horizontal furnace using Ga_2O_3, NH_3 and activated carbon as Ga, N sources and reducing agent respectively.
- To synthesize GaN NSs at low temperature by exploiting a two stage oven system at atmospheric pressure using Ga_2O_3 as a precursor.
- To use GaN as a catalyst support for cinnamaldehyde hydrogenation reaction.
- To test the new GaN as a chemical gas sensor for H_2.
- To coat pre-produced GaN with carbon using acetylene and to functionalize the material.

The new materials were characterized using different techniques i.e. transmission electron microscopy (TEM), scanning electron microscopy (SEM), Raman

spectroscopy, Brunauer-Emmett and Teller (BET) surface area analysis, X-ray energy dispersive spectroscopy (EDS), powder X-ray diffraction (PXRD), X-ray photo-electron spectroscopy (XPS), High resolution TEM (HRTEM), thermal gravimetric analysis (TGA) and Photoluminescence (PL).

1.3 Thesis outline

Chapter 1: This chapter briefly gives the background of the GaN materials studied some applications and gives an overview of the Thesis.

Chapter 2: This chapter gives a literature review that covers the synthesis, morphology, growth mechanism, properties and applications of GaN nanostructures.

Chapter 3: This chapter describes in detail the experimental procedure and characterisation techniques that were used to make, test and characterize the materials.

Chapter 4: This chapter explains the synthesis of pure GaN materials using different CVD procedures using a (i) single and (ii) double stage furnace.

This chapter is currently under review as; Thobeka Kente, Neil J. Coville, Sabelo D. Mhlanga, Hendrik. C. Swart, Rudolph M. Erasmus, Sandip Dhara, Catalyst free vapour-solid growth of novel GaN nanostructures at low temperature, Journal of Material Chemistry and Physics.

Chapter 5: This chapter gives an explanation of the synthesis, functionalization and characterization of carbon coated pre-produced GaN NSs.

Chapter 6: This chapter reports on the preparation and testing of Pt/Pd catalysts using carbon doped GaN as a support for gas sensing.

This chapter will be submitted for publication as Thobeka Kente, Arun K. Prisada, Sandip Dhara, Sabelo D. Mhlanga and Neil J. Coville, Synthesis and functionalization of carbon doped GaN NSs for hydrogen gas sensing.

Chapter 7: This chapter reports on the synthesis and use of nanostructures of gallium nitride (GaN NSs) and nitrogen doped carbon spheres (NCSs) as support materials for the hydrogenation of cinnamaldehyde.

*This chapter has been published as: Thobeka Kente, Sibongile M. A. Dube, Neil J. Coville, Sabelo D. Mhlanga**,** Application of Gallium Nitride Nanostructures and Nitrogen Doped Carbon Spheres as Supports for the Hydrogenation of Cinnamaldehyde, Journal of Nanoscience and Nanotechnology,Volume 13, Number 7, pp 4990-4995, 2013.*

Chapter 8: This chapter gives the general conclusions and recommendations to the study.

1.4 References

1. B. S. Kang, H-T Wang, L. C Tien , F. Ren , B. P. Gila, D. P. Norton, C. R. Abernathy, J. Lin and S. J. Pearton, Sensors, 6 (2006) 643.
2. A. L. Spetz, P. Tobias, L. Uneus, H. Svenningstorp, L-G. Ekedahl, I. Lundstrom, Sens. Actuators, B 70 (2000) 67.
3. H. Svenningstorp, P. Tobias, I. Lundstrom, P. Salomonsson, P. Mårtensson, L-G. Ekedahl, A .L. Spetz, Sensors and Actuators B 57 (1999) 159.
4. Y. Irokawa, Sensors, 11 (2011) 674.
5. S. S. Kim, J. Y. Park, S-W. Choi, H. S. Kim, H. G. Na, J. C. Yang, C. Lee, H. W. Kim, Int. J. Hydrogen Energ. 36 (2011) 2313.
6. K. Matsuo, N. Negoro, J. Kotani, T. Hashizume, H. Hasegawa, Appl. Surf. Sci. 244 (2005) 273.
7. G. Nabi, C. Cao , W. S. Khan, S. Hussain, Z. Usman, T. Mahmood, N. A. D. Khattak, S. Zhao, X. Xin, D. Yu, X. Fu, Mater. Chem. and Phys. 133 (2012) 793.
8. W. Han and A. Zettl, Appl. Phys. Lett, 80 (2002) 2.
9. X. M Cai, A. B Djurisic, M. H Xie, Thin Solid Films 515 (2006) 984.
10. S. Y. Bae, H.W Seo, J. Park, H. Yang, S. A.Song, Chem. Phys. Lett. 365 (2002) 525.
11. S. Dhamodaran, D. SathishChander, J. Ramkumar, Appl. Surf. Sci. 257 (2011) 9612.
12. G. Nabi, C. Cao, Z. Usman, S. Hussain, W. S. Khan, F. K. Butt, Z. Ali, D. Yu, X. Fu, Mater. Lett. 70 (2012) 19.

13. G. Nabi, C. Cao, W.S. Khan, S. Hussain, Z. Usman, N. A. D. Khattak, Z. Ali, F. K. Butt, S. H. Shah, M. Safdar, Mater. Lett. 66 (2012) 50.

14. S. C. Lyu, O. H. Cha, E. K. Suh, H. Ruh, H. J. Lee, C. J. Lee, Chem. Phy. Lett. 367 (2003) 136.

15. L. Luo, K. Yu, Z. Zhua, Y. Zhang, H. Ma, C. Xue, Y. Yang, S. Chen, Mater. Lett. 58 (2004) 2893.

16. G. Nabi, C. Cao, W. S. Khan, S. Hussain, Z. Usman, S. Muhammad, S. S. Hussain, N. A. D. Khattak, Appl. Surf. Sci. 257 (2011) 10289.

17. D. V. Dinh, S. M. Kang, J. H. Yang, S-W. Kim, D. H. Yoon, J. Cryst. Growth, 311 (2009) 495.

18. G. Nabi, C. Cao , S. Hussain , W. S. Khan , R. R. Sagar , Z. Ali , F. K. Butt , Z. Usman and D. Yu, Cryst. Eng. Comm, 14 **(**2012), 8492.

19. B. Liu, Y. Bando, C. Tang, F. Xu, J. Hu, and D. Golber, J. Phys. Chem. B, 109 (2005) 17082.

20. J. Liu, X-M. Meng, Y. Jiang, C-S. Lee, I. Bello and S-T. Lee, Appl. Phys. Lett. 83 (2003) 4241.

21. L. Dai, S.X. Fu, L.P. You, J.J. Zhu, B.X. Lin, J.C. Zhang, G.G. Qin, J. Chem. Phys. 122 (2005) 104713.

22. C. Xue, Y. Wu, H. Zhuang, D. Tian, Y. Liu, X. Zhang, Y. Ai, L. Sun, F. Wang, Physica E, 30 (2005) 179.

23. X. He, G. Meng, X. Zhu and M. Kong, Nano. Res, 2 (2009) 321.

24. H. Qiu, C.Cao, J. Li, F. Ji, H. Zhu, J. Cryst. Growth, 291 (2006) 491.

25. P. Sahoo, S. Dhara, S. Dash, S. Amirthapandian, A.K Prisad, A.K. Tyagi, Int. J. Hydrogen Energy, 38 (2013) 3513.

26. P. Sahoo, S. Dhara, S. Amirthapandian, M. Kamruddin, S. Dash, B.K. Panigrahi, A.K. Tyagi, Cryst. Growth Des. 12 (2012) 2375.

27. S. Cho, J. Lee, I.Y. Park and S. Kim, Jpn. J. App. Phys. 41 (2002) 5533.

28. R. Koester, J. S Hwang, C. Durand, D. Le Si Dangand. J. Eymery, Nanotechnol. 21 (2010) 015602 (9pp).

29. M. C. Lu,Y. L. Chueh, L. J. Chen, L. J. Chou , H. L. Hsiao, and An-Ban Yang, Electr. Chem. Solid-State Lett, 8(2005) (7) G153.

30. C. Hemmingsson, G. Pozina, S. Khromov and B. Monemar, Nanotechnol. 22 (2011) 085602 (8pp).

31. M. J. Shin, J.Y. Moon, H.Y. Kwon, Y. J. Choi, H. S. Ahn, S. N. Yi, D.H. Ha, Y. Huh, Mater. Lett. 64 (2010) 1238.

32. M. Drygas, J. F. Janik, Mater. Chem. Phys. 133 (2012) 932.

33. Y. Wu, C. Xue, H. Zhuang, D. Tian, Y. Liu, Appl. Surf. Sci. 253 (2006) 485.

34. L. L. Low, F. K. Yam, K. P. Beh, Z. Hassan, Appl. Surf. Sci. 257 (2011) 10052.

35. X. Hao, J. Zhan, Y. Wu, S. Liu, X. Xu, M. Jiang, J. Cryst. Growth, 280 (2005) 341.

36. X. Sun and Y. Li, Angew. Chem. Int. Ed, 43 (2004) 3827.

37. L. C. Tien, H. T. Wang, B. S. Kang, F. Ren, P. W. Sadik, D. P. Norton, S. J. Pearton, J. Electrochem. Solid-State Lett. 8 (2005) G230.

38. I. Sayago, E. Terrado, E. Lafuente, M .C. Horrillo, W. K. Maser, A. M. Benito, R. Navarro, E. P. Urriolabeitia, M. T. Martinez, J. Gutierrez, Synth. Met. 148 (2005) 15.

39. B. Wang, L. F. Zhu, Y. H. Yang, N. S. Xu, G.W. Yang, J. Phys. Chem. C 112 (2008) 6643.

40. X. J. Huang and Y. K. Choi, Sens. Actuators, B 122 (2007) 659.

41. A. Ponzoni, E. Comini, G. Sberveglieri, J. Zhou, S. Z. Deng, N. S. Xu, Y. Ding and Z. L. Wang, Appl. Phys. Lett. 88 (2006) 203101.

42. O. Lupan, G. Chai, L. Chow, Microelectron. J. 38 (2007) 1211.

43. I. Sayago , E. Terrado, E. Lafuente, M. C. Horrillo, W. K. Maser, A. M. Benito, R. Navarro, E. P. Urriolabeitia, M. T. Martinez, J. Gutierrez, Synth. Met. 148 (2005) 15.

44. Y. Lu, J. Li, J. Han, H-T. Ng, C. Binder, C. Partridge, M. Meyyappan. Chem. Phys. Lett. 391 (2004).

45. L. C. Tien, H. T. Wang, B. S. Kang, F. Ren, P. W. Sadik, D. P. Norton, S. J. Pearton and J. Lin, Electrochem. Solid-State Lett. 8 (2005) G230.

46. J. S. Wright, W. Lim, B. P. Gila, S. J. Pearton, J. L. Johnson, A. Ural, F. Ren, Sensors and Actuators B 140 (2009) 196.

47. W. Lim, J. S. Wright, B. P. Gila, J. L. Johnson, A. Ural, T. Anderson, F. Ren, and S. J. Pearton, Appl. Phys. Lett. 93 (2008) 072109.

48. M. Epifani, T. Andreu, R. Zamani, J. Arbiol, E. Comini, P. Siciliano, G. Faglia and J. R. Morante, CrystEngComm, 14 (2012) 3882.

Chapter 2

Literature Review

2.1 Introduction

The synthesis of group III-nitride (group13-nitride) materials and in particular gallium nitride, have been investigated for a long time. Group III-nitride nanomaterials have been considered as promising systems for use in semiconductor devices [1]. Among the various semiconductor nanostructures, GaN is a promising candidate material for short wavelength optoelectronic devices such as light emitting diodes (LEDs), laser diodes (LDs) as well as high power and high temperature operation devices [2]. GaN is an important semiconductor with a wide direct band gap (3.39 eV at room temperature). The band gap of GaN is useful since it corresponds to the edge of the ultraviolet spectrum and therefore it could be applicable to the entire visible spectrum [3-4]. There is much interest on using these materials for chemical gas sensing applications, such as for the detection of H_2, O_2, NH_3 and ethanol [5]. Sensing materials are known to play a key role in detecting chemical and biological reagents [6].

In recent years it has become apparent that the shape and size of materials can impact on the properties. One dimensional nanostructures such as nanotubes, nanowires and nanorods are thus being studied because of their potential applications in novel nanoelectronic and optoelectronic devices, due to their unique electronic and optical properties [7]. Many attempts have been made to synthesize one dimensional GaN nanorods or nanowires using different techniques such as the carbon nanotube-confined reactions [8], anodic alumina template methods [9] arc discharge [10], laser

ablation [11, 12], chemical vapour deposition (CVD) [13] and metal organic vapour phase epitaxy (MOVPE) [14]. Among the different synthesis methods, the CVD process in a horizontal tube furnace reactor is of particular interest due to the low cost of the equipment and the simplicity of the experimental procedure. However, there are factors that can affect the morphology and the properties of the synthesized GaN nanostructures in such a system. The system geometry, gas flow, pressure during growth, Ga/N ratio, temperature, source material, substrate and catalyst used, all affect the obtained results [15]. Chander et al. have studied the controlled growth mode transition from 1-D to 3-D GaN nanostructures. The shape of nanostructures can be varied from a 1-D nanowire to a 3-D polyhedron depending on the growth conditions [16]. While much new information has been accumulated on GaN structures, especially nanostructures no attempt has been made in recent years to summarize this information. Herein, we report on some of the important results that have been obtained on GaN. The information will provide a perspective to place the thesis work in context. This review covers the synthesis, morphology, growth mechanism, properties and applications of GaN nanostructures.

2.2 Crystalline structure of GaN

The crystalline structure of GaN can have the wurtzite (hexagonal) or zinc-blende (cubic) structures under ambient conditions. These structures differ in their stacking sequence of close-packed Ga-N planes; the energy difference between the two structures is small. The wurtzite structure has a stacking sequence of ABABAB and belongs to the space group *P63mc*. This structure has alternating layers of close packed (0001) Ga metal atoms and nitrogen atoms. The zinc-blende structure belongs to the space group *F43m* and has an ABCABC stacking sequence of (111) close packed planes (Fig. 2.1) [17]. The change of the sequence during growth can produce defects e.g. stacking faults.

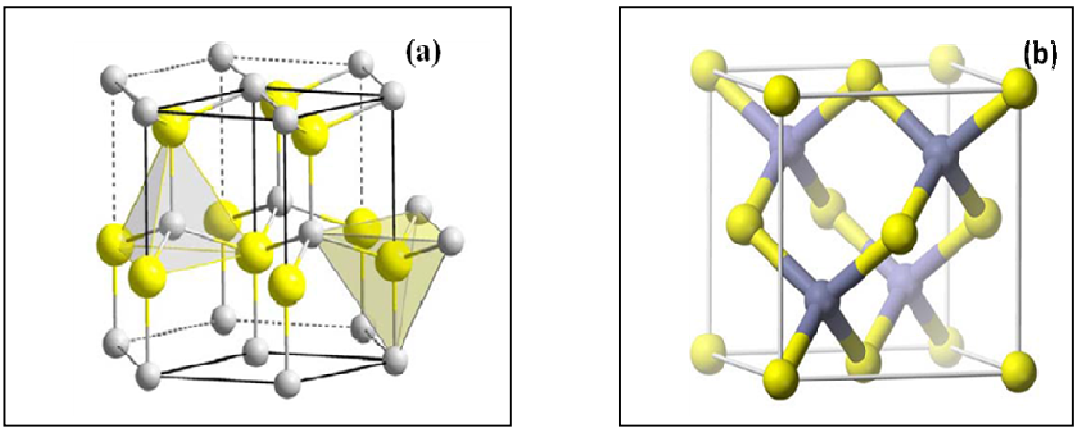


Fig. 2.1: Crystal structure of (a) Wurzite GaN and (b) Zinc-blende GaN [17].

The two structures have different physical (Table 2.1) and electronic (Table 2.2) properties [18].

Table 2.1: Physical properties of GaN

Physical Properties (300K)	Hexagonal GaN	Cubic GaN
Energy band gap (eV)	3.39	3.2
Density (g/cm^3)	6.15	6.15
Melting point (^oC)	2500	2500
Lattice constant (Å)	a=3.189, c=5.186	a=4.52
Thermal conductivity (W/cm·K)	2.1	2.1
Thermal expansion Coefficient (1/K)	$\alpha a=5.59\times10^{-6}$ $\alpha c=3.17\times10^{-6}$	N/A
Thermal diffusivity (cm^2/s)	0.43	0.43
Heat capacity (J/mol·K)	35.3	35.3
Dielectric constant (static)	8.9	9.7
Refractive index	2.3	2.3
Bulk modulus (GPa)	210	210

The properties of GaN have been compared with other widely used semiconductor materials e.g. (GaAs, AlN etc). GaN shows some advantages over the other

semiconductors for high power and high frequency applications. It is the best of all semiconductor materials except for diamond [18].

GaN based electronics are more advanced than GaAs based devices. GaN devices can withstand much higher electric fields than GaAs devices due to its larger bandgap of 3.4 eV. GaN is highly thermally stable material [19].

Table 2.2: Electronic properties of GaN

Electronic Properties	Hexagonal GaN	Cubic GaN
Electron mobility ($cm^2/V \cdot s$)	≤1000	≤1000
Hole mobility ($cm^2/V \cdot s$)	≤200	≤350
Effective electron mass (m_o)	0.20	0.13
Effective hole mass ($m_{o)}$		
Heavy	1.4	1.3
Light	0.3	0.2
Electron affinity (eV)	4.1	4.1
Breakdown field (V/cm)	~5×10^6	~5×10^6
Diffusion coefficient (cm^2/s)		
Electrons	25	25
Holes	5	9
Electron thermal velocity (m/s)	2.6×10^5	3.2×10^5
Hole thermal velocity (m/s)	9.4×10^4	9.5×10^4

2.3 Synthesis of GaN nanostructures

The different methods that have been used to synthesize GaN nanostructures can be classified into two types: the catalyst-assisted and the catalyst-free methods. The catalyst-assisted growth method typically occurs via a vapor-liquid-solid (VLS) process. Most GaN nanowires are currently obtained using metal catalysts by the MOVPE method [20]. The VLS process begins with the suspension of vapor phase reactants into a catalytic liquid metal (typically Ni or Au for the growth of GaN nanostructures) to form a supersaturated solution [21-25]. GaN material with different diameters and lengths in one dimension can be achieved by controlling the size of the catalyst particle, the growth time and the temperature [24].

A number of catalyst-free methods are known and these include the metal organic vapor-phase epitaxy (MOVPE), hydride-vapor-phase-epitaxy (HVPE) and plasma-assisted molecular-beam-epitaxy (PAMBE) methods [26]. The MOVPE process has been widely used for epitaxial film growth and involves a delivery of reactants in the form of metal-organic precursors onto a heated substrate using a carrier gas, followed by thermal decomposition of the precursors and surface migration of the resulting constituents. A surface chemical reaction then takes place between the migrating reactants, resulting in nucleation and subsequent crystal growth. MOVPE is a method that involves use of metal oxides to produce high quality GaN nanostructures for light emitting diode (LED) applications.

The HVPE process is similar to the MOVPE process and it is based on vapor-phase-epitaxy but uses gaseous gallium chlorides and hydrides and separate nitrogen sources respectively [27-31] to make GaN. The HVPE produces high growth rates and thus is advantageous for bulk film growth. However, because fine control of the nanostructure growth is not trivial at such high rates, synthesizing nanostructures via HVPE is difficult [26].

The PAMBE process uses Ga metal in ultrapure form. The GaN is heated slowly and sublimes to form Ga while nitrogen plasma is used as the nitrogen source. The Ga atomic source and activated-nitrogen gas then contact the heated substrates in an ultrahigh-vacuum (UHV) environment, where they diffuse and eventually give the nanostructure growth. This technique can produce high quality single crystalline GaN nanostructures with atomic scale control [32-37]. A summary of the various approaches used to make GaN nanostructures is given in Table 2.3.

Table 2.3: Synthetic parameters related to the synthesis of GaN nanostructures.

Catalyst	**Morphology of GaN**	**Gas atmosphere**	**Temperature and time.**	**Synthesis method**	**References**
(1:2) mixture of gallium dimethylamide and ferrocene.	Nanorods	NH_3 (~ 20 – 30 ml/min)	1000 °C (first stage) 900 °C (second stage) reaction time of 15 min.	CVD. Two stage furnace system.	Han et al. [38]
Metallic Ga on Si (111), Si (100) substrates with metal catalysts (Au and Ni).	Nanowires and stacked-cone nanowires	NH_3 (50/125 sccm) and Ar (100/25 sccm)	Varied from (800 – 1000 °C), reaction time of 30 min.	CVD. Single stage furnace system.	Cai et al. [39]
Catalyst- free	Nanowires	SiH_4 (45 sccm) NH_3 (4000 sccm) N_2 (8000 sccm)	1000 °C Reaction time varied (50, 100, 200, 400 s)	MOVPE	Koester et al. [40]

Si(100) substrates gold-catalyzed.	Nanotubes	NH_3 (200 sccm) and TMGa + N_2 (150 sccm), H_2 (200 sccm)	450 – 600 °C	MOCVD	Lu et al. [41]
GaCl, Al_2O_3 (0001) and Au coated Al_2O_3 (0001) substrates.	Nanotubes	NH_3 (500 – 2000 ml/min) N_2 (carrier gas)	Varied from 480 - 520 °C, reaction time of 90 min.	Vertical HVPE reactor	Hemmingsson et al. [42]
Ga, Ga_2O_3 and B_2O_3 mixture. $NiCl_2$ deposited on the substrate.	Nanobelts	NH_3 (200 sccm)	Ga source was set at 1100 °C and substrate was ~ 1000 °C, reaction time of 1 h.	CVD	Bae et al. [43]
Ga metal, Si (001) and AlN substrates.	Nanoflowers	NH_3 (25-50 sccm)	1050 °C reaction time of 3h.	CVD	Dhamodaran et al. [44]

Ga:GaN:C (4:4:1) Ga, c-plane sapphire substrates, Ni was deposited on the substrate.	Nanowires	NH_3 (100 sccm)	1st furnace 1000 °C 2nd furnace 950 °C reaction time of 30 min.	Horizontal two – furnace system	Low et al. [45]
$Ga_2O_3$with and without pre-heating with NH_3 (aq) at 120 °C. Si (001) substrate coated with $NiCl_2$/ethanol solution.	Nanowires	NH_3 (200 sccm)	1050 °C reaction time of 2 h	Horizontal tube furnace (CVD)	Nabi et al. [46]
$Ga_2O_3$with and without pre-heating with NH_3 (aq) at 100 °C. Si (001) substrate coated with $NiCl_2$/ethanol solution.	Grass like	NH_3 (200 sccm)	1200 °C reaction time of 2 h	Horizontal tube furnace (CVD)	Nabi et al.[47]

Ga/GaN (1:1), NiO catalyzed Al substrate	Nanowires	NH_3 (500 sccm)	1000 °C, reaction time of 1 h	CVD	Lyu et al. [48]
1st stage: (Ga $(OC_2H_5)_3$) was dissolved in ethanol (40 ml) 2nd stage: Ga_2O_3 gel	Nanorods	N_2/NH_3 (400 sccm)	Room temperature 1000 °C, reaction time of 20 min.	Ball milling process. Horizontal quartz tube furnace (CVD)	Wu et al. [49]
Ga_2O_3 thin films were deposited on Si (111) substrates.	Nanobelts with herringbone morphology	NH_3 (300 ml/min)	950 °C , reaction time of 15 min.	CVD	Luo et al. [50]
Ga metal pre-treated with aqueous NH_3 at 120 °C.	Durian-like	NH_3 (200 sccm)	1200 °C, reaction time of 2 h	CVD	Nabi et al. [51]
Ga_2O_3 + Graphite powder (1:1) treated with aqueous NH_3 at 120 °C.	Dandelion-like	NH_3 (200 sccm)	1200 °C, reaction time of 2 h	Horizontal quartz tube furnace CVD	Nabi et al. [52]

GaN powder + molten Ga metal (1:1), Au thin films were deposited onto the Si (100) substrates.	Triangular - shaped nanowires	NH_3 (20 sccm)	950 °C, reaction time of 15 – 30 min.	Horizontal quartz-tube hot-wall VPE system	Dinh et al. [53]
GaN pre-treated with aqueous NH_3 at 120 °C	Conical shape nanorods	NH_3 (200 sccm)	Varied from 1000, 1100 and 1200 °C, reaction time of 2 h.	CVD	Nabi et al. [54]
Ga_2O_3, Si wafer coated with a Au film was put on the Al_2O_3 boat, with the Au film directly facing the reactants.	Needle- like nanowire	NH_3 (300 ml/min) Ar (200 ml/min)	1150 °C, reaction time of 30 min.	Horizontal resistance furnace	Liu et al. [55]
Ga_2O_3 + graphite powder (1:1) using Si(100) wafer pre-coated with 6 mn Au film	Nanowires	NH_3 (100 sccm)	900 °C, reaction time of 1.5 h	CVD	Liu et al. [56]

HCl + GaCl →GaCl GaCl + NH_3 → GaN Grown on Si (111) substrate with AlN buffer layer.	Nanochestnuts	NH_3 (725 sccm) HCl (29 sccm) N_2 (1140 sccm) carrier gas.	600 -1050 °C reaction time of 2 h.	HVPE	Shin et al. [57]
HCl + GaCl →GaCl 20 sccm of HCl was diluted in 83 sccm of N_2 on the liquid gallium source. Si (111) and c-plane sapphire substrate were used.	Individual, Tripod, bunched and hyper- bunched.	NH_3 (25 – 600 sccm) N_2 (1460 sccm) H_2 (500 sccm)	625- 800°C reaction time of 30 min.	HVPE	Lekhal et al. [58]

In + Ga (1:4) were placed on Mo boat and Si (111) wafer covered with a 3C- SiC epilayer were placed on the other boat to serve as substrate.	Nanotip triangle pyramids.	NH_3 (50-100 sccm)	850-900°C 900-950°C reaction time of 15 min.	CVD	Dai et al. [59]
Ga_2O_3/BN film was ammoniated and was deposited on Si (111) substrate by RF magnetron sputtering system.	nanowires	NH_3 (800 ml/min.)	1100°C reaction time of 15 min.	CVD	C. Xue et al. [60]
Gallium imide.	nanopowder (smallest crystallites)	NH_3	350,450,600,700 °C for 4h and 800 °C for 16 h	Pyrolysis	M. Drygas et al. [61]
Solution of gallium nitrate in various solvent (DMF+ MeOH,	Intermediate to large crystallites.		950°C for 12 h and 975 °C for 6h		

DMF, MeOH and H_2O).					
Gallium oxide.	Largest crystallites.	NH_3	950 °C for 12 h		
$Ga/NaN_3/Li_3N$ NaN_3 and Li_3N were used as nitrogen source to react with Ga.	Nanospindle	N_2	400 °C for reaction time of 40 h	Stainless steel autoclave	X. Hao et al. [62]
Au catalyst was thermally evaporated onto γ-$LiAlO_2$ (100) substrate. Metallic Ga was used as a precursor.	Nanowires	NH_3 (25-28 sccm)	1000 °C for the reaction time of 15 min.	CVD	X. He et al. [63]

Ga_2O_3 was dissolved in HNO_3 and the pH was adjusted by adding NH_4OH. Citrate was added into the solution. The solution was dried and form multilayer sheet-like. The sheet-like was crushed and used as a Ga source.	Leaf –like crystals	NH_3 (75-100 ml/min)	1080 °C for reaction time of 1h	CVD	H. Qiu et al. [64]
Ga metal and Au coated Si substrate.	Nanotubes	NH_3 (10 sccm)	900 °C for reaction time of 2 h	CVD	P. Sahoo et al. [65]
Ga nodules were initially annealed at 500°C for 10 min.	Nanotips	NH_3 (10 sccm)	900 °C for reaction time of 2 h	CVD	P. Sahoo et al. [66]
Ga nodules were initially annealed	Nanoparticles				

at 300 °C for 10 min.					
GaOOH powder was initially prepared by adding NH_4OH into $Ga(NO_3).xH_2O$	Fine particles	NH_3 (500 sccm)	500 -1000 °C for reaction time of 4 h	CVD	S. Cho et al. [67]

2.4 GaN nanostructure morphologies and the growth processes

GaN can be grown to give different structures (rods, wires, tubes etc) and the data generated on their synthesis and growth processes are described below (see also Table 2.3).

2.4.1 GaN nanorods

Different methods have been reported for the synthesis of GaN nanorods (GaN NRs). The pyrolysis approach is one of the methods that have been reported using a two-stage furnace system involving the pyrolysis of gallium dimethylamide and ferrocene under an ammonia atmosphere [38]. Fig. 2.2 shows the TEM images of GaN nanorods including a tip (low and high magnification). The growth process of the GaN nanorods is suggested to occur via a vapor–liquid-solid (VLS) mechanism (Fig. 2.3). Firstly, the separation of iron leads to an increase in the size of iron clusters on the surface of the quartz tube. Then Ga and N were introduced in the vapour phase; the Ga and N dissolved into the iron oxide clusters to form liquid catalyst centers. Continuous dissolution of Ga and N leads to a supersaturated solution. GaN nanorod growth takes place by the precipitation from the supersaturated liquid catalyst centers [39].

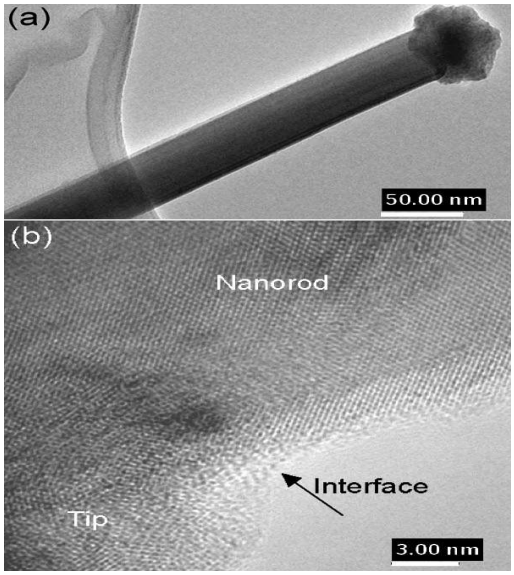


Fig. 2.2: (a) Low-magnification image of a GaN nanorod including its tip, (b) a high-magnification image of the interface of the tip and the nanorod [38].

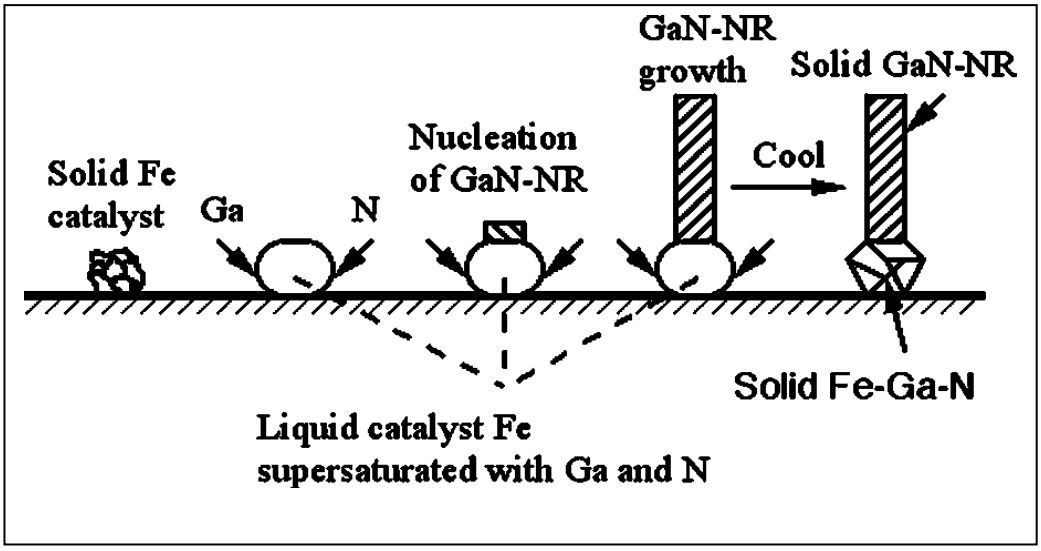


Fig. 2.3: Schematic illustration of VLS process for GaN nanorod (GaN-NR) growth by a pyrolysis route [38].

Lekhal et al. studied the synthesis of bunched structures of nanorods. These nanorods were synthesized on a c-plane sapphire and a silicon (111) substrate by catalyst free HVPE at 740 °C with a NH_3 flow rate of 100 sccm. These nanostructures were formed through the following process. Gaseous HCl was reacted with liquid gallium at 800 °C to form GaCl vapor species. Ammonia (NH_3) gas was used and the species were directly introduced into the central zone of the furnace. The central zone of the furnace was heated at high temperature in order to mix the gas species and reduce parasitical nucleation. A mixture of N_2 and H_2 was used as a carrier gas and HCl was diluted in N_2 on the liquid gallium source. The flow rate for NH_3 was varied between 25 and 600 sccm and the growth temperature was between 625, 670, 740 and 785 °C for a 30 min reaction time. Fig. 2.4 shows single NRs, bunched NRs and hyperbunched NRs formed on silicon and c-plane sapphire substrates.

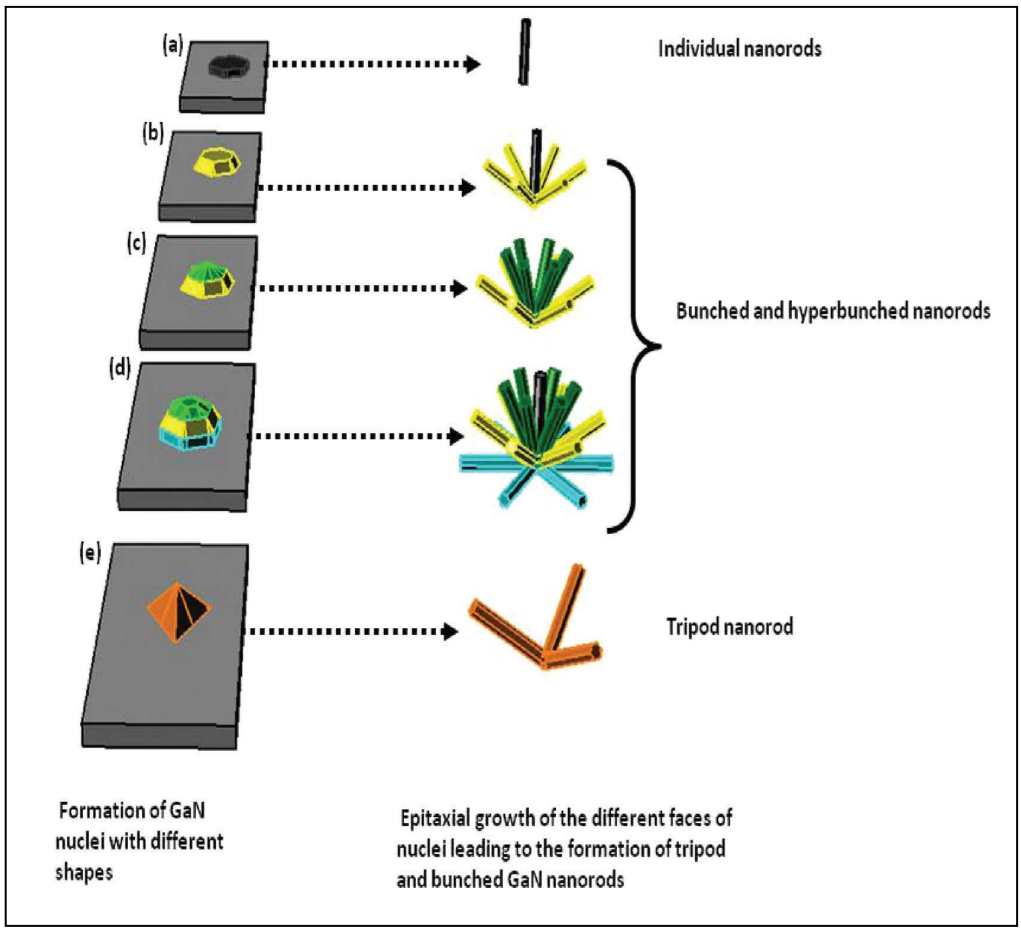


Fig. 2.4: Schematic illustration of the condensation growth mechanism for GaN nanorods. (Left) GaN nuclei responsible for the tripod, bunched and hyperbunched growth. (Right) Final GaN NR morphologies depending on the crystal symmetry of the nuclei [58].

2.4.2 GaN nanowires

The term 'nanowire' is generally used to describe a large aspect ratio rod, 1-100 nm in diameter [68]. Synthesis of GaN nanowires have been studied by a number of research groups. Cai et al studied the CVD growth of GaN nanowires by the reaction of metallic Ga on a Si substrate with NH_3 in the presence of a metal catalyst. They found that the use of metallic catalysts, such as Ni and Au, resulted

in better purity of the obtained materials. Increasing the quantity of Ga and/or the use of a $Ni(NO_3)_2$ catalyst resulted in formation of a mixture of GaN nanowires and SiOx nanowire bundles. Fig. 2.5 shows the growth of GaN nanowires on different substrates Si(100) and (111) [40].

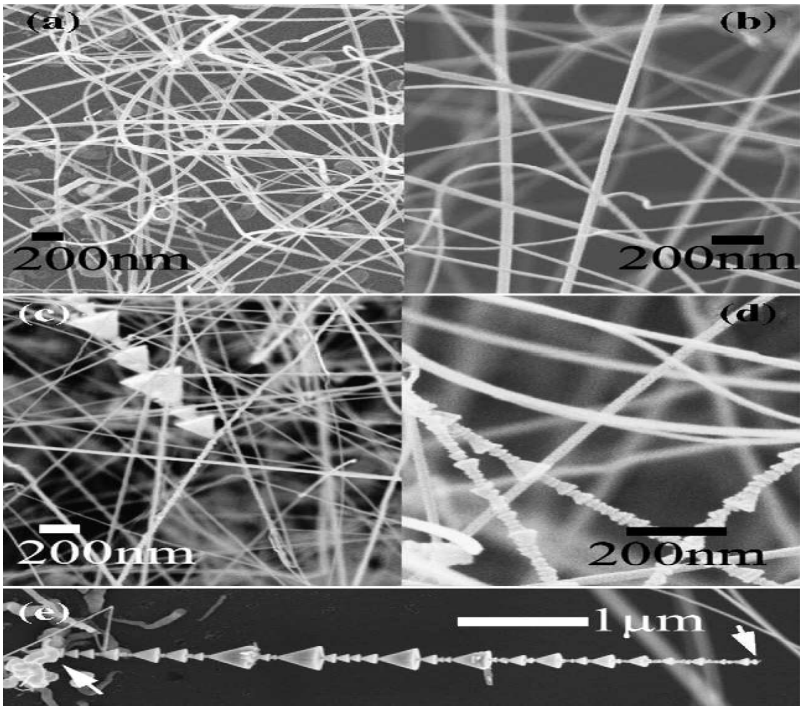


Fig. 2.5: GaN nanowire growth on different substrates. (a, c) Si(100), (b, d) Si(111). In the case of (a) and (b), the flow rates were 50 sccm for NH_3 and 100 for Ar, and in the case of (c) and (d), the flow rates are 125 sccm for NH_3 and 25 sccm for Ar; (e) higher magnification image of the cones [40].

Koester et al studied a non-catalytic MOVPE approach to give self-assembled GaN single-crystal wires on c-plane sapphire substrates, which do not require *ex-situ* surface preparation before growth. The method is based on three main steps: (i) the initial substrate treatment including in-situ deposition of a thin SiN*x* layer, (ii) the GaN seed nucleation, and (iii) the vertical growth. The spontaneous self-organization of the wire seeds was performed on a thin SiN*x* layer (~2 nm) deposited in situ on a *c*-plane sapphire using silane and ammonia. Typical wires

grown with this method are shown in Fig. 2.6 [41]. The MOVPE process has been usually used for epitaxial film growth. The process involves a delivery of reactants in the form of metal-organic precursors onto the heated substrate using a carrier gas, followed by thermal decomposition of the precursors and surface migration of the resulting constituents. A surface chemical reaction takes place between the migrating reactants, resulting in nucleation and subsequent crystal growth [26]. The growth process of GaN nanowires by a MOVPE mechanism is shown in Fig. 2.7.

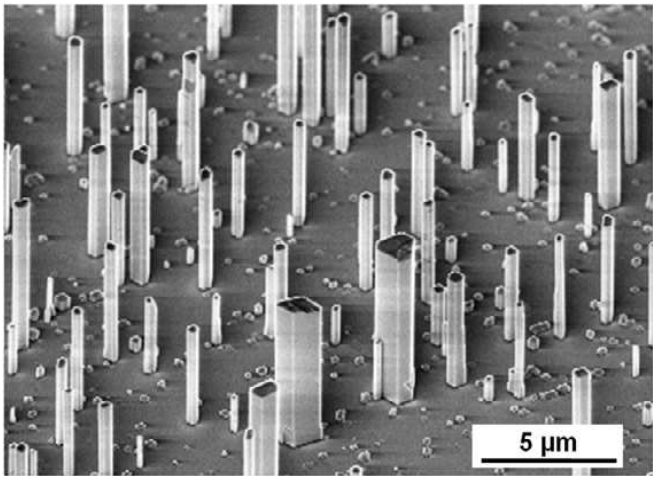


Fig. 2.6: 45°-Tilted scanning electron microscopy (SEM) view of a typical non-catalytic MOVPE growth of self-assembled GaN single-crystal wires on a c-plane sapphire substrate. The growth is homogeneous on the whole 2 inch wafer surface [41].

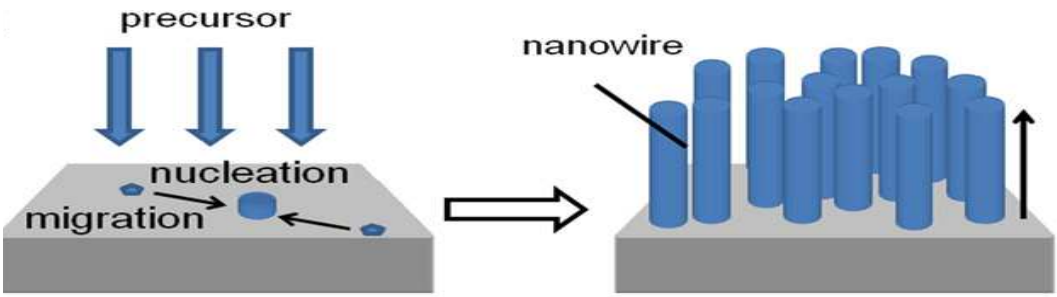


Fig. 2.7: Growth mechanism of GaN nanowires by catalyst free MOVPE [26].

2.4.3 GaN nanotubes

Single-crystal wurtzite GaN nanotubes have been synthesized by the Au-catalyzed MOCVD process [42]. GaN nanotubes with or without Ga-filled cores were observed. Fig. 2.8 (a) shows the TEM images of dispersed tubes with hollow cores; dark clusters of Au were found inside some tubes. Fig. 2.8 (c) shows an FESEM image of one dimensional tubular nanostructure; some of the tubes show open ends.

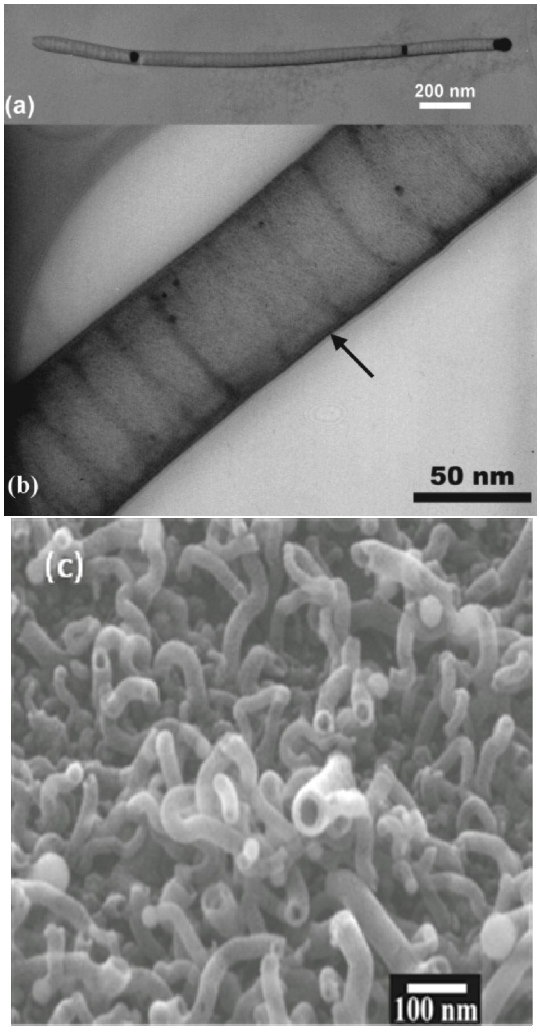


Fig. 2.8: (a) TEM image of a GaN nanotube and (b) magnified view of (a) and (c) scanning electron micrograph of GaN nanotubes [42].

Hemmingsson et al. investigated the low temperature growth of GaN nanostructures using the HVPE process on c-oriented Al_2O_3 and Au coated Al_2O_3 substrates. When the GaCl partial pressure increased, the structure changed from dot-like structures to nanotubes and when the growth temperature was changed, the radius of the inner diameter could be controlled. Fig. 2.9 shows the HVPE mechanism proposed for the growth process of the GaN nanotubes.

When 5nm thick Au film on a substrate was used (Fig. 2.9(a)) nanodroplets of Au were formed during heating to the growth temperature (Fig. 2.9(b)). When GaCl was introduced (Fig. 2.9(c)), Au droplets were converted to an alloy of Au and Ga and nanotubes were grown assisted by the droplets which were acting as catalysts. As the growth continued, the Au in the droplet was used up, and only Ga was left (Fig. 2.9(d)). Ga droplets were formed spontaneously on the substrate. The tube-like shape was formed (Fig. 2.9(e)). The growth of the nanotube is determined by supersaturation within the droplet, which is established by catalytic absorption of the gaseous reactants from the surroundings [42].

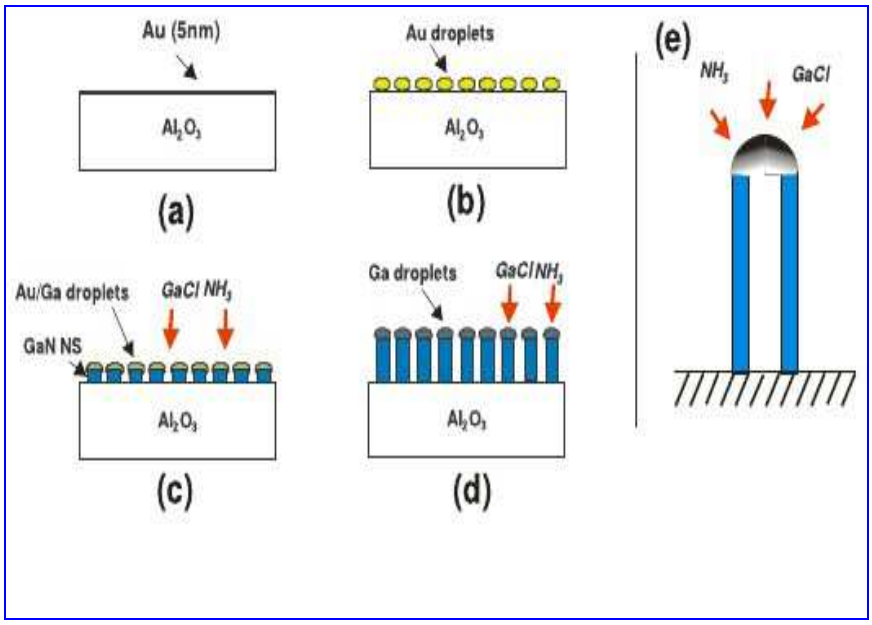


Fig. 2.9: A schematic illustration of the formation process of GaN nanotubes: (a) substrate before growth; (b) formation of Au droplets upon heating to growth temperature; (c) initial growth of GaN nanotubes using an Au/Ga alloy as catalyst; (d) continuous growth of nanotubes using Ga droplets as catalyst; (e) cross-sectional image of a nanotube illustrating the diffusion-limited growth process. The N concentration in the Ga droplet is schematically depicted by the gray scale (darker indicates higher N concentration) [42].

2.5 Other Structures

2.5.1 GaN nanobelts

Bae et al. investigated the growth of GaN nanobelts grown on a Ni-deposited silicon substrate by a catalyst assisted CVD reaction of a Ga, Ga_2O_3, and B_2O_3 mixture with NH_3. The use of Ni nanoparticles and B_2O_3 as catalysts yields the formation of high density single-crystalline wurtzite structured GaN nanobelts [43]. Fig. 2.10 shows the SEM images of GaN nanobelts grown on a silicon substrate.

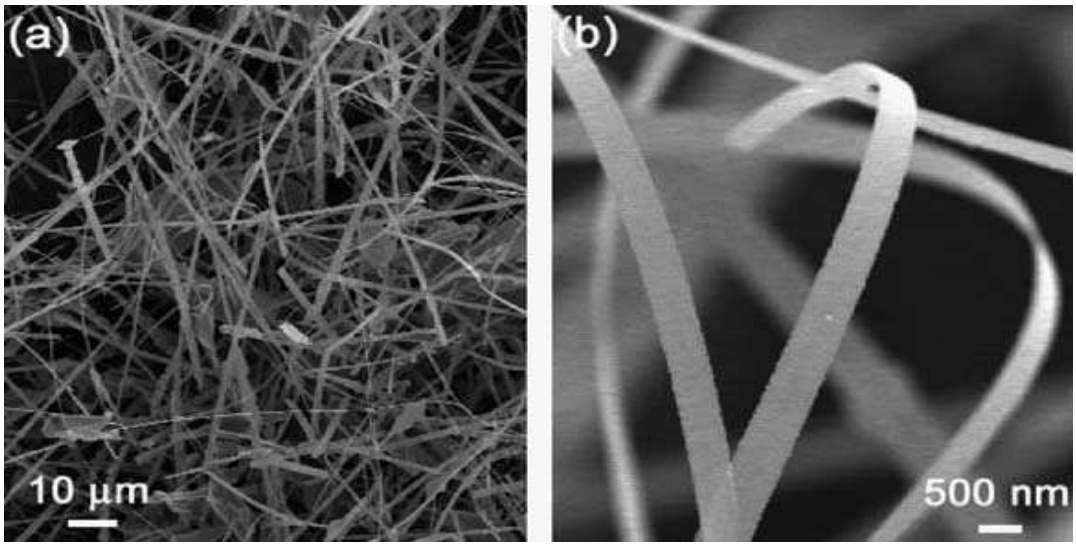


Fig. 2.10: (a) A SEM micrograph showing high-density GaN nanobelts grown on a large area of the silicon substrate. (b) A magnified view revealing the belt-like structure [43].

2.5.2 GaN nanobelts with herringbone morphology

Gallium nitride (GaN) nanobelts with herringbone morphology were successfully synthesized on Si (111) substrates by ammoniating Ga_2O_3 thin films deposited by radiofrequency magnetron sputtering (Fig. 2.11) [50].

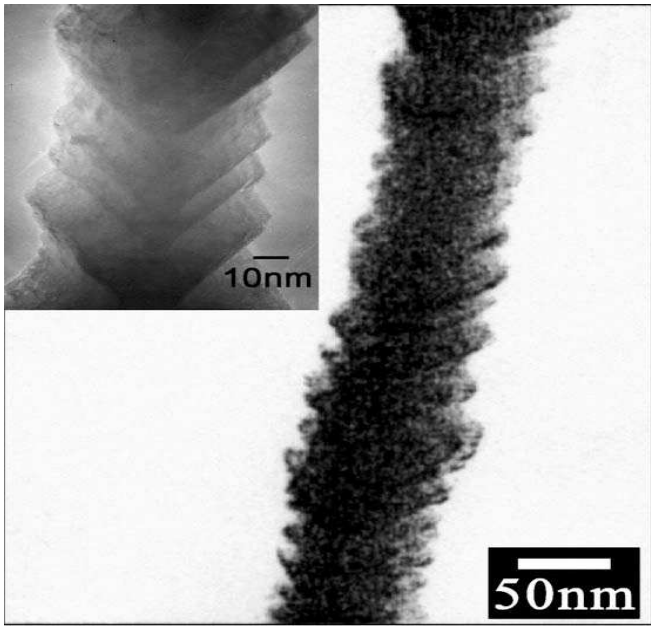


Fig. 2.11: Low-magnification TEM image of an individual GaN nanobelt and the inset shows corresponding high-magnification TEM image [50].

2.5.3 GaN nano-flowers

Dhamodaran et al. studied the growth of GaN nano-flowers using a simple CVD reactor without any catalyst using an NH_3 atmosphere. The nanostructures grown on three different substrates had similar shapes with slight variation in size [44]. Fig. 2.12 shows SEM images of GaN nanoflowers grown on (a) silicon substrate (b) at different flow rates and grown on (a) GaN and (b) AlN substrate respectively.

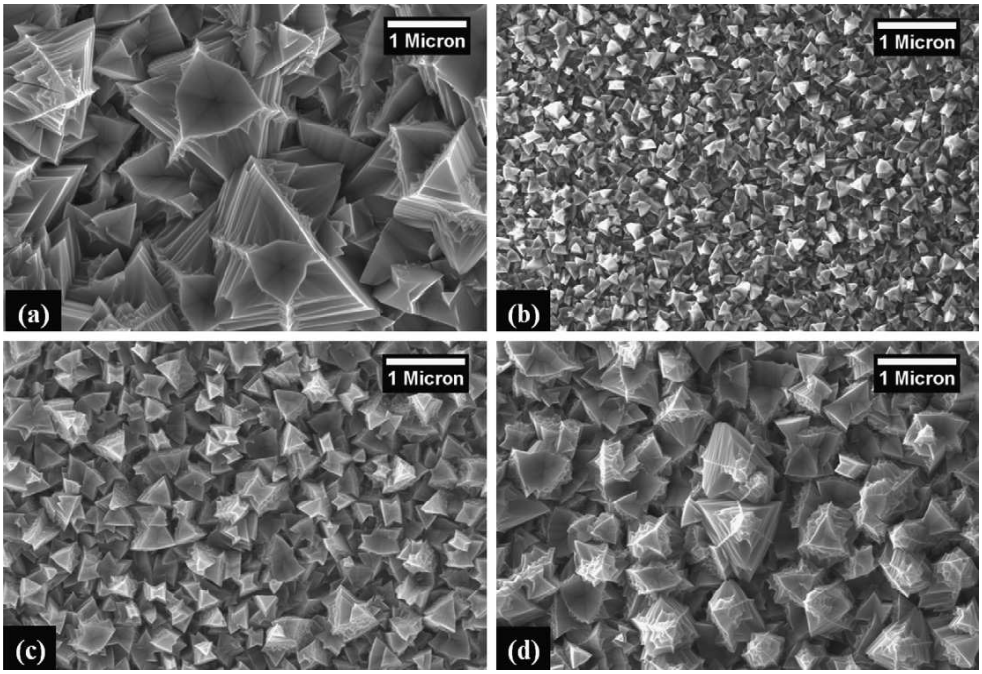


Fig. 2.12: SEM images of GaN nanostructures (a) and (b) grown on a silicon substrate at 1323 K/25 SCCM and 1323 K/50 SCCM (c) and (d) on GaN and AlN substrates respectively grown with 1323 K/25 SCCM [44].

2.5.4 Durian-like GaN

Nabi et al. have obtained a novel durian-like morphology of GaN microstructures by pre-treating Ga metal with aqueous NH_3 via a catalyst assisted chemical vapor deposition (CVD) method at 1200 °C. Durian-like microstructures have a high density of scales with very sharp tips. Fig. 2.13 shows the SEM images of durian-like GaN [51].

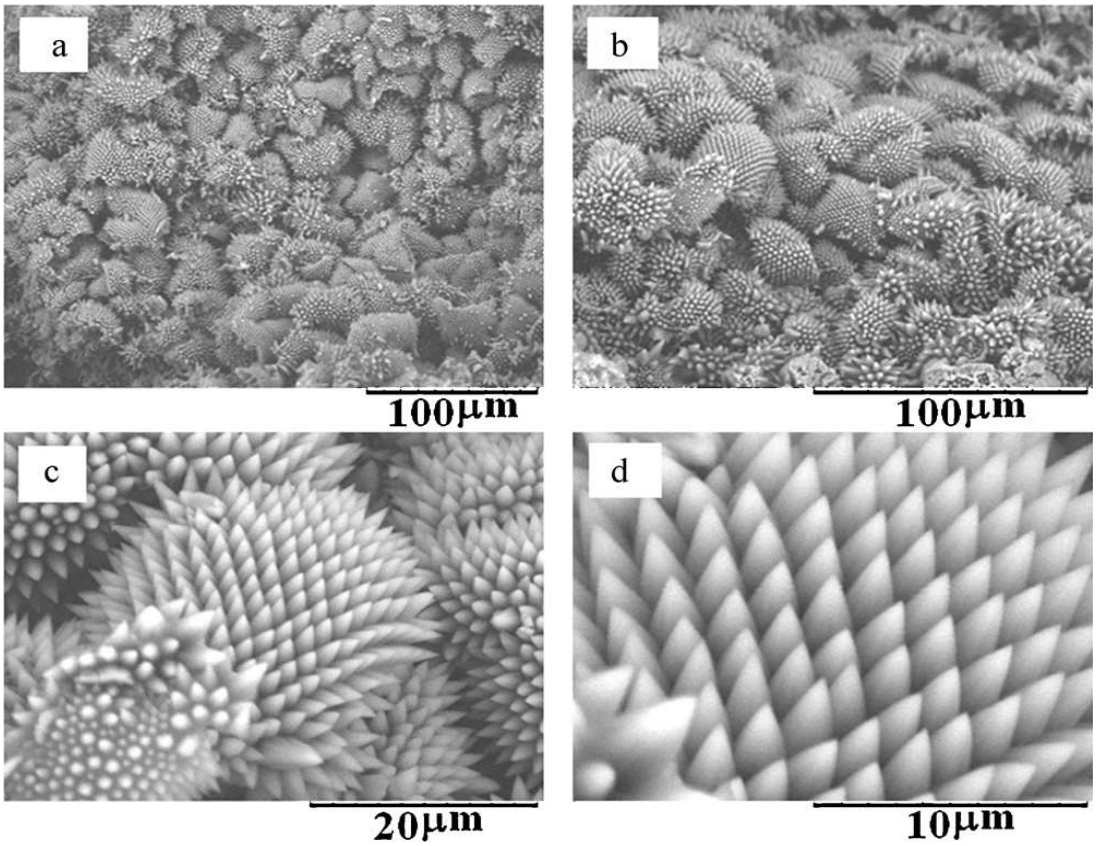


Fig. 2.13: (a and b) Low magnification SEM images of durian-like GaN. (c) Medium magnification of durian-like GaN. (d) High magnification images of durian-like GaN having sharp tips [51].

2.5.5 Dandelion-like GaN

Nabi et al. have synthesized a unique morphology of high quality dandelion-like GaN on nickel coated Si (100) substrates, using an ammonia atmosphere at 1200 °C. A CVD method was used and the precursors were pre-treated with aqueous ammonia at 120 °C. Fig. 2.14 shows the SEM images of dandelion-like GaN [52]. The VLS mechanism for the growth of dandelion–like GaN was proposed. This was achieved by heating the source material; gallium droplets were formed since gallium has a lower melting temperature than silicon. The Ga droplets that evaporated were collected on a silicon substrate on energy favorable sites as shown in Fig. 2.15 (b and c). These droplets reacted slowly with nitrogen as the temperature of the furnace and the reaction time increased. These droplets were

consumed and converted into nanowires as shown in Fig. 2.15 (d). Finally they were converted into a dandelion-like structure (Fig. 2.15 (e)).

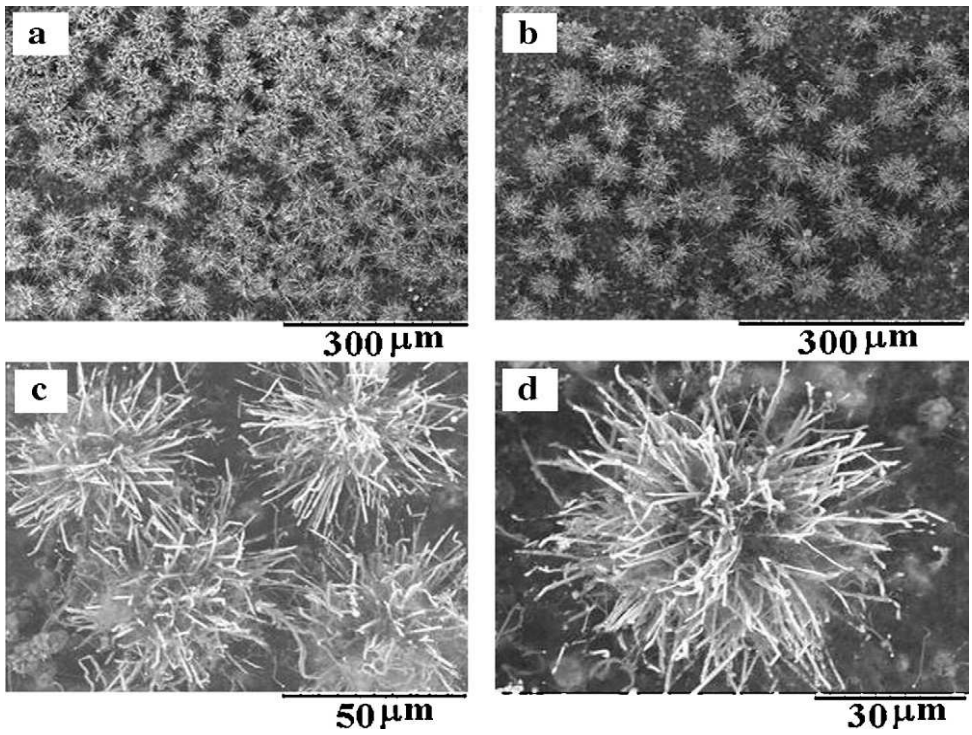


Fig. 2.14: (a and b) shows the low magnification images and (c and d) shows high magnification of SEM images of dandelion-like GaN microstructures [52].

The mechanism for the generation of the dandelion is shown in Fig. 2.15 [52].

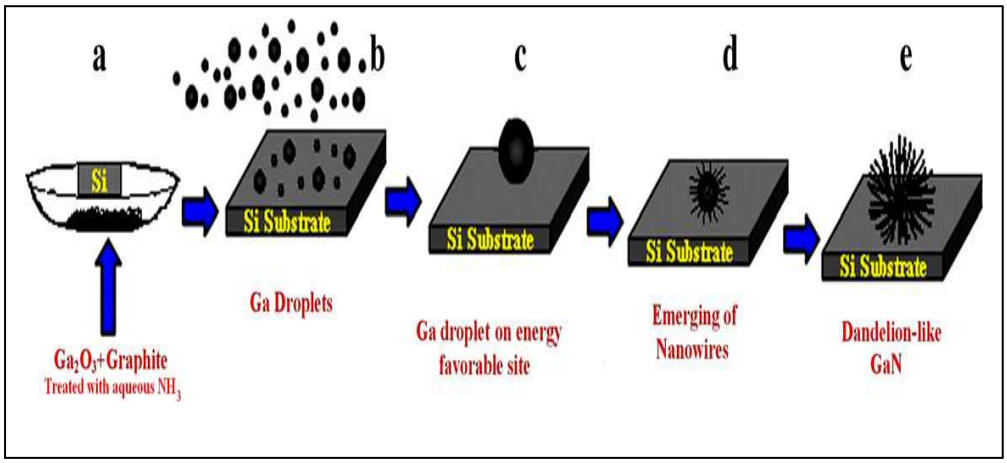


Fig. 2.15: The growth mechanism for the formation of dandelion-like GaN microstructures [52].

2.5.6 Triangular nanowires

Dinh et al. have also synthesized GaN unique nanowires, grown on gold-coated n-type Si (100) substrates, using the vapor-phase epitaxy method. The grown GaN nanowires, with diameters in the range 20 – 60 nm and lengths of several micrometers, were uniformly distributed on Si substrates (Fig. 2.16) [53].

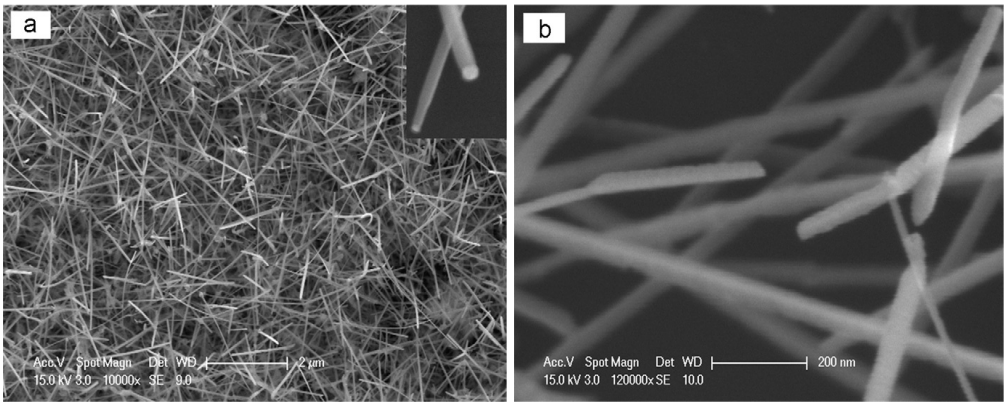


Fig. 2.16: FESEM images of GaN nanowires grown on Si (100) at (a) low magnification and (b) high magnification. The inset shows the existence of the Au catalysts at the end of the nanowires [53].

2.5.7 Conical shape nanorods

Nabi et al. have prepared vertically well aligned, well patterned and high density conical shaped GaN nanorods (Fig. 2.17) on a Si substrate by pre-treating GaN powder with aqueous NH_3 via a facile CVD method without any catalyst. It was observed that the angle of the sharp tip of the tilted GaN at high magnification is approximately 55 °C and these nanorods tips have good field emission properties [54].

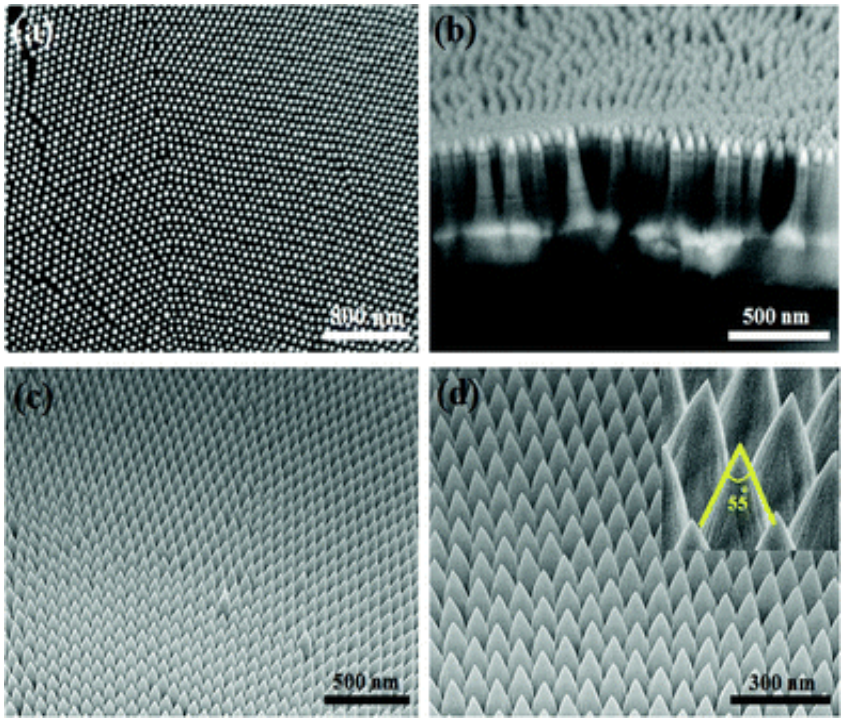


Fig. 2.17: FESEM images of GaN nanorods prepared at 1100 °C (a) top view, (b) side view, (c) low magnification tilted view and (d) high magnification tilted view (inset is the tip angle) [54].

2.5.8 Needle- like nanowire array

Liu et al. have synthesized crystalline GaN nanowires on a substrate; a piece of a Si wafer coated with an Au film (~ 20 nm) via a simple thermal evaporation process. The majority of the GaN nanowires have bicrystalline structures with a needle like shape, triangular prism morphology, and a uniform diameter of ~100 nm (Fig. 2.18) [55].

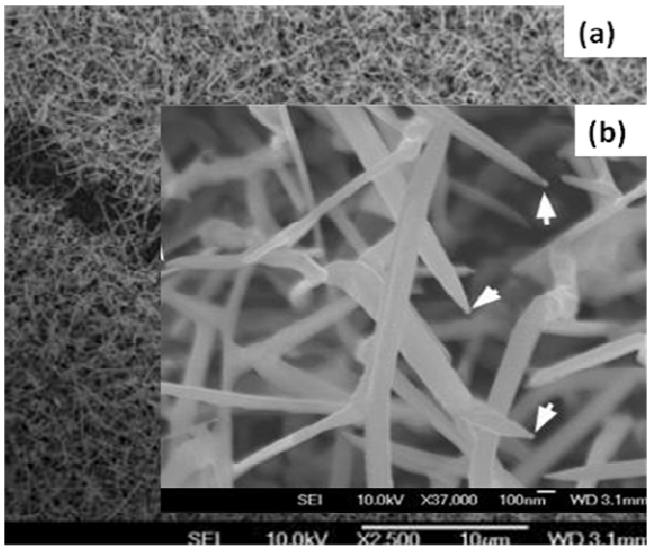


Fig. 2.18: (a) Low magnification and (b) high magnification SEM images for the needle-like GaN nanowires [55].

2.5.9 GaN hollow spheres

Li et al. reported the synthesis of monodispersed GaN hollow spheres using surface layer absorption (SLA) templating technique. Carbon spheres were used as templates for the formation of GaN hollow spheres. The formation of GaN hollow spheres involves three steps: (1) gallium ion absorption from the solution into a surface layer; (2) removal of the carbon core by calcination of the composite spheres in air which resulted to the formation of oxide hollow spheres; (3) oxide spheres were converted into nitride using an in-situ method in the

presence of ammonia at 700 – 900 ºC. Fig. 2.19 shows the TEM images of GaN hollow spheres obtained by ammoniating Ga_2O_3 hollow spheres at 700 °C and 900 °C respectively. Fig. 2.20 shows a schematic mechanism for the formation of GaN hollow spheres [69]. Yin et al. also reported the growth of GaN hollow spheres and nanotubes. The GaN structures were synthesised by use of liquid droplets of $GaCl_3$ as a precursor deposited on a sapphire substrate and grown by an in-situ chemical reaction. The NH_3 was introduced and reacted with liquid Ga. The gallium droplet acted as a reactant and a template for the formation of hollow GaN structures. Fig. 2.21 shows the schematic illustration of the formation process of hollow GaN spheres and hollow nanotubes [70].

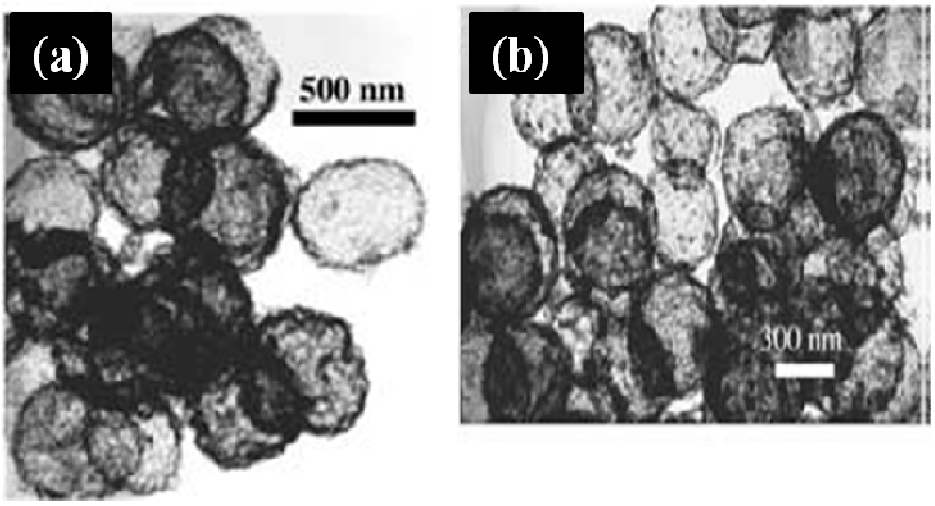


Fig. 2.19: TEM images of GaN hollow spheres synthesized at (a) 700 °C and (b) 900 °C [69].

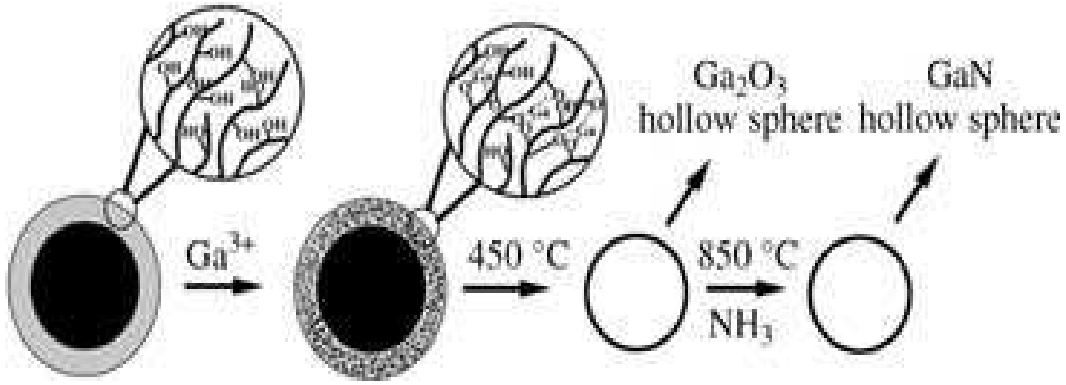


Fig. 2.20: Schematic mechanism for the formation of GaN hollow spheres using carbon spheres as templates [69].

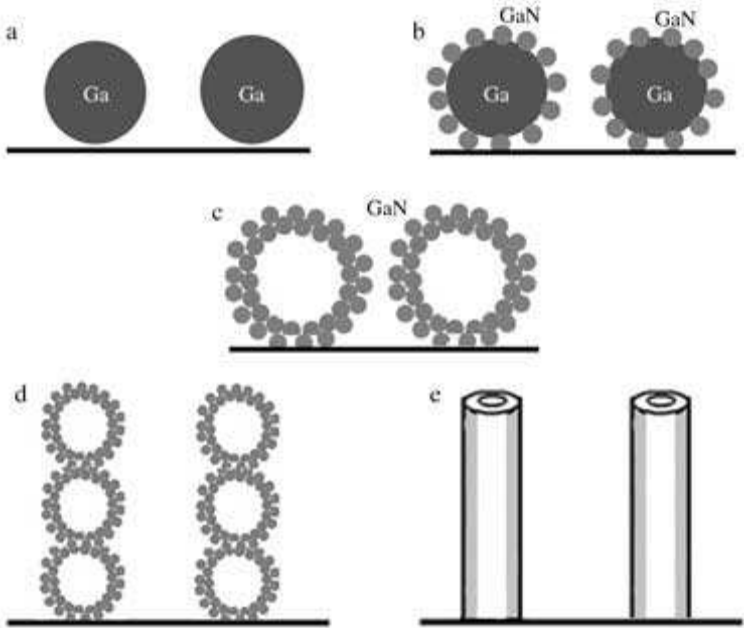


Fig. 2.21: A schematic illustration of the formation process of hollow GaN spheres and hollow nanotubes: a) Generation of nanosized liquid Ga droplets; b) GaN nanocrystal nucleation and growth on the surface of Ga liquid droplets; c) the hollow GaN sphere is formed with small shell size; d, e) at high temperatures

they formed hollow GaN spheres aggregate and hollow GaN nanotubes are formed by the coalescence of the nanosized hollow GaN spheres [70].

2.5.10 GaN nanochestnuts

Shin et al. have reported the synthesis of GaN nanochestnuts. The nanochestnuts structures were grown through the following process. Liquid Ga was reacted with HCl at 850°C to form GaCl vapour. The NH_3 and N_2 gases were used as nitrogen source and carrier gas respectively. When the temperature increased to 1050°C in the reaction zone the NH_3 precursor decomposed to form nitrides and hydrides leading to nucleation of GaN. Most GaN nuclei produce GaN droplets on the substrate in the growth zone, at 600 or 650 °C, and they mingled to form GaN nanostructures. However, some GaN nuclei floated in the N_2 carrier gas and act as colloidal particles. These colloidal particles formed chestnut-like structures which gradually grew in size while the nanostructures grew vertically on the substrate. The individual nanostructure chestnut fell and grew larger together with the nanoneedle structures under them [57]. Fig. 2.22 (a) and (c) shows the FE-SEM images of a GaN nanorod chestnut grown at 650 °C and a nanoneedle chestnut grown at 600 °C, respectively. Fig. 2.22 (b) and (d) shows cross-sectional images of nanorod and nanoneedle chestnuts respectively, and revealed that the spheres are surrounded by burs of nanorods and nanoneedles. Fig. 2.23 shows a schematic diagram of one possible growth mechanism of GaN chestnut-like nanostructures in a thermodynamic process and the morphologies are shown in the inset.

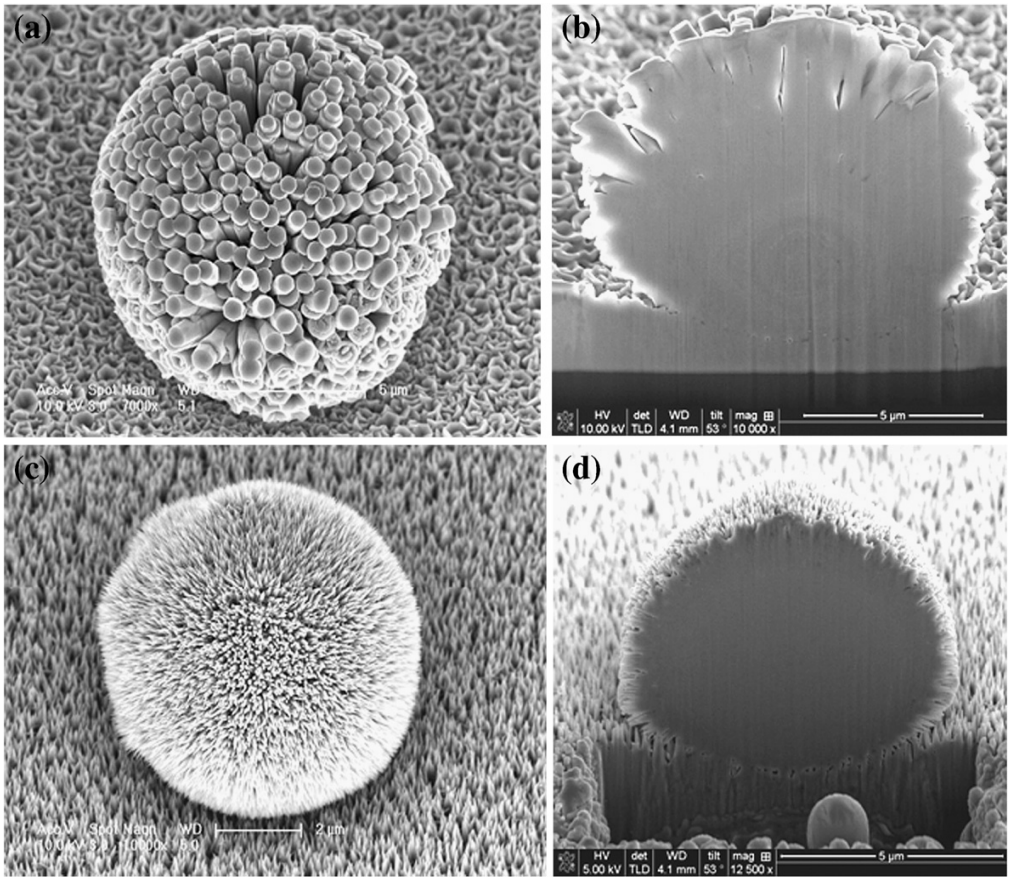


Fig. 2.22: FE-SEM images of (a) a GaN nanorod chestnut, (b) a cross-sectional image of a nanorod chestnut, (c) a nanoneedle chestnut, and (d) a cross-sectional image of a nanoneedle chestnut [57].

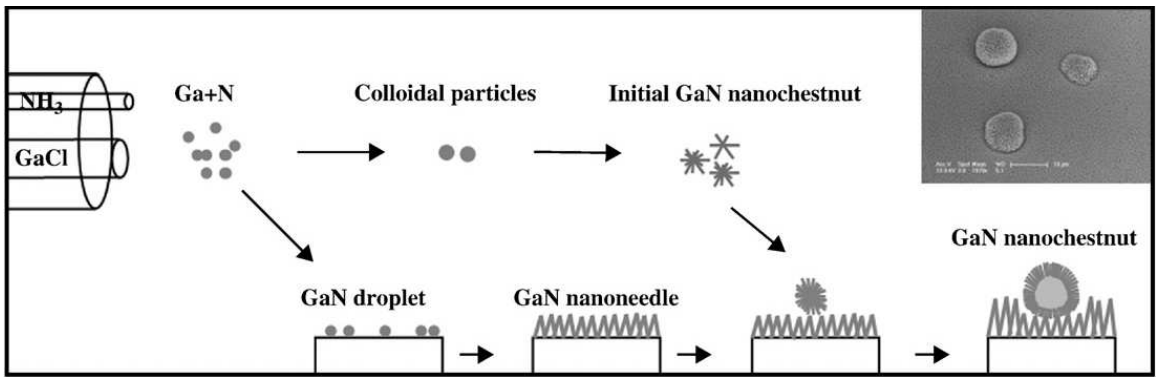


Fig. 2.23: Schematic diagram of a possible growth mechanism of GaN chestnut-like nanostructures [57].

In summary the type of substrate and Ga source used to grow GaN NSs can affect the morphology of the material, e.g.:

- Au and Ni supported on Si (111) and Si (100) substrates catalyzed the formation of nanowires and stacked cone nanowires respectively using Ga metal as a precursor.
- Au supported on Si (100) and Al_2O_3 (0001) substrates catalyzed the formation of nanotubes using $GaMe_3$ and GaCl as a precursor.
- Ga metal deposited on Si (001) and AlN substrate formed GaN nanoflowers.
- Ga metal deposited on a c-plane sapphire substrate together with a Ni catalyst formed nanowires.
- Ga_2O_3 deposited on a Si (001) substrate coated with $NiCl_2$ formed grass-like nanostructures.
- Ga_2O_3 thin film deposited on Si (111) substrate formed nanobelts with herringbone.
- An Au thin film deposited on a Si (100) substrate formed triangular shaped nanowires in the presence of GaN powder and molten Ga (1:1).
- Needle-like nanowires formed on Si wafer coated with Au film using Ga_2O_3 as a precursor.
- Nanochestnuts were formed from GaCl deposited on Si (111) substrate with AlN buffer layer.
- Au supported on a γ-$LiAlO_2$ (100) substrate catalysed formation of nanowires using metal Ga as a precursor.

Transition metals such as Fe, Ni, Co and their oxides were discovered to be efficient catalysts for the precipitation of GaN materials from a molten catalyst droplet supersaturated with metal vapor [18]. Au was found to be a better choice of catalyst for synthesizing GaN NSs due to its high defect formation energy (~4 eV) in GaN as compared to low defect formation energy for Ni substitution (1.2 eV). Therefore less diffusion of Au atoms into the lattice of GaN can be expected [71]. Fe and Ni have been commonly used as catalysts mostly in the VLS growth of GaN

NWs because Ga and N are soluble in the liquid metals. However the disadvantage of using Fe and Ni catalysts is contamination in the GaN NWs resulting in unwanted variations in their electronic properties [71]. Catalyst metals based on Au, Ni, Pd or various metal alloys were preferably used to produce GaN NWs because they provide high growth rates. GaN NWs grown on a Ni catalyst were reported as a VLS or VSS phase. However, the nature of the catalyst droplets remain unclear and the GaN NW nucleation process is complex [72].The Au catalyst product purity is expected to be better though it has poor solubility for N as compared to other transition metals like Fe and Ni [18].

In most cases NH_3 has been used as a N source to make GaN NSs. There is an exceptional case where Li_3N was also used as N source in a stainless steel autoclave to form nanospindles [62].

There are a few studies in which a double stage furnace CVD synthesis method [38, 45, 73] had been used rather than single stage furnace to make GaN NSs. In most cases horizontal furnaces have been used but there are few studies have described the use of vertical reactors. Kim et al. used a vertical CVD reactor to make GaN nanowires using Ga over Ni catalysts supported on Si substrate [74] and Hemmingson et al. used a vertical HVPE reactor to make GaN nanotubes from GaCl supported on Au coated Al_2O_3 (0001) substrate [42].

This led to the aim of this work where we have exploited the synthesis of GaN NSs at lower temperature by using a double stage horizontal furnace to preheat NH_3 at high temperature and grow GaN NSs at low temperatures using Ga_2O_3 as a precursor. GaN NSs were also made using a single stage horizontal furnace; Ga_2O_3, NH_3 and activated carbon were used as Ga, N sources and reducing agent respectively.

2.6 Properties and Applications of GaN nanostructures

Properties of GaN-based materials and related semiconductors are very attractive for high temperature applications, as well as for optoelectronic and electronic devices. The quality of GaN materials has improved gradually over the past few

years and this has opened up new opportunities for GaN related devices [75]. GaN has a high melting point (2500 ºC), high thermal conductivity (2.1 W/cm.K), and a large bulk modulus (210 GPa) [76]. These properties of GaN materials are related to strong ionic and covalent bonding between Ga and N [77]. Spontaneous and piezoelectric polarizations are one of the important properties of wurtzite GaN. A surface charge can be induced and this can create a large internal electric field in a GaN film. This electric field can strongly affect the electrical and optical properties of GaN based devices [78 - 79].

The wide direct band gap of GaN and its good thermal conductivity also contribute to its application in high temperature and high power electronics where devices based on Si or GaAs are not applicable [19]. GaN nanostructures have also been used in research fields and in commercial applications because of their important properties [75]. GaN nanostructured materials can be used for short-wavelength light-emitting diodes (LEDs), laser diodes and optical detectors as well as for high-temperature, high-power and high-frequency electronic devices [80].

LEDs have the advantages of high efficiency, lower energy consumption and longer life time compared to conventional lights [19]. Other important applications of GaN-based LEDs, water purification systems and in medical devices [81].

2.6.1 GaN Alloy nanostructures

Ternary group III-nitride systems have been studied for their tunable emission properties (Fig. 2.24). For example, indium gallium nitride (InGaN) has been reported as the active layer for the most high-brightness LED devices. The bandgap of AlN can be reduced systematically by increasing Ga incorporation in the network [82]. GaN has the advantage compared to SiC in that it can readily grow heterostructures e.g. AlGaN/GaN. Heterostructures formed by radio-frequency plasma-assisted molecular beam epitaxy show a two dimensional

electron gas (2DEG) system that serves as the conductive channel at the AlGaN/GaN heterojunction [83]. The electron mobility of an AlGaN/GaN heterostructure was found to decrease with increasing Al content and thickness of the $Al_xGa_{1-x}N$ layer. Optical and electrical properties could be tuned in the ternary systems to make it attractive for use in optoelectronics [84]. These material properties show that GaN is a good candidate for next generation high-power/high-temperature microwave applications [81].

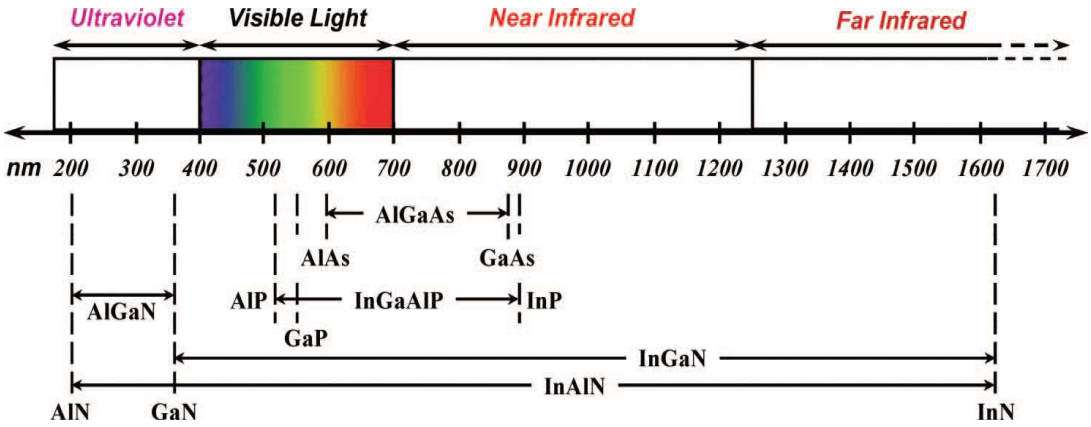


Fig. 2.24: Various ternary and quaternary materials used for LEDs with the wavelength ranges indicated [84].

2.7 Properties and Applications of GaN nanostructures in Sensors

GaN has been a candidate for high temperature gas sensing applications due to its wide band gap and chemical stability. This type of semiconductor can be used in harsh conditions e.g. considerable interest has been shown in developing hydrogen gas sensors that can operate in a harsh environment. A GaN gas sensor has a unique advantage; it can be integrated into GaN based optical devices or high power/temperature electronic devices on the same chip [85].

Schottky diode or field-effect transistor structures fabricated on GaN and SiC are sensitive to a number of gases, including hydrogen and hydrocarbons. Fig. 2.25 shows a schematic of a completed device, while Fig. 2.26 shows a scanning

electron micrograph diode or field-effect transistor structures fabricated on GaN and SiC [86-87]. There has been extensive development of SiC-based gas sensors [5, 88, 89], while the work on GaN is still at an early stage [90]. However, there has been much recent activity based on the relative advantages of GaN for sensing [90 - 94]. These advantages include the presence of the polarization-induced charge, the availability of a heterostructure and the fast rate of device technology development for GaN which borrows from the commercialized light-emitting diode and laser diode businesses [95].

The ability of this material to function at high temperature, high power and high flux/energy radiation conditions will allow a huge improvement in a wide variety of applications e.g. spacecraft, mining, nuclear power etc. and in applications in high temperature pressure sensing for coal and fossil energy applications [86]. GaN is a known material for H_2 gas sensing in part due to its sensitivity to surface charge and its wide temperature stability [96]. One-dimensional (1-D) nanomaterials (nanowires, nanotubes, nanorods, and nanobelts) show increasing potential as H_2 gas sensors due to their high surface to volume ratio [97–102]. Many groups have already reported the use of H_2 sensors based on carbon nanotubes (CNTs) [99], ZnO nanorods [103], and SnO_2 nanowires [100] with excellent response and recovery characteristics, although there are few studies on H_2 gas sensors based on GaN nanowires, which may offer excellent environmental stability [104].

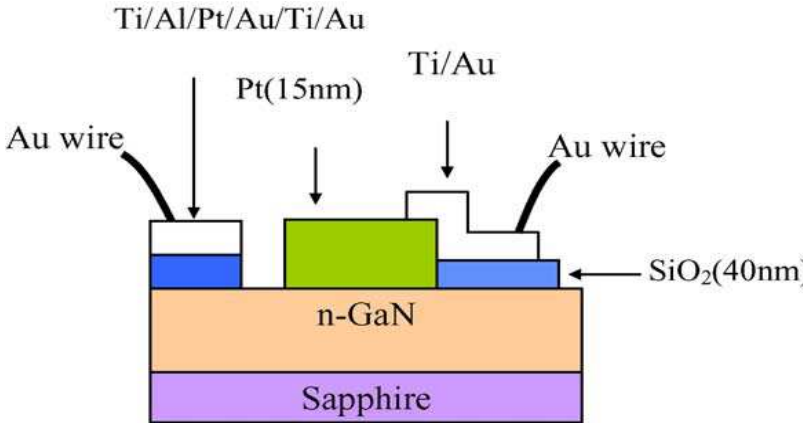


Fig. 2.25: Schematic of Pt/GaN Schottky diode for hydrogen gas sensing [86].

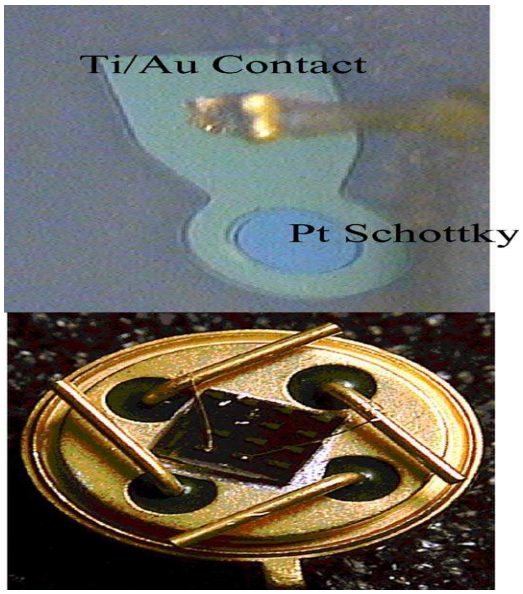


Fig. 2.26: SEM micrograph of completed device, showing bond wire attached (top) and photograph of device bonded into header [86].

2.8 Catalyst support

Catalyst supports that are typical used include Al_2O_3, TiO_2, SiO_2 and many carbons. The use of classical semiconductors such as GaN is rarely used as catalyst supports. In this study we have used this material for the first time as a support for palladium nanoparticles [105].

2.9 References

1. O. Ambacher, Appl. Phys. 31(1998) 2653.

2. S. M. Kang, T. I. Shin, Duc V. Dinh, J. H. Yang, S.-W. Kim, and D. H. Yoan, Microelectron. J. 40 (2009) 373.

3. J. Hu, Y. Bando, D. Golberg, and Q. Liu, Angew. Chem. Int. Ed. 42 (2003) 3493.

4. K. Adhikary and S. Chaudhuri, Trans. Ind. Ceram. Soc. 66 (1**)** (2007)1.

5. J. S. Wright, W. Lim , D.P. Nortton, S.J. Pearton, F. Ren, J. L. Johnson, A. Ural, Semicond. Sci. Technol. 25 (2010) 024002 (8pp).

6. G. Korotcekov, Chemical Sensors: Fundamentals of Sensing Materials, Vol. 2: Nanostructured Materials, © Momentum Press, LLC, 2010.

7. Z. Wu, M. G. Hahm, Y. J. J, L. Menon, J. Mater. Chem, 19 (2009) 437.

8. W. Han, S. Fan, Q. Li, and Y. Hu, Science. 277 (1997) 1287.

9. G. S. Cheng, L.D. Zhang, Y. Zhu, G.T. Fei, L. Li, C.M. Mo, and Y.Q. Mao, Appl. Phys. Lett. 75 (1999) 2455.

10. W. Han, P. Redlich, F. Ernst, and M. Ruhle, Appl. Phys. Lett. 76 (2000) 652.

11. X. Duan, and C.M. Lieber, J. Am. Chem. Soc. 122 (2000) 188.

12. W. Shi, Y. Zheng, N. Wang, C. Lee, and S. Lee, Adv. Mater. 13 (2001) 59.

13. X. Chen, J. Xu, R. M. Wang, and D. Yu, Adv. Mater. 15 (2003) 419.

14. R. Koester, J. S. Hwang, C. Durand, D. Lee, S. Dang and J. Eymery, Nanotechnol. 21 (2010) 5602.

15. X. M. Cai, A. B. Djurisic, and M. H. Xie, Thin Solid Films 515 (2006) 984.

16. D. S Chander, J. Ramkumar, and S. Dhamodaran, Physica E 43 (2011) 1683.

17. A. Hill, Growth, Characterization, and Thermodynamics of III-Nitride Semiconductors, PhD Thesis, 2011.

18. M. E. Levinshtein, S. L. Rumyantsev, M. S. Shur, Properties of Advanced Semiconductor Materials: GaN, AlN, InN, BN, and SiGe, John Wiley and Sons, New York, 2011.

18. P. K. Sahoo, Quasi One Dimensional GaN Nanostructures: Growth Kinetics, Physical Properties, and Applications, PhD Thesis, 2012.

19. H. Li, Novel processes for large area gallium nitride single crystal and nanowire growth, Phd Thesis, December 2005.

20. T. Kuykendall , P. J Pauzauskie, Y. Zhang , J. Goldberger , D. Sirbuly, J. Denlinger and P. Yang Nat. Mater. 3 (2004) 528.

21. Y. Huang, X. Duan, Y. Cui, and C. M. Lieber, Nano Lett. 2 (2002) 101

22. J. T. Hu, T.W. Odom, and C. M. Lieber, Acc. Chem. Res. 32 (1999) 435.

23. J. T. Hu, M. Ouyang, P. Yang, and C. M. Lieber, Nature 399 (1999) 48.

24. Y. Wu, and P. Yang, Chem. Mater. 12 (2000) 605.

25. Z. Zhong, F. Qian, D. Wang, and C. M. Lieber, Nano Lett. 3 (2003) 343.

26. M. S Kang, C. Lee, J. B Park, H. Yoo, and G. Yi, Nano Energy 1 (2012) 391.

27. H. M. Kim, D. S. Kim, D.Y. Kim, T.W. Kang, Y.H. Cho, and K. S. Chung, Appl. Phys. Lett. 81 (2002) 2193.

28. H. P. Maruska, and J. J. Tietjen, Appl. Phys. Lett. 15 (1969) 327.

29. H. M. Kim, T. W. Kang, and K. S. Chung, J. Ceram. Proc. Res. 5 (2004) 241.

30. H. M. Kim, Y. H. Cho, H. Lee, S. I. Kim, S. R. Ryu, D. Y. Kim, T. W. Kang, and K. S. Chung, Nano Lett.4 (2004) 1059.

31. Y. H. Kwon, K. H. Lee, S.Y. Ryu, T.W. Kang, C. H. You, and T. W. Kim, Appl. Surf. Sci. 254 (2008) 7014.

32. M. Yoshizawa, A. Kikuchi, M. Mori, N. Fujita, and K. Kishino, Jpn. J. Appl. Phys 36 (1997) L459.

33. M. A. S Garcia, E. Calleja, E. Monroy, F. J. Sanchez, F. Calle, E. Munoz , and R. Beresford, J. Cryst. Growth 183 (1998) 23.

34. E. Calleja, J.Risti´c, S. Fernandez-Garrido, L. Cerutti, M. A. Sanchez-Garca, J. Grandal, A. Trampert, U. Jahn, G. Sanchez, A. Griol, B. Sanchez, Phys. Status Solid b 244 (2007) 2816.

35. H. Sekiguchi, K. Kishino, and A. Kikuchi, Appl. Phys. Lett. 96 (2010) 231104.

36. M. Kesaria, S. Shetty, and S. M. Shivaprasad, J. Cryst. Growth 326 (2011) 191.

37. L. Geelhaar, C. Cheze, B. Jenichen, O. Brandt, C. Pfuller, S. Munch, R. Rothemund, S. Reitzenstein, A. Forchel, T. Kehagias, P. Komninou, G. P. Dimitrakopulos, T. Karakostas, L. Lari, P. R. Chalker, M. H. Gass, and H. Riechert, IEEE J. Sel. Top. Quant. Electr. 17 (2011) 878.

38. W. Han and A. Zettl, Appl. Phys. Lett, 80 (2002) 2.

39. X. M Cai, A. B Djurisic, and M. H Xie, Thin Solid Films 515 (2006) 984.

40. R. Koester, J. S Hwang, C. Durand, D. Le Si Dangand, and J. Eymery, Nanotechnol. 21 (2010) 015602 (9pp).

41. M. C. Lu,Y. L. Chueh, L. J. Chen, L. J. Chou , H. L. Hsiao, and An-Ban Yang, Electr. Chem. Solid-State Lett, 8(2005) (7) G153.

42. C. Hemmingsson, G. Pozina, S. Khromov and B. Monemar, Nanotechnol. 22 (2011) 085602 (8pp).

43. S. Y. Bae, H.W Seo, J. Park, H. Yang, and S. A. Song, Chem. Phys. Lett. 365 (2002) 525.

44. S. Dhamodaran, D. SathishChander, and J. Ramkumar, Appl. Surf. Sci. 257 (2011) 9612.

45. L. L. Low, F. K. Yam, K. P. Beh, and Z. Hassan, Appl. Surf. Sci. 257 (2011) 10052.

46. G. Nabi, C. Cao, Z. Usman, S. Hussain, W. S. Khan, F. K. Butt, Z. Ali, D. Yu, and X. Fu, Mater. Lett. 70 (2012) 19.

47. G. Nabi, C. Cao, W.S. Khan, S. Hussain, Z. Usman, N. A. D. Khattak, Z. Ali, F. K. Butt, S. H. Shah, and M. Safdar, Mater. Lett. 66 (2012) 50.

48. S. C. Lyu, O. H. Cha, E. K. Suh, H. Ruh, H. J. Lee, and C. J. Lee, Chem. Phy. Lett. 367 (2003) 136.

49. Y. Wu, C. Xue, H. Zhuang, D. Tian, and Y. Liu, Appl. Surf. Sci. 253 (2006) 485.

50. L. Luo, K. Yu, Z. Zhua, Y. Zhang, H. Ma, C. Xue, Y. Yang, and S. Chen, Mater. Lett. 58 (2004) 2893.

51. G. Nabi, C. Cao, W. S. Khan, S. Hussain, Z. Usman, T. Mahmood, N. A. D. Khattak, S. Zhao, X. Xin, D. Yu, and X. Fu, Mater. Chem. Phys. 133 (2012) 793.

52. G. Nabi, C. Cao, W. S. Khan, S. Hussain, Z. Usman, S. Muhammad, S. S. Hussain, and N. A. D. Khattak, Appl. Surf. Sci. 257 (2011) 10289.

53. D. V. Dinh, S. M. Kang, J. H. Yang, S-W. Kim, and D. H. Yoon, J. Cryst. Growth, 311 (2009) 495.

54. G. Nabi, C. Cao , S. Hussain , W. S. Khan , R. R. Sagar , Z. Ali , F. K. Butt , Z. Usman and D. Yu, Cryst. Eng. Comm, 14 **(**2012), 8492.

55. B. Liu, Y. Bando, C. Tang, F. Xu, J. Hu, and D. Golber, J. Phys. Chem. B, 109 (2005) 17082.

56. J. Liu, X-M. Meng, Y. Jiang, C-S. Lee, I. Bello and S-T. Lee, Appl. Phys. Lett. 83 (2003) 4241.

57. M.J. Shin, J.Y. Moon, H.Y. Kwon, Y.J. Choi, H.S. Ahn, S.N.Yi, D.H. Ha, and Y. Huh, Mater. Lett. 64 (2010) 1238.

58. K. Lekhal, Y. Andre, A. Trassoudaine, E. Gil, G. Avit, J. Cellier, and D. Castelluci, Cryst. Growth Des. 12 (2012) 2251.

59. L. Dai, S.X. Fu, L.P. You, J.J. Zhu, B.X. Lin, J.C. Zhang, and G.G. Qin, J. Chem. Phys. 122 (2005) 104713.

60. C. Xue, Y. Wu, H. Zhuang, D. Tian, Y. Liu, X. Zhang, Y. Ai, L. Sun, and F. Wang, Physica E, 30 (2005) 179.

61. M. Drygas, and J. F. Janik, Mater. Chem. Phys. 133 (2012) 932.

62. X. Hao, J. Zhan, Y. Wu, S. Liu, X. Xu, and M. Jiang, J. Cryst. Growth, 280 (2005) 341.

63. X. He, G. Meng, X. Zhu and M. Kong, Nano. Res, 2 (2009) 321.

64. H. Qiu, C.Cao, J. Li, F. Ji, and H. Zhu, J. Cryst. Growth, 291 (2006) 491.

65. P. Sahoo, S. Dhara, S. Dash, S. Amirthapandian, A. K Prisad, and A.K. Tyagi, Int. J. Hydrogen Energy, 38 (2013) 3513.

66. P. Sahoo, S. Dhara, S. Amirthapandian, M. Kamruddin, S. Dash, B. K. Panigrahi, and A. K. Tyagi, Cryst. Growth Des. 12 (2012) 2375.

67. S. Cho, J. Lee, I.Y. Park and S. Kim, Jpn. J. App. Phys. 41 (2002) 5533.

68. A. I. Hochbaum, and P. Yang, Chem. Rev. 110 (2010) 527.

69. X. Sun and Y. Li, Angew. Chem. Int. Ed, 43 (2004) 3827.

70. L-W. Yin, Y. Bando, M-S. Li, and D. Goldberg, small, 1 (2005) 1094.

71. C-K. Kuo, C-W. Hsu, C-T. Wu, Z-H. Lan, C-Y. Mou, C-C. Chen, Y-J. Yang, L-C. Chen and K-H. Chen, Nanotechnol. 17 (2006) S332.

72. K. Lekhal, G. Avit, Y. Andre, A. Trassoudaine, E. Gil, C. Varenne, C. Bougerol, G. Monier and D. Castelluci, Nanotechnol.,23 (2012) 405601 (6pp).

73. N. Liu, W. Tian, X. Zhang, J. Su, Q. Zhang and Y. Gao, Opt. Express, 20 (2012) 20753.

74. T. Y. Kim, S. H. Lee, Y. H. Mo, H.W. Shim, K. S. Nahm, E. K. Suh, J. W. Yang, K.Y. Lim, and G.S. Park, J. Cryst. Growth, 257 (2003) 97.

75. F. A Ponce and D. P Bour Nature 386 (1997) 351.

76. V. Jindal, Development of group III nitride nanostructures by MOCVD, State Univ. of New York, ProQuest LLC, 2009.

77. M. B. Kanoun, S. Goumri-Said, A. E. Merad, G. Merad, J. Cibert and H. Aourag, Semicond. Sci. Technol. 19 (2004) 1220.

78. O. Ambacher, J. Smart, J. R. Shealy, N. G. Weimann, K. Chu, M. Murphy, R. Dimitrov, L. Wittmer, M. Stutzmann, W. Rieger, and J. Hilsenbeck, J. Appl. Phys. 85 (1999) 3222.

79. M. Stutzmann, O. Ambacher, M. Eickhoff, U. Karrer, A. Lima Pimenta, R. Neuberger, J. Schalwig, R. Dimitrov, P. Schuck, and R. Grober, Phys. Status Solid B 288 (2001) 505.

80. M. B. Kanoun, S. Goumri-Said, A. E. Merad, G. Merad, J. Cibert and H. Aourag, Semicond. Sci. Technol. 19 (2004) 1220.

81. M. C .J .C .M Kramer, Gallium Nitride Based Microwave High Power Heterostructure Field Effect Transistors, Phd Thesis, 2006.

82. D. Brunner, H. Angerer, E. Bustarret, F. Freudenber, R. Hopler, R. Dimitrov, O. Ambacher, and M. Stutzman, J. Appl. Phys., 82 (1997) 5090.

83. I. P. Smorchkova, C. R. Elsass, J. P. Ibbetson, R. Vetury, B. Heying, P. Fini, E. Haus, S. P. Den Baars, J. S. Speck, and U. K. Mishra, J. Appl. Phys., 86 (1999) 4520.

84. S. Chattopadhyay, A. Ganguly, K-H Chen, and L-C Chen, Crit. Rev. Solid State Mater. Sci., 34 (2009) 224.

85. Y. Irokawa, Sensors (Basel). 11(1) (2011) 674.

86. S. J Pearton, B. S Kang, S. Kim, F. Ren, B. P Gila, C. R Abernathy, J. Lin and S. N.G Chu, J. Phys: Condens. Matter 16 (2004) R96.

87. A. E .L. Kouche, J. Lin, M. E. Law, S. Kim, B. S. Kim, F. Ren, and S. J. Pearton, Sens. Actuators B 105 (2005) 329.

88. A. L Spetz, A. Baranzahi, P. Tobias and I. Lundstrom, Phys. Status Solidi a 162 (1997) 493.

89. A. L Spetz, P. Tobias, L. Uneus, H. Svenningstorp, L-G Ekedahl and I. Lundstrom, Sens. Actuators B70 (2000) 67.

90. R. Neuberger, G. Muller, O. Ambacher and M. Stutzmann, Phys. Status Solidi a 185 (2001) 85.

91. J. Schalwig, G. Muller, O. Ambacher and M. Stutzmann, Phys. Status Solidi a 185 (2001) 39.

92. J. Schalwig, G. Muller, M. Eickhoff, O. Ambacher and M. Stutzmann, Sens. Actuators B 81 (2002) 425.

93. M. Stutzmanna, G. Steinhoff, M. Eickhoff, O. Ambacher, C. E. Nebel, J. Schalwig, R. Neuberger, G. Muller, Diamond Relat. Mater. 11 (2002) 886.

94. M. Eickhoff , J. Schalwig, G. Steinhoff, O. Weidemann, L. Gorgens, R. Neuberger, M. Hermann, B. Baur, G. Muller, O. Ambacher, and M. Stutzmann, Phys. Status Solidi C 6 **(**2003) 1908.

95. H-T. Wang, T. J. Anderson, F. Ren, C. Li, Z-N Low, J. Lin, B. P Gila, S. J. Pearton, A. Osinsky and A. Dabiran, Appl. Phys. Lett. 89 (2006) 242111.

96. L. Voss, B. P. Gila, S. J. Pearton, H. Wang, and F. Ren, J. Vac. Sci. Technol. B 23 (2005) 2373.

97. L. C. Tien, P. W. Sadik, D. P. Norton, L. F. Voss, S. J. Pearton, H. T. Wang, B. S. Kang, F. Ren, J. Jun, and J. Lin, Appl. Phys. Lett. 87 (2005), 222106 (1-3pp).

98. L. C. Tien, H. T. Wang, B. S. Kang, F. Ren, P. W. Sadik, D. P. Norton, S. J. Pearton, and J. Lin, Electrochem. Solid-State Lett. 8 (2005) G230.

99. I. Sayago, E. Terrado, E. Lafuente, M. C. Horrillo, W. K. Maser, A. M. Benito, R. Navarro, E. P. Urriolabeitia, M. T. Martinez, and J. Gutierrez, Synthetic Met. 148 (2005) 15.

100. B. Wang, L. F. Zhu, Y. H. Yang, N. S. Xu, and G. W. Yang, J. Phys. Chem. C 112 (2008) 6643.

101. T. Zhang, S. Mubeen, N. V Myung and M. A Deshusses, Nanotechnol. 19 (2008) 332001 (14pp).

102. Y. M. Wong, W. P. Kang, J. L. Davidson, A. Wisitsora, K. L. Soh, Sens. Actuators B, 93 (2003) 327.

103. O. Lupan, G. Chai, L. Cho, Microelectron. Eng. 85 (2008) 2220.

104. J. S.Wright, W. Lim, B.P. Gila, S. J. Pearton, J. L. Johnson, A. Ural, F. Ren, Sens. Actuators B, 140 (2009) 196.

105. T. Kente, S. M. A. Dube, N.J. Coville, S.D. Mhlanga, J. Nanosci. Nanotechnol. 13 (2013) 4990.

Chapter 3

Experimental and characterization techniques

3.1 Introduction

Many methods have been reported to make GaN such as, chemical vapour deposition (CVD) [1-3], metal-organic chemical vapour deposition (MOCVD) [4], molecular beam epitaxy [5], halide vapor-phase epitaxy [6-9], arc discharge [10], magnetron sputtering [11], chemical thermal-evaporation process [12], MOVPE [13], laser ablation [14], pyrolysis [15], etching [16], and ammonolysis [17–20]. Among these techniques, CVD is regarded as one of the best methods to use since the process is cheap and it can be used to produce large surface area GaN in a fast growth process. However, a major challenge for the synthesis of GaN nanostructures (NSs) is the requirement of a high temperature used in the CVD method [21]. The GaN NSs in this study were characterized by different techniques listed below in section 3.4 where they are explained in detail. Details on the operation of these techniques are also given.

3.2 Synthesis of GaN NSs and carbon coated GaN

GaN NSs were synthesized using a CVD method in both a single and double stage furnace (see Fig. 3.1 and 3.2). The synthesis of GaN in a single stage furnace typically requires higher temperatures (> 1000 °C). The synthesis of GaN in a double stage furnace can be achieved at lower temperatures (< 1000 ºC). Carbon coated GaN (GaN-C) nanostructures were also made using CVD in a single stage

furnace at lower temperatures (500 – 650 ºC). The synthesis of these materials is explained in detail in Chapters 4 and 5.

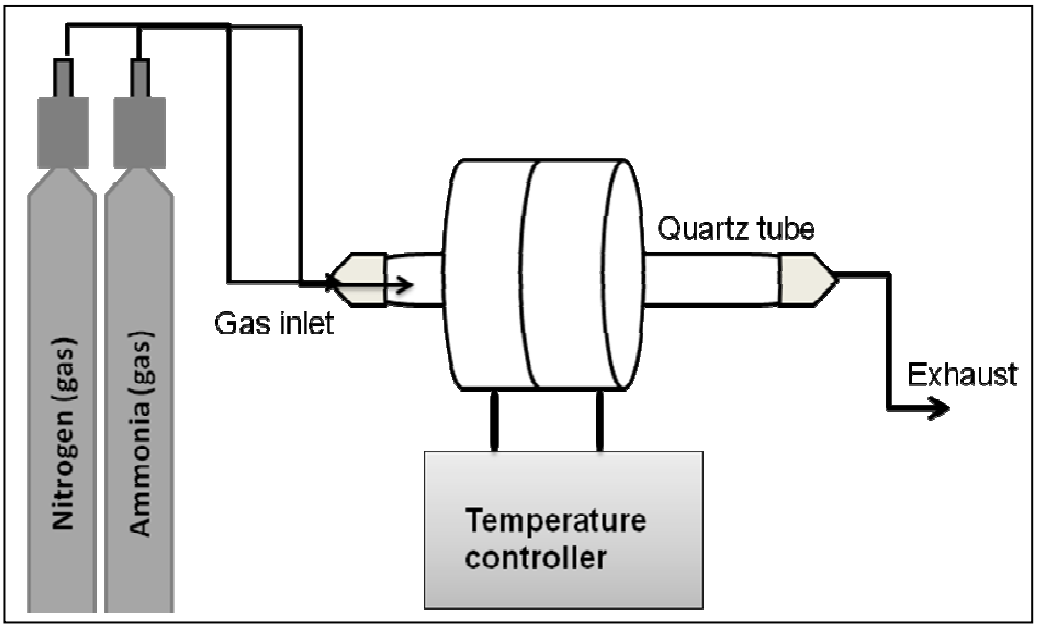


Fig. 3.1: Single stage furnace for CVD synthesis of GaN materials.

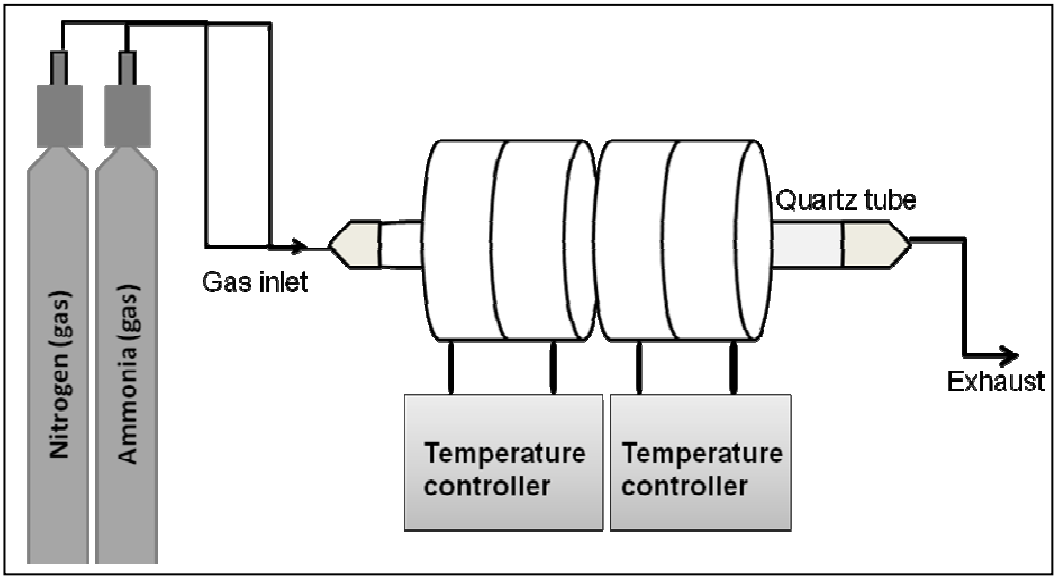


Fig. 3.2: Double stage furnace used in CVD synthesis of GaN materials.

3.3 Functionalization of GaN NSs

The GaN NSs and GaN-C materials were functionalized with nitric acid (HNO_3) at room temperature for 1 h and a piranha solution (HNO_3/H_2SO_4) was used to introduce the organic functional groups on the surface. The functionalised GaN nanostructure materials were used to support palladium (Pd) and platinum (Pt) catalysts. The catalysts were prepared with metal loadings of 1 and 3 wt %. The catalysts, supports and GaN-C material were evaluated by using different characterization techniques that are discussed in section 3.4. The catalysts were used on sensors to determine the presence of hydrogen gas at different temperatures (RT - 200ºC). They were also used in hydrogenation reactions (cinnamaldehye to hydrocinnamaldehyde) at (40 and 60 °C) using the experimental setup shown in Fig. 3.3.

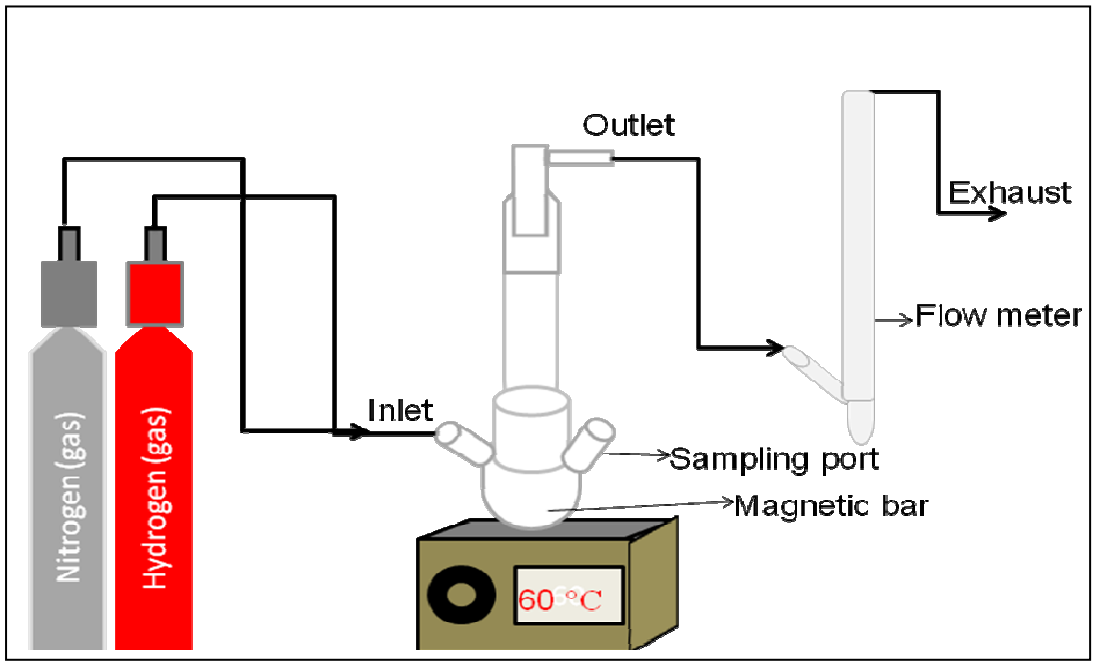


Fig. 3.3: Reaction setup used for hydrogenation reaction.

3.4 Characterization techniques

3.4.1 Transmission and scanning electron microscopy (TEM and SEM)

The structural morphology of the GaN NSs was ascertained by scanning electron microscopy (JEOL 7500F SEM) and transmission electron microscopy (FEI Tecnai G^2 Spirit electron microscope at 120 kV). TEM and SEM were also used to determine the size (i.e. diameter and the length) and the purity of the synthesized materials.

The materials for TEM analysis were prepared by sonicating the sample in methanol for about 10 minutes so that the sample could be well dispersed. One drop of the suspension was transferred to a SPI Cu-grid using a Pasteur pipette. The grid was placed on a single tilt sample holder and the holder was inserted into the TEM (Fig. 3.4). When the sample was in place, a good vacuum has been created, the beam was turned on and the column valves were opened the sample was ready to be viewed.



Fig. 3.4: FEI Tecnai G^2 Spirit electron microscope used to study the GaN NSs.

The materials for SEM analysis were prepared by placing a carbon tape on a sample stub; a first layer of a carbon tape was removed. A small amount of material was mounted on a stub with carbon tape. Then the sample was loaded in a chamber using a pin stub mount gripper. Fig 3.5 shows a JEOL 7500F scanning electron microscope.



Fig. 3.5: JEOL 7500F scanning electron microscope used to study the GaN NSs.

3.4.2 Raman spectroscopy

Raman spectra (Jobin-Yvon LabRAM) were collected using the 514.5 nm line of an argon ion laser. A 600 gr/mm grating and a liquid cooled CCD detector were used to investigate the vibrational properties. Resonance Raman spectroscopic studies were performed in the backscattering configuration using a micro-Raman setup (InVia, Renishaw) with 325 nm excitation from a He-Cd laser, 2400 gr/mm grating and a thermoelectrically cooled CCD detector. This technique has been established as a valuable tool for probing phonon excitations in semiconductors

[22] and provides information about the dispersion of raman active optical phonons. The main use in this study was to determine the frequencies of longitudinal optical (LO) and transverse optical (TO) modes near the Brillouin zone center [000] [23]. This technique could also finger print excitation modes attributed to the graphitic (G) layers and disorder (D) bands in a carbon coated material. The ratio between the D and G bands indicated the quality of the sample.

3.4.3 Photoluminescence

Photoluminsence (PL) spectroscopic studies were performed in the backscattering configuration using a micro-Raman setup (InVia, Renishaw) with 325 nm excitation from a He-Cd laser, 2400 gr/mm grating and thermoelectrically cooled CCD detector. PL is a process of re-emission of light after absorbing a photon of higher energy and it's a radiative recombination process among excited charge carriers, such as electrons/holes or wannier excitons in a semiconductor during an external optical/radiative excitation process [23].

3.4.4 Brunauer Emmett Teller (BET) surface area

A BET TRISTAR 3000 analyzer was used to measure the surface area and porosity of the materials. BET is based on a theory that uses the Langmuir adsorption isotherms, multi-molecular layers and adsorption. The adsorption or desorption isotherms are used to investigate the surface area and pore structure of the material [24]. Approximately 0.2 g of the sample was weighed and degassed under N_2 ambient at 150 °C to remove moisture for ~ 4 hours before the analysis.

3.4.5 Thermogravimetric analysis

Thermogravimetric analysis (TGA), using a Perkin Elmer STA 4000 analyzer was used to study the thermal stability and decomposition temperature of the materials. The derivative weight curves were used to identify the decomposition temperature maxima. Approximately 10 mg of the sample was heated from room temperature to 900 °C at 10 °C/min under air with a gas flow rate of 20 ml/min.

3.4.6 Electron Dispersive X-ray (EDX) analysis

This technique was used to identify the elemental composition of a material. EDX equipment was attached to a JEOL 7500F SEM electron microscopy (SEM/EDX). The generated data shows the peaks that correspond to the elements and the composition of the sample being analysed.

3.4.7 Powder X- ray diffraction (PXRD) analysis

Powder X-ray diffraction (Bruker D2 Phaser) with Cu-Kα (1.789Å) radiation was used to identify the phases of the crystalline material. The samples were finely ground. The data was collected at 2θ from ~10° to 90°, angles that are present in the X-ray scan using θ/θ Brentano geometry. Debye Scherrer equation was used to calculate the particle size of the material and is limited to nanoscale particles.

3.4.8 X-ray photo-electron spectroscopy (XPS)

XPS (PHI 5000 Versaprobe – Scanning ESCA Microprobe) is a quantitative spectroscopic technique that was used to measure the elementary composition and chemical bonding of the GaN materials.

3.5. Gas measurement system

GaN NSs were dispersed in methanol and then ultrasonicated for 5 minutes. The sample was prepared for gas sensing by spin coating. Spin coating was done on the gold (Au) electrode which was deposited by sputtering on a SiO_2 substrate. The prepared solution was added dropwise onto Au deposited on a SiO_2 substrate. It was then dried to remove the solvent. Then the sample was ready for sensing. The conductivity of the sample was confirmed before the sample was loaded into the chamber. The gases studied in the system are nitrogen, hydrogen, oxygen, methane, ammonia and nitrous oxide. All gas flows were controlled by a Mass Flow Controller (MFC). A heater was connected at the bottom of chamber and can go up to 500°C. The oxidation was minimized by purging Ar.

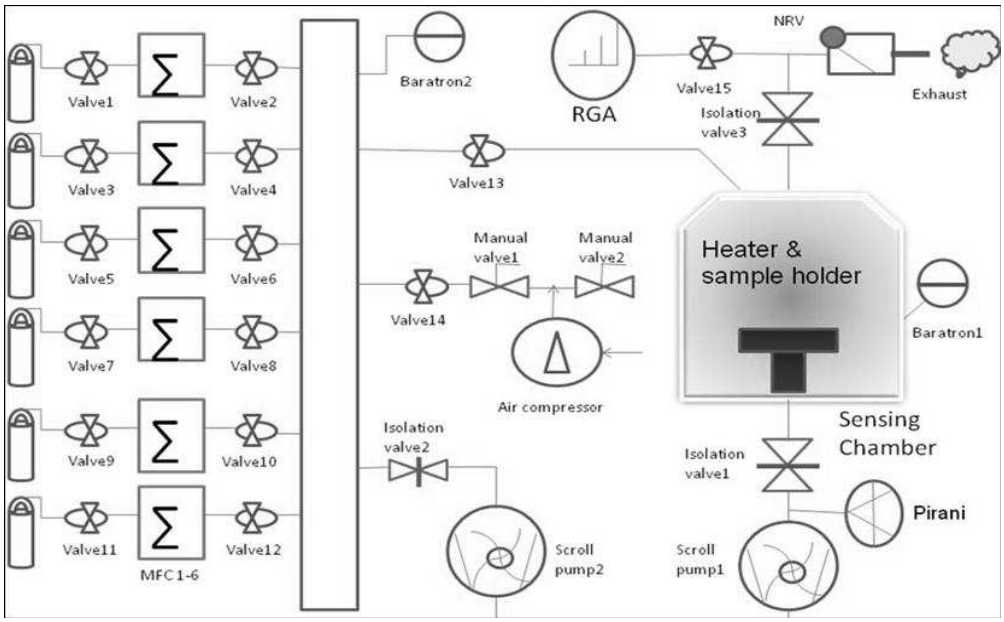


Fig. 3.6: Schematic diagram of gas measurement system.

*RGA – Residual gas analyser.

3.6 References

1. S. Y. Bae, H.W Seo, J. Park, H. Yang, S. A. Song, Chem. Phys. Lett. 365 (2002) 525.

2. S. Dhamodaran, D. S. Chander, J. Ramkumar, Appl. Surf. Sci. 257 (2011) 9612.

3. G. Nabi, C. Cao, Z. Usman, S. Hussain, W. S. Khan, F. K. Butt, Z. Ali, D. Yu, X. Fu, Mater. Lett. 70 (2012) 19.

4. Z. Yu, Z. Yang, S. Wang, Y. Jin, J.G. Liu, M. Gang, X. Sun, Chem. Vap. Deposition, 11(2005) 433.

5. K. A. Bertness, A. Roshko, L. M. Mansfield, T. E. Harvey, N. A. Sanford, J. Cryst. Growth, 300 (2007) 94.

6. T. B. Wei, Q. Hu, R. F. Duan, X. C. Wei, Z. Q. Huo, J. X. Wang, Y. P. Zeng, G. H. Wang, J. M. Li, J. Cryst. Growth, 311(2009) 4153.

7. C. Hemmingsson, G. Pozina, S. Khromov, B. Monemar, Nanotechnol. 22 (2011) 085602 (8pp).

8. M. J. Shin, J.Y. Moon, H.Y. Kwon, Y. J. Choi, H. S. Ahn, S. N.Yi, D. H. Ha, Y. Huh, Mater. Lett. 64 (2010) 1238.

9. K. Lekhal, Y. Andre, A. Trassoudaine, E. Gil, G. Avit, J. Cellier, and D. Castelluci, Cryst. Growth Des. 12 (2012) 2251.

10. W. Q. Han, P. Redlich, F. Ernst, and M. Ruhle, Appl. Phys. Lett., 76 (2000) 652.

11. L. Yang, C. Xue, C. Wang, and H. Li, Nanotechnol., 14 (2003) 50.

12. B. D. Liu, Y. Bando, C. C. Tang, G. Z. Shen, D. Golberg, and F. F. Xu, Appl. Phys. Lett., 88 (2006) 88.

13. R. Koester, J. S Hwang, C. Durand, D. Le Si Dangand. J. Eymery, Nanotechnol. 21 (2010) 015602 (9pp).

14. X. Duan and C. Lieber, J. Am. Chem. Soc. 122 (2000) 188.

15. W. Han and A. Zettl, Appl. Phys. Lett, 80 (2002) 2.

16. S. C. Hung, Y. K. Su, S. J. Chang, S. C. Chen, T. H. Fang, and L. W. Ji, Physica E, 28 (2005)115.

17. A. P. Purdy, S. Case, and N. Muratore, J. Cryst. Growth, 252 (2003) 136.

18. S. Y. Bae, H. W. Seo, J. Park, H. Yang, J. C. Park, and S. Y. Lee, Appl. Phys. Lett., 81(2002) 126.

19. S. Kikkawa, K. Nagasaka, T. Takeda, M. Bailey, T. Sakurai, and Y.Miyamoto, J. Solid State Chem., 180 (2007) 1984.

20. S. Cho, J. Lee, I. Y. Park, and S. Kim, Jpn. J. Appl. Phys., Part 1, 41 (2002) 5533.

21. Wright, S.; Lim, W.; Norton, D.P.; Pearton, S. J.; Ren, F.; Johnson, J. L.; and Ural, A.; Semicond. Sci. Technol. 25 (2010) 024002.

22. F. Xu, Y. Xie, X. Zhang, S. Y. Zhang, X. M. Liu, W. Xi, X. B. Tian, Adv. Funct. Mater. 14 (2004) 464.

23. P. K. Sahoo, Quasi One Dimensional GaN Nanostructures: Growth Kinetics, Physical Properties, and Applications, PhD Thesis, 2012.

24. S. Brunauer, The adsorption of Gases and Vapors. Vol. I, Physical Adsorption, Princeton University Press, Princeton, N.J. (1943).

Chapter 4

Catalyst free vapour-solid growth of novel GaN nanostructures at low temperature

4.1 Introduction

Among the various semiconductor nanostructures, GaN is a promising candidate material for short wavelength (from green to ultraviolet) optoelectronic devices such as light emitting diodes (LEDs) and laser diodes (LDs) as well as high power and high temperature operation devices. These uses are associated with GaN because of its high melting temperature, high breakdown field, and high saturation drift velocity [1]. GaN is an important semiconductor with a wide direct band gap (~3.9 eV at room temperature) and it is useful as a blue and ultraviolet light emitter [2]. Several attempts have been made to synthesize one dimensional GaN nanorods or nanowires using different techniques such as carbon nanotube-confined reactions which result in the growth of GaN nanorods with diameters of 4 ~ 50 nm [3], anodic alumina template methods [4], arc discharge [5], laser ablation [6,7], chemical vapour deposition (CVD) [8] and metal organic vapour phase epitaxy (MOVPE) [9]. Among these techniques, CVD is well recognized due to the low cost constraints as well as the ability to produce large area GaN in a fast growth process. However, a major challenge for the synthesis of GaN nanostructures (NSs) is the requirement of a high temperature in the CVD method [10].

There are several reports of nitridation of Ga_2O_3 at high temperatures (900 – 1100 °C) to obtain GaN, as the sublimation temperature of GaN is ~ 1000 °C although there is a possibility of a decrease of the sublimation temperature with reduction of GaN nanocrystal size [11]. In addition, GaN decomposes at temperatures above 850 °C in high vacuum [12] and close to 1000 °C under atmospheric pressure

[13]. Thus, a synthesis below 1000 °C is desired to overcome these disadvantages that occur at higher temperatures. Moreover, there is a requirement for a catalyst free growth to avoid interference of catalyst in device applications [14]. Catalyst assisted low temperature growth of GaN NSs is however reported to occur at a temperature of ~ 650 °C using either metallic Ga or gallium acetyacetate as the Ga source material using the CVD technique [15,16] but no detailed optical analysis of the presence of the catalysts was described in those studies.

This study aims for catalyst free growth of GaN nanostructures (NSs) at low temperature by exploiting a two stage oven system; the first heating zone is used to preheat the NH_3 at high temperature (T = 1100 °C) and the second heating zone is used for the growth of GaN NSs at a lower temperature. Table 4.1 shows results obtained by others using a similar setup to synthesize GaN nanostructures under the influence of catalysts. Surprisingly; use of the readily available Ga_2O_3 has not been used to synthesize GaN in a two stage reactor system.

Table 4.1: Previous work on the synthesis of GaN in a double stage furnace.

Material used	Cluster size	Synthesis temperature	Reference
Ga metal on Ni coated c-plane sapphire substrate.	35 – 80 nm and 0.4 – 1.3 µn	Stage 1 = 1000 °C Stage 2 = 950 °C	[17]
Ga metal on Ni coated c-plane sapphire substrate.	25 - 215 nm	Stage 1 = 1000 °C Stage 2 = 750 – 1000 °C	[18]
Mixture (1:2) of galliumdimethyleamide and ferrocene.	15 – 70 nm	Stage 1 = 1000 °C Stage 2 = 900 °C	[19]

4.2. Experimental details

4.2.1 Growth of GaN Nanostructures

The GaN NSs were synthesized using a double stage furnace. In this experimental setup the first heating zone (zone 1) of the double stage furnace was heated to 1100 °C to preheat NH_3 and cause its dissociation into NH_2, NH, and N reactive species. At this temperature a complete dissociation of constituent species is reported [20]. The second heating zone (zone 2), where the synthesis of GaN occurred, was heated to temperatures between 700 – 900 °C.

Ga_2O_3 powder was placed in a crucible in the center of a quartz tube in zone 2. Pure N_2 was allowed to flow through the quartz tube at a flow rate of 12 mL/min while heating the two zones of the reactor. When the desired temperatures were reached, NH_3 at different flow rates was introduced. The dissociated products of NH_3 reacted with Ga_2O_3 in zone 2 to grow the GaN NSs. The NH_3 flow rate was varied (12 mL/min at 900 ºC, 72 mL/min at 850 ºC and 210 mL/min at 750 ºC and 800 ºC) while N_2 was kept at a flow rate of 12 mL/min. After 1 h the furnace was then cooled to room temperature while N_2 was passed through the reactor and the crucible was then removed from the reactor and weighed and analyzed to establish the amount of GaN product formed. We have also grown NSs at the NH_3 preheating temperature of 1100 °C in a single stage oven using the same precursor and reactant gas for comparison purposes. The NH_3 and N_2 flow rates were both 12 mL/min with a reaction time of 45 min.

4.2.2 Characterization of the GaN nanostructures

The morphology and structure of the GaN NSs were ascertained by scanning electron microscopy (SEM; JEOL 7500F SEM) and transmission electron microscopy (TEM; FEI Tecnai G^2 Spirit electron microscope at 120 kV), respectively. Powder X-ray diffraction (PXRD; Bruker D2 Phaser) was used to study the chemical composition and crystallinity of the materials. A Brunauer-Emmett-Teller (BET) TRISTAR 3000 analyzer was used to measure the surface

area and porosity. The formation of chemical bonding was determined by X-ray photo-electron spectroscopy (XPS) using a PHI 5000 Versaprobe – Scanning ESCA Microprobe. Raman spectroscopy (Jobin-Yvon LabRAM) with the 514.5 nm line of an argon ion laser, a 600 gr/mm grating and a liquid cooled CCD detector was used to investigate the vibrational properties. Resonance Raman and photoluminescence (PL) spectroscopic studies was performed in the backscattering configuration using a micro-Raman setup (InVia, Renishaw) with 325 nm excitation from a He-Cd laser, 2400 gr/mm grating and thermoelectrically cooled CCD detector.

4.3. Results and discussion

4.3.1 Morphological analysis

SEM images of the GaN materials synthesized at different temperatures are shown in Fig. 4.1. The SEM images show that the materials consist of randomly oriented rod-like structures that appear solid. The corresponding TEM images of the materials are also given in Fig. 4.1 (inset images). Detailed TEM analysis however, revealed that what appear to be solid rods under SEM are actually nanorods constituted of mainly agglomerated nanoparticles (Fig. 4.2a). Indeed the particles that agglomerate to form the nanorods are less than 20 nm in diameter. TEM analysis of the sample grown at 1100 ^{o}C, however show a relatively smooth surface.

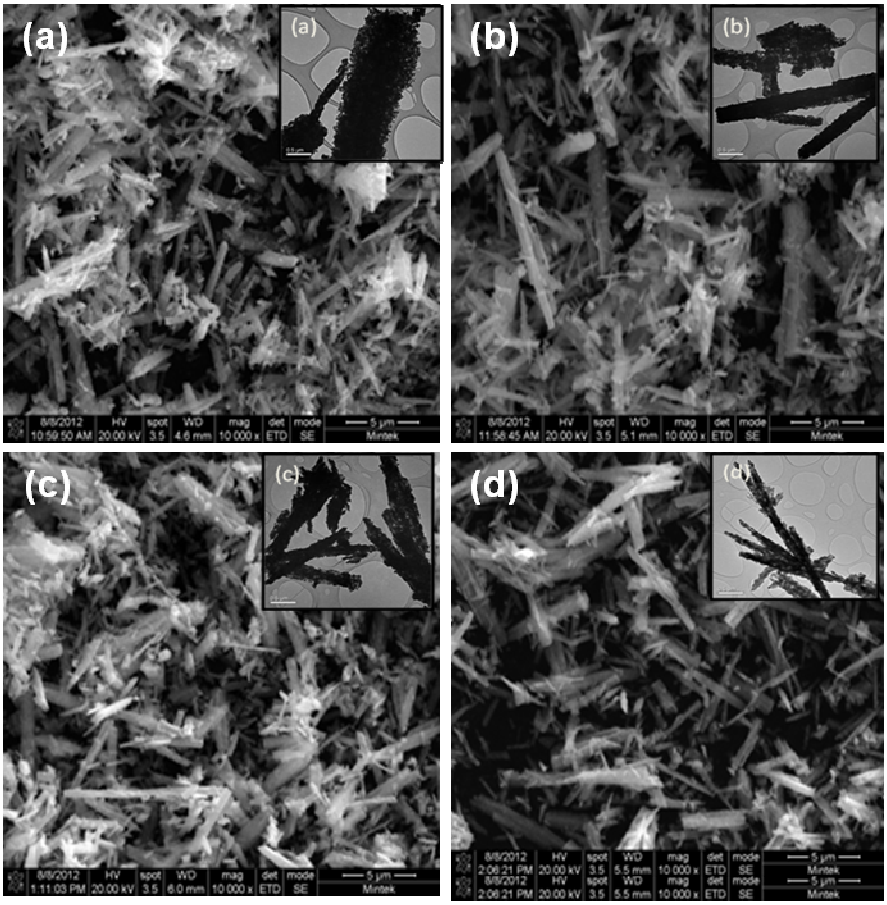


Fig. 4.1: SEM and TEM (inset) images of GaN nanostructures grown in the two stage furnace at (a) 750 °C, and (b) 800 °C, for 2 h; (c) 850 °C and (d) 900 °C for 1 h.

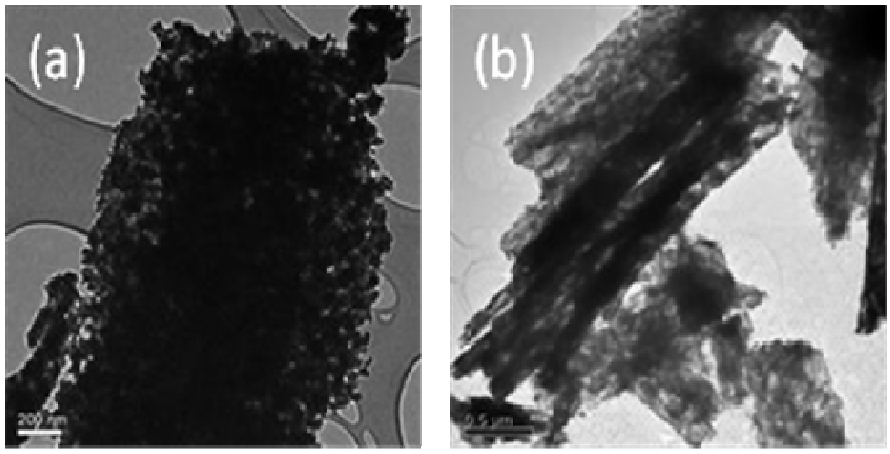


Fig. 4.2: TEM image shows the (a) agglomerated nanoparticles typically grown in the two stage furnace at 750 ^{o}C (b) morphology of the GaN materials at 1100 °C grown in single stage furnace.

4.3.2 PXRD analysis

The peaks at 2θ values of 32.55 ^{o}, 34.83°, 36.99 ^{o}, 48.30 ^{o}, 57.89 ^{o}, 63.76 ^{o}, 68.20°, 69.34 ^{o}, 70.64 ^{o}, and 73.22^{o} corresponding to (*hkl*) planes (100), (002), (101), (102), (110), (103), (200), (112), (201) and (004), respectively showed (Fig. 4.3) the presence of wurtzite GaN phase (JCPDS # 02-1078) in these NSs. Ga_2O_3 was completely converted to GaN even at temperatures as low as 750 °C. Below this temperature, no GaN was obtained. Thus GaN was successfully synthesized using a double stage furnace at temperatures lower than 900 ^{o}C, which is the typical reaction temperature reported in the literature. By pre-heating the NH_3, the synthesis of pure hexagonal wurtzite GaN could be achieved at 750 °C.

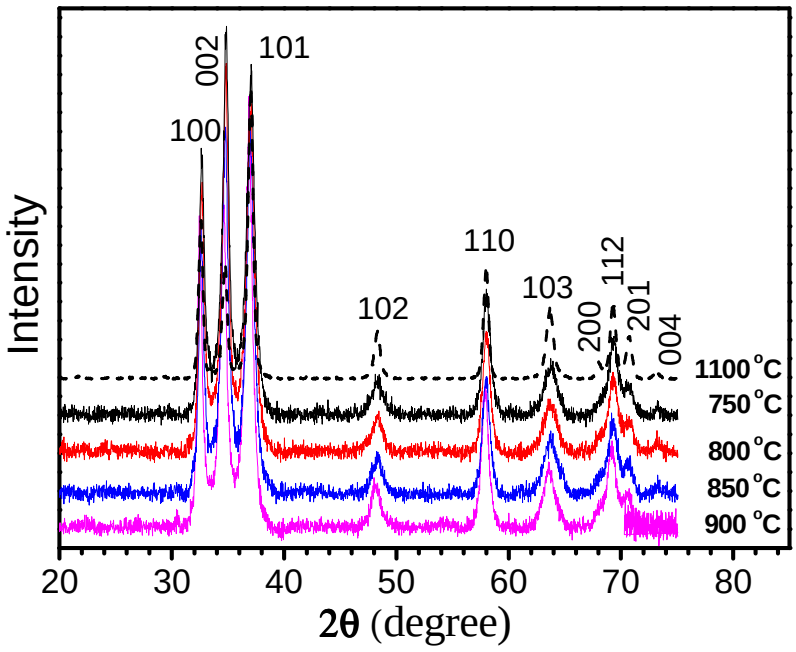


Fig. 4.3: PXRD pattern of GaN nanostructures synthesized using Ga_2O_3 and NH_3 at various growth conditions. Spectra are shifted vertically for clarity.

The grain size of the GaN materials synthesized at different temperatures was quantified using the Scherrer equation [21] and the prominent peak which corresponds to the (101) plane of GaN was used for the study. Very small grains in the range of 12 - 16 nm were obtained, smaller than the size of the material ~14 - 22 nm synthesized in a single stage furnace at an elevated temperature of 1100 ^{o}C. The grain size of the materials increased with an increase in synthesis temperature as shown in Fig. 4.4. This is due to the low flow rate of NH_3 at high temperature.

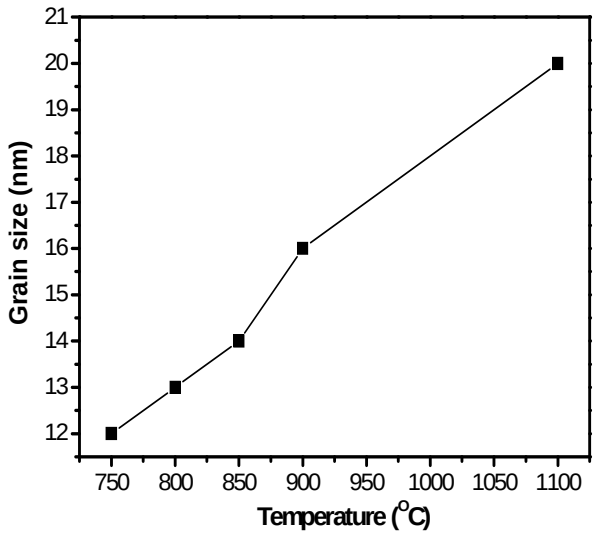


Fig. 4.4: Average grain sizes of the GaN nanostructures synthesized at different growth temperatures (750 – 900 °C) in a double stage furnace and 1100 °C in a single stage furnace. The line acts as a guide to the eye.

4.3.3 BET surface area analysis

Table 4.2 shows the surface area of the GaN NSs synthesized at different temperatures. Comparison of these materials to those synthesized in the single stage furnace using the same precursors revealed that the surface area of these materials doubled from 10 m^2/g to 20 m^2/g. Such materials could be exploited for use as supports for catalysts where high surface areas are desirable. The lowest temperature used i.e (750 °C) to synthesize the GaN NSs gave good surface area (~ 20 m^2/g), this renders the method ideal for the synthesis of these materials.

Table 4.2: BET surface areas of the GaN NSs synthezised at different temperatures in a double stage furnace (synthesis time = 1 h for 850 °C and 900 °C and 2 h for 750 °C and 800 °C).

Temperature (°C)	Surface area (m^2/g)	Pore volume (cm^3/g)
1100 (single stage)	10.8	0.06
750	19.6	0.12
800	20.2	0.12
850	20.8	0.12
900	20.9	0.13

4.3.4 X-ray photo-electron spectroscopy (XPS) analysis

Figure 4.5 shows typical XPS analysis of the GaN NSs synthesized at 800 °C. The data for temperatures at 850, 900 and 1100 °C are shown in Fig. 4.6, 4.7 and 4.8 respectively in the two stage reactor and Fig. 4.8 (1100 °C) in a single stage reactor and confirmed the presence of elemental Ga and N. Fig. 4.5, 4.6, 4.7 and 4.8 show a high resolution spectra of the N1s, $Ga2p_{3/2}$ and O1s present in the materials with expected binding energy peak positions (see Table 4.3). The N1s peaks were deconvoluted into two peaks at~395.9 and~397.4 eV, 395.7 and 397.5 eV, 391.2 and 396.3 eV, 392.0 and 396.5 eV for GaN NSs synthesized at 800 °C, 850 °C, 900 °C and 1100 °C respectively. The peaks at 395.9, 395.7, 391.2 and 392.0 eV are due to nitrogen that is bonded to the Ga (Auger peak; Ga LMM 1) and the peak at 397.4, 397.5, 396.3 and 396.5 eV are nitride peak with ~ 0.1- 1.00 eV shift from the reported value of nitrides (see Fig. 4.5 (a)). The binding energy peaks for $Ga2p_{3/2}$ were~1117.9, 1118.1 eV for GaN NSs synthesized at 800, 850 °C. The binding energy peaks for $Ga2p_{3/2}$ of GaN NSs synthesized at 900 °C and 1100 °C were decovoluted into two peaks at 1115.8 and 1117.1 eV, 1117.7 and 1115.9 eV.

The O1s peaks were also deconvoluted into two peaks at 530.7 and 531.8 eV, 530.9 and 531.8 eV, 530.3 and 531.4 eV, 530.6 and 531.4 eV for GaN NSs synthesized at different temperatures. These two peaks are due to oxygen that is bonded to Ga (LMM1) and absorbed oxygen when GaN is exposed to the atmosphere respectively. The position of the binding energies of Ga and N confirms the bonding between Ga and N [22].

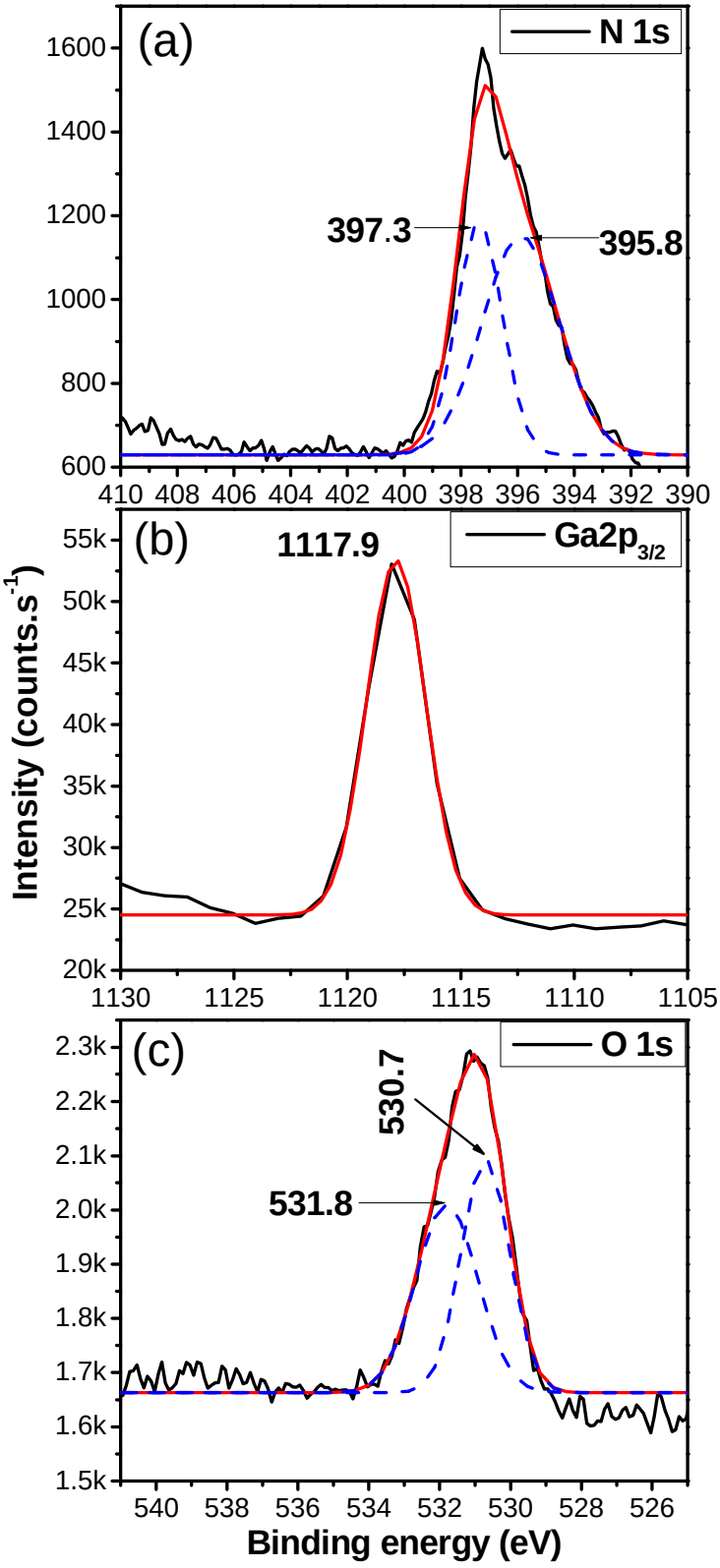


Fig. 4.5. Typical high resolution binding energy spectra of the N1s (a), $Ga2p_{3/2}$ (b) and O1s (c) observed in the GaN nanostructures synthesized at 800 °C in the two stage furnace.

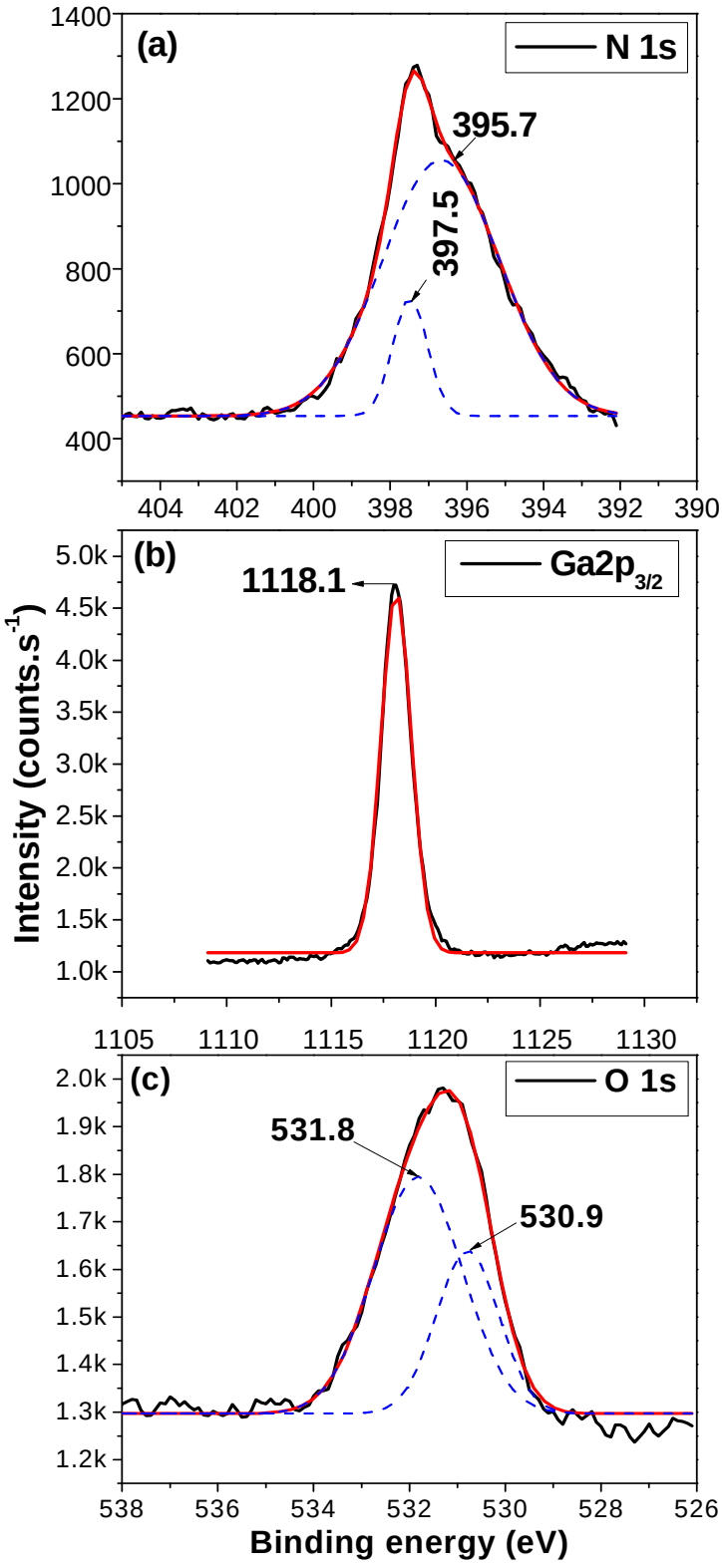


Fig. 4.6. Typical high resolution binding energy spectra of the N1s (a), $Ga2p_{3/2}$ (b) and O1s (c) observed in the GaN nanostructures synthesized at 850 °C in the two stage furnace.

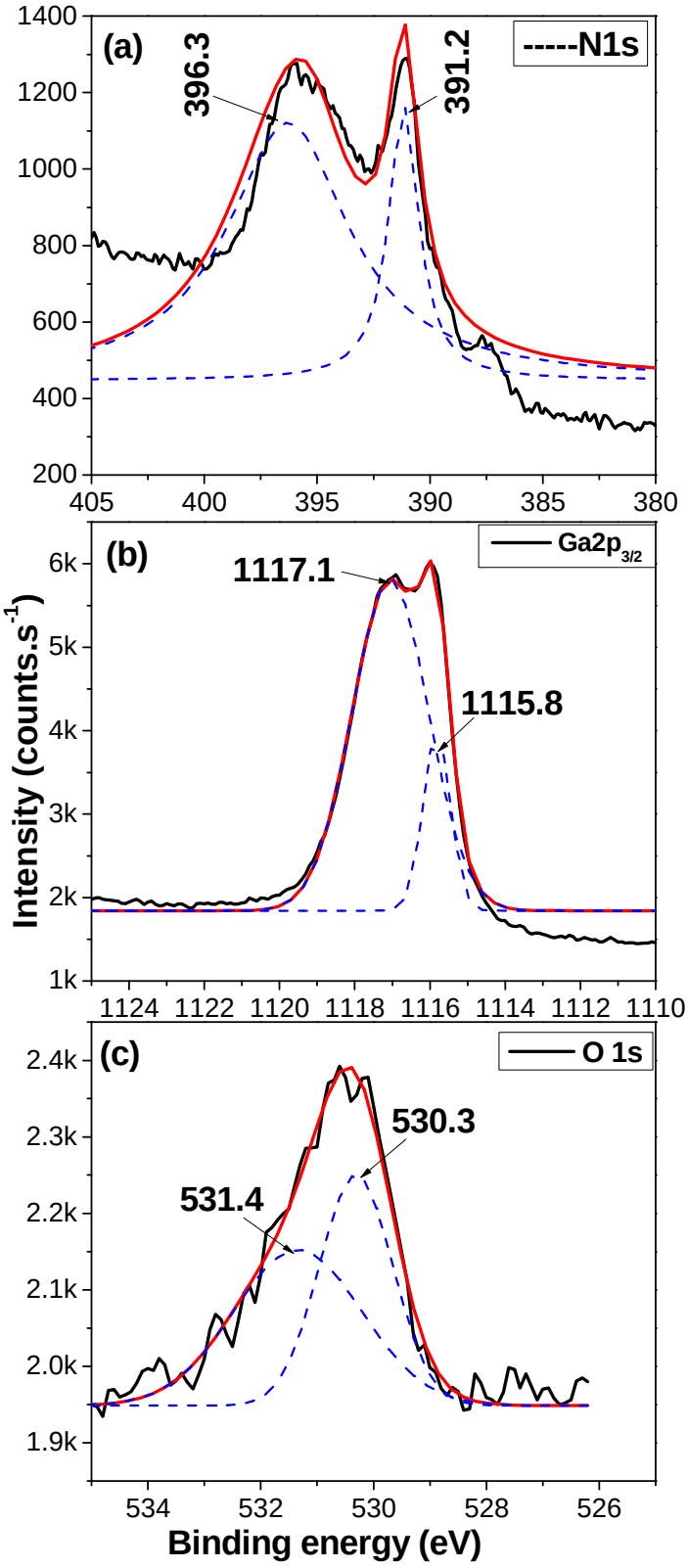


Fig. 4.7. Typical high resolution binding energy spectra of the N1s (a), $Ga2p_{3/2}$ (b) and O1s (c) observed in the GaN nanostructures synthesized at 900 °C in the two stage furnace.

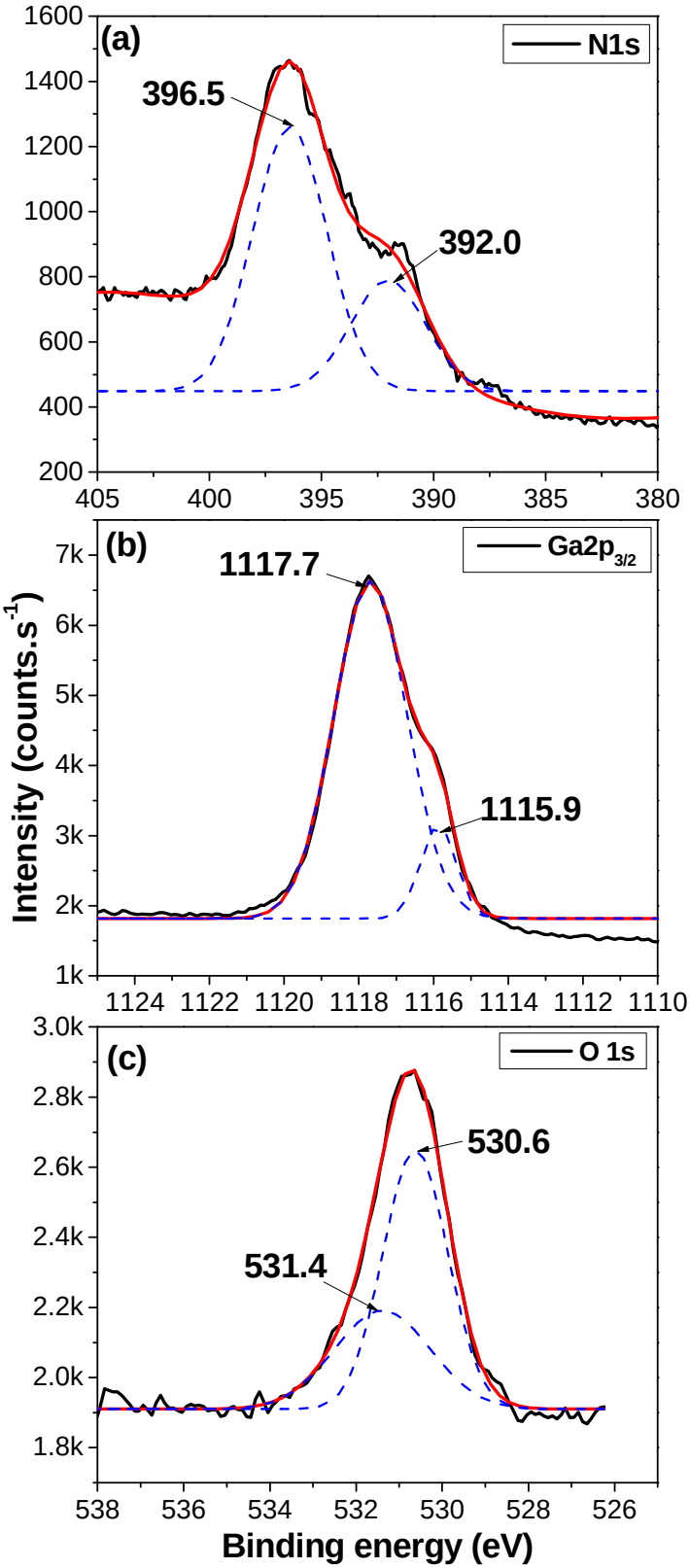


Fig. 4.8. Typical high resolution binding energy spectra of the N1s (a), $Ga2p_{3/2}$ (b) and O1s (c) observed in the GaN nanostructures synthesized at 1100 °C in the single stage furnace.

Table 4.3: The binding energies of the GaN synthesized at various growth temperatures.

Temperature (°C)	$Ga2p_{3/2}$ (eV)	N1s (eV)	O1s (eV)
800	1117.9	397.4	531.8
		395.9	530.7
850	1118.1	397.5	530.9
		395.7	531.8
900	1117.1	396.3	530.3
	1115.8	391.2	531.4
1100	1117.7	396.5	530.6
	1115.9	392.0	531.4

4.3.5 Raman spectroscopic analysis

Fig. 4.6a clearly shows prominent phonon modes at ~ 249, 418, 562, and 724 cm^{-1} in the Raman spectra of the samples grown at various growth temperatures using Ar^{+} (514.5 nm) excitation. The peaks at 562 and 724 cm^{-1} can be assigned to symmetry allowed E_2(high) and A_1(LO) Raman modes corresponding to wurtzite GaN, respectively [23]. Peaks at 249 and 418 cm^{-1} may be assigned to a zone boundary (ZB) phonon in the finite sized NSs [23]. A higher intensity of A_1(LO) compared to that for E_2(high) indicates a superior electronic quality in these samples. The peaks marked as '*' are unknown, and they disappear with increasing growth temperature (Fig. 4.9a). These peaks may be due to minor structural defects in the samples grown at lower temperatures.

We have also performed resonance Raman spectroscopy in these samples using a He-Cd laser (325 nm ≈ 3.81 eV). A strong A_1(LO) phonon mode was observed at

~ 730 cm^{-1} along with an E_2(high) mode at 575 cm^{-1} (Fig. 4.9b). These mode frequencies deviate slightly from that reported at 725 and 569 cm^{-1} corresponding to A_1(LO) and E_2(high) phonon modes, in the non-resonant condition [23]. At an excitation energy greater than the reported band gap of GaN (3.47 eV at room temperature) electrons in the conduction band couple with LO phonons, giving rise to Frolich interactions, which are responsible for the observation of a strong A_1(LO) mode intensity along with a possible shift of Raman peak positions [24]. Peaks at 1454 and 2196 cm^{-1} may be assigned to 2^{nd} and 3^{rd} order modes of A_1(LO) designated as $2A_1$(LO) and $3A_1$(LO) in Fig. 4.9b. These peak positions are also not the exact integral multiple of the fundamental mode as the higher order modes are not zone centre phonons.

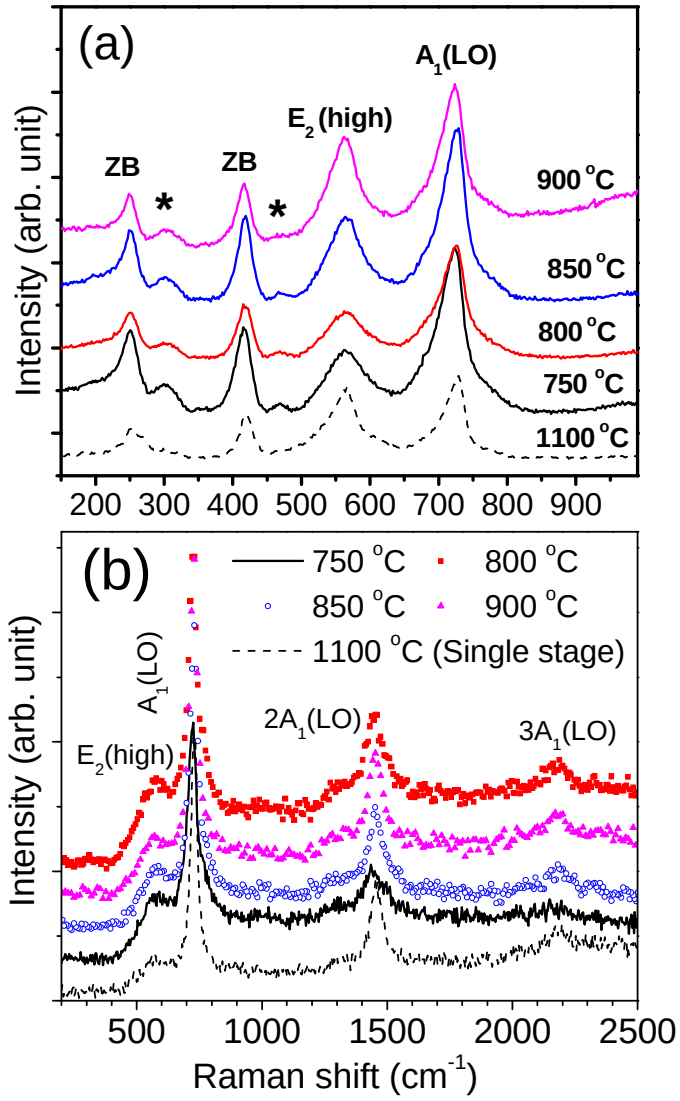


Fig. 4.9: a) Raman spectra of GaN nanostructures synthesized at different growth temperatures using 514.5 nm excitation. b) Resonance Raman spectra of GaN nanostructures synthesized at different growth temperatures using 325 nm excitation. Spectra are shifted vertically for clarity.

4.3.6 Photoluminescence (PL) analysis

Room temperature PL spectra of the pristine samples at various growth temperatures (Fig. 4.10a) show a dominant peak in the range of 1.7-2.1 eV using a 325 nm excitation from a He-Cd laser. A weak peak around 3.25 eV is also observed as shown in the zoomed spectra and the sharp peaks at 3.50 – 3.75 eV are Raman peaks (inset in Fig. 4.10). The broad intense peak around 1.7-2.1 eV may be assigned to a nitrogen di-vacancy [25]. A strong depletion in N is expected in the growth process with high preheating temperature of NH_3 at 1100 ^oC. As reported in the literature, dissociation of NH_3 starts at a temperature as low as 430 ^oC [20]. Thus a di-vacancy of N may be energetically favoured in this case. The peak at 3.25 eV may be assigned to free-to-bound (FB) recombination related emission [14]. In the present study Ga clusters in the absence of N will energetically favour the creaction of a deep level acceptor state [26], which may radiatively recombine with the free electron to give the FB band emission. In the absence of H, as the constituent is depleted at high preheating temperature, the FB band is supressed with un-compensated surface states present in the system.

Noting the low dissociation temperature of NH_3 [20], we have post-annealed these samples at the same time in NH_3 at 750 ^oC and atmospheric pressure for 30 min in order to demonstrate compensation for a nitrogen vacancy (V_N) as well to show passivation of the surface states using N and H, respectively. An elevated temperature of 750 ^oC was optimized keeping in mind the high energy required for the compensation of vacancy related point defects. We could clearly observe the decrease in the defect emission intensity and increase of the FB emission line in the annealed samples (Fig. 4.10b) as compared to that observed in the pristine sample (Fig. 4.10a). The N vacancies have been demonstrated to be compensated partially in the moderate annealing temperature for a short duration. The constituent H has also been demonstrated to passivate the surface states effectively as indicated by the clear increase in the FB band intensity.

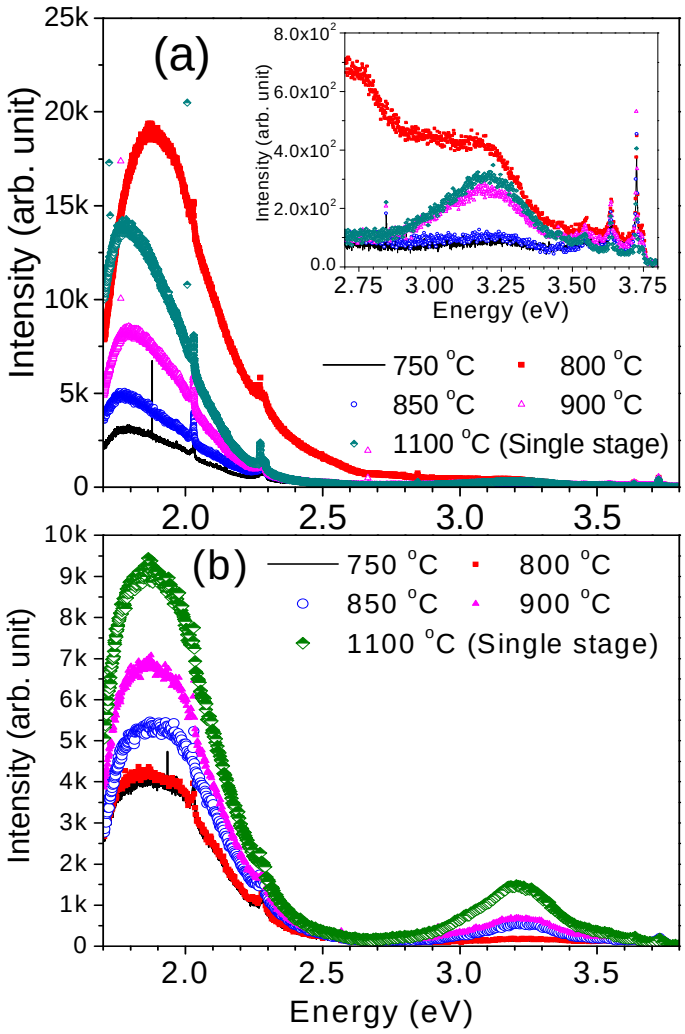


Fig. 4.10: Room temperature PL spectra a) for pristine GaN nanostructures synthesized at various growth temperatures showing broad and intense peak in the range of 1.7-2.1 eV. Inset shows the zoomed spectra for free-to-bound emission at around 3.25 eV, b) for post-annealed GaN nanostructures synthesized at various growth temperatures showing clear free-to-bound emission peak at around 3.25 eV.

4.4 Conclusion

The study shows formation of novel GaN nanostructures, made of small particulates of GaN with diameters in the range 12 - 16 nm at a very low temperature of 750 ^{o}C using the technique of pre-heating the reactant gas. A large surface area of 20 m^2/g has been achieved in the reported nanostructures. The effect of growth parameters such as reaction temperature, time, and flow rate on the synthesis of good quality GaN have been optimized in this study. The study has demonstrated that the NH_3 decomposition process plays an important role in the formation of GaN. A nitrogen vacancy related defect state at 1.7 – 2.1 eV is demonstrated to be partially compensated with post-annealing treatment in NH_3 along with the passivation of the surface states at 750 °C.

4.5 References

1. S. M. Kang, T. I. Shin, D. V. Dinh, J. H. Yang, S.-W. Kim, D. H. Yoan, Microelectr. Journ. 40 (2009) 373.
2. J. Hu, Y. Bando, D. Golberg, Q. Liu, Angew. Chem. Int. Ed. 42 (2003) 3493.
3. W. Han, S. Fan, Q. Li, Y. Hu, Sci. 277 (1997) 1287.
4. G. S. Cheng, L. D. Zhang, Y. Zhu, G. T. Fei, L. Li, C. M. Mo, Y. Q. Mao, Appl. Phys. Lett. 75 (1999) 2455.
5. W. Han, P. Redlich, F. Ernst, M. Ruhle, Appl. Phys. Lett. 76 (2000) 652.
6. X. Duan, C. M. Lieber, J. Am. Chem. Soc. 122 (2000) 188.
7. W. Shi, Y. Zheng, N. Wang, C. Lee, S. Lee, Adv. Mater. 13 (2001) 59.
8. X. Chen, J. Xu, R. M. Wang, D. Yu, Adv. Mater. 15 (2003) 419.
9. R. Koester, J. S. Hwang, C. Durand, D. Lee, S. Dang, J. Eymery, Nanotechnol. 21 (2010) 5602.
10. S. Wright, W. Lim, D.P. Norton, S. J. Pearton, F. Ren, J. L. Johnson, and A. Ural, Semicond. Sci. Technol. 25 (2010) 024002.
11. F. Xu, Y. Xie, X. Zhang, S. Y. Zhang, X.M. Liu, W. Xi, X. B. Tian, Adv. Funct. Mater. 14 (2004) 464.
12. B.V. L'vov, Thermochim. Acta 360 (2000) 85.
13. H. Z. Zhao, M. Lei, X. Yang, J. K. Jian, X. L. Chen, J. Am. Chem. Soc.127 (2005) 15722.
14. P. Sahoo, S. Dhara, S. Amirthapandian, M. Kamruddin, S. Dash, B. K. Panigrahi, A. K Tyagi, Cryst. Growth Des. 12 (2012) 2375.
15. K-W Chang, J-J Wu, J. Phys. Chem. B 106 (2002) 7796
16. L. Yu, Y. Ma, Z. Hu, J. Crystal Growth 310 (2008) 5237.
17. L. L. Low, F. K. Yam, K. P. Beh, Z. Hassan, Appl. Surf. Scie. 257 (2011) 10052.
18. L. L. Low, F. K. Yam, K. P. Beh, Z. Hassan, Appl. Surf. Scie. 258 (2011) 542.
19. W. Han and A. Zettl, Appl. Phys. Lett, 80 (2002) 2.
20. V. Hacker, K. Kordesch, in: W. Vielstich, A. Lamm, H.A Gasteiger (Eds.) Fundamentals, Technology and Application, Chichester, 2003, pp. 121-127.

21. P. Magudapathy, P. Gangopadhyay, B. K. Panigrahi, K. G. M. Nair and S. Dhara, Physica B 299 (2001) 142.
22. L. Chang, J. Chang, J. Yeh, H. Lin, and H. C. Shih, AIP Adv. 1 (2011) 032114.
23. P. Sahoo, S. Dhara, C. R Das, S. Dash, A. K Tyagi, B. Raj, P. Chandramohan, M. P. Srinivasan, Intl. J. of Nanotechnol. 7 (2010) 823.
24. S. Dhara, S. Chandra, G. Mangamma, S. Kalavathi, P. Shankar, K. G. M. Nair, A. K. Tyagi, C.W. Hsu, C. C. Kuo, L.C. Chen, K. H. Chen and K. K. Sriram, Appl. Phys. Lett. 90 (2007) 213104.
25. A. E. Younvich, Semiconductor, 32 (1998) 1054.
26. P. Boguslawski, E. L. Briggs and J. Bernholc, Phys. Rev. B 51 (1995) 17255.

Chapter 5

Functionalization and characterization of carbon coated GaN nanostructures

5.1 Introduction

Synthesis and characterization of GaN nanowires and their nanocomposites has been of great interest recently because this type of GaN is an important semiconductor in many applications [1]. Many attempts have been made to incorporate C into GaN [2]. However, the role of carbon introduced as an impurity into GaN is an unresolved issue [3].Carbon incorporated on GaN has been used to p-type dope the GaN and to form semi-insulating nitride layers for use in high electron mobility transistors (HEMTS) and for other devices [4]. However, Klein et al. observed a current collapse in HEMTS which they contributed to an unexpected deep C- related acceptor in the semi-insulating region [5].

The synthesis of GaN-carbon nanocomposites was first demonstrated using the arc discharge method. The method produced GaN nanorods and GaN carbon composite nanotubes [6]. Han and Fan also produced GaN nanorods through a carbon nanotube confined reaction [7]. Han and Zettl reported the synthesis of GaN nanorods coated with graphitic carbon layers by the deposition of carbon onto pre-produced GaN nanorods [8]. Sutter et al. reported the encapsulation of GaN nanowires in a crystalline carbon shell in the presence of carbon [9]. Studies thus reveal that GaN/C composites have been made and studied but an understanding of the materials has still to be realised. To investigate these materials further we have chosen to study GaN/C composites by using a simple CVD process.

In this study we report the synthesis of carbon coated GaN nanostructures using acetylene as carbon source on pre-produced GaN nanostructures by a CVD method. The functionalization of the material has also been investigated.

5.2 Experimental

5.2.1 Synthesis of carbon coated GaN (GaN/C)

A GaN/C composite was synthesised by decomposing acetylene (C_2H_2) (Afrox) on a pre-produced GaN nanostructure. The synthesis method to make GaN NSs was described in chapter 4. The GaN was placed in a quartz boat in the centre of a quartz tube. First, pure N_2 was allowed to flow through the quartz tube at a flow rate of 12 mL/min and then the GaN was heated between the temperatures of 500 - 650 ºC at 10 °C/min. The flow rate for C_2H_2 was varied from 50 to 100 mL/min. When the temperature reached the desired value, C_2H_2 was introduced at a flow rate of 100 ml/min at the required temperature while N_2 was used with the same flow rate. The reaction was allowed to take place for 1 h. At the optimum temperature of 600 °C and a flow rate of 50 mL/min, the reaction was allowed to take place for 1 h and 2 h. The furnace was then cooled to room temperature while N_2 was passed through the reactor and the crucible was removed from the reactor and weighed to establish the amount of GaN-carbon product formed.

5.2.2 Functionalisation of GaN/C

Concentrated nitric acid (55% HNO_3) and diluted nitric acid (30% HNO_3) was used to functionalise the GaN/C material synthesized at 600 °C for 1 h. The functionalization of GaN/C material was performed to introduce functional groups on the surface. GaN/C was immersed and stirred in 55% and 30% HNO_3 solution respectively for 6 hours in each of the solution at room temperature. The functionalized materials were washed with distilled water until the filtrate had a pH ~ 7 (neutral). The product was then dried in an oven overnight at 110 °C.

5.3 Results and discussion

5.3.1 HRTEM analysis

Fig. 5.1 shows TEM images of GaN/C nanostructures (T = 600 °C, t = 1 h) before functionalization. Fig. 5.2 and Fig. 5.3 show TEM images of the GaN/C after functionalization. This later product is referred to fGaN/C. It was observed that the surface of the GaN/C nanostructures was partially covered with carbon but the lattice fringes for carbon were not visible. This may be due to the carbon in the material being amorphous. The morphology of the GaN NSs did not change when carbon was deposited on the material. The structure still comprised of small crystallites of GaN in the form of a rod. It has been reported that GaN does not react with carbon although the small amount of carbon may be included as a dopant in the GaN [10]. This is due to the fact that graphitic carbon layers act as chemically inert protecting layers for GaN [8]. Han et al. also observed that both the composition and the morphology of GaN did not change during carbon deposition [8]. As such the interaction between the GaN and C is purely a physical one (such as van der waals forces). Selected area electron diffraction (SAED) patterns (inset in Fig. 5.2 and Fig. 5.3) show clearly visible diffraction spots when compared to Fig. 5.1 (inset) that can be indexed to the reflections of hexagonal GaN [11].

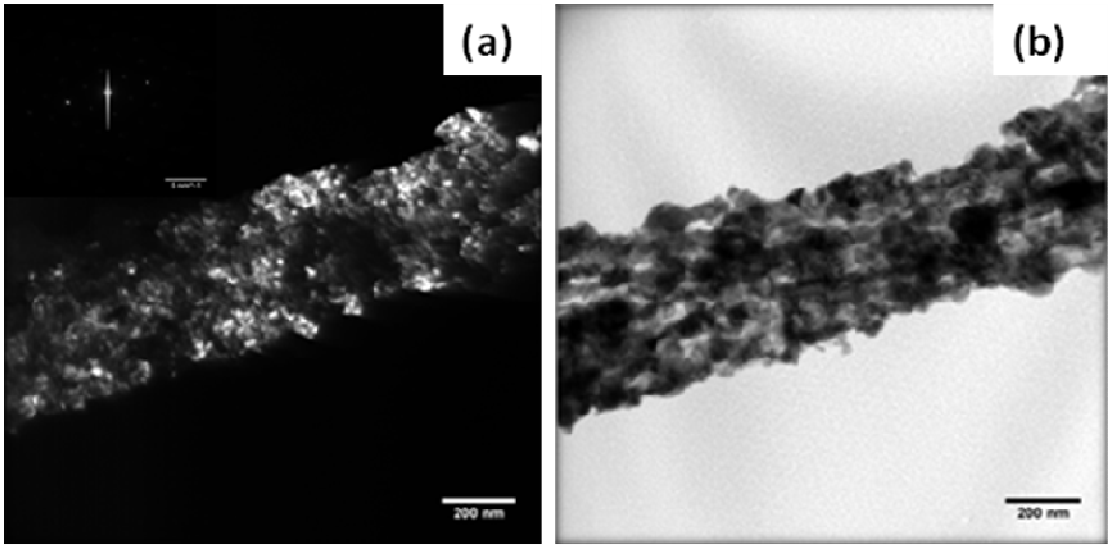


Fig. 5.1: TEM images. (a) Dark field image and SAED pattern (inset) (b) bright field image of GaN/C.

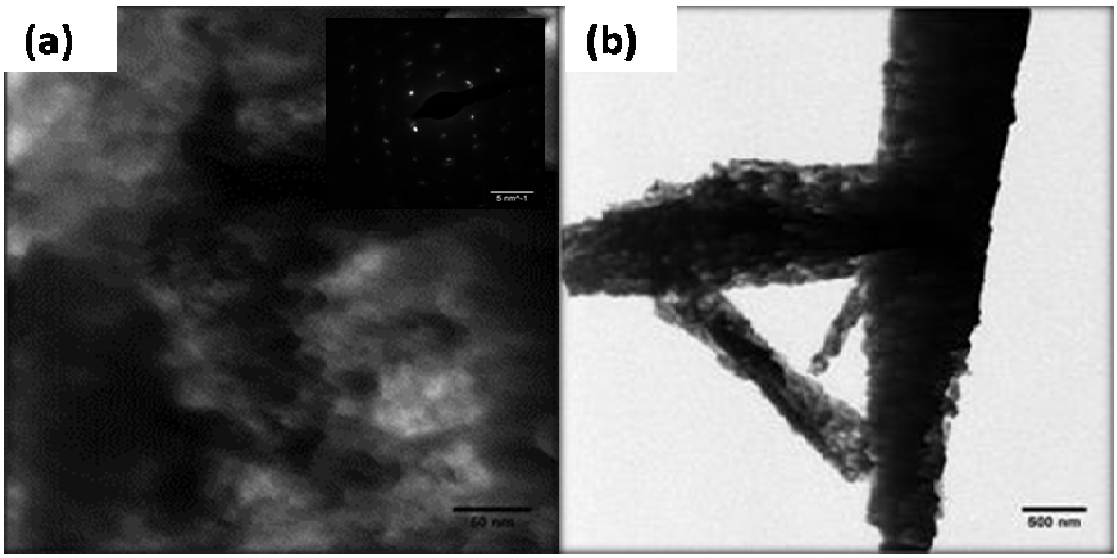


Fig. 5.2: (a) High magnification TEM images and SAED (inset) (b) TEM images of 30% fGaN/C.

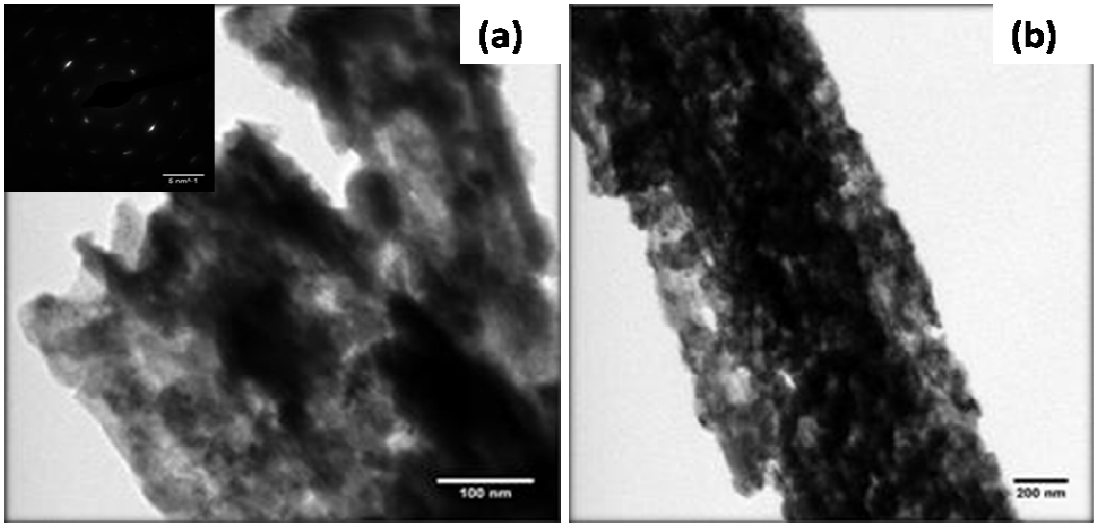


Fig. 5.3: (a) High magnification TEM images and SAED (inset) (b) TEM images of 55% fGaN/C.

5.3.4 TGA analysis

TGA analysis has been used to determine the thermal stability and composition of carbon in the GaN/C material. This material was first synthesised at different temperatures (500 - 650 °C) using a flow rate of 100 mL/min. Fig. 5.4 shows the TGA profiles run in air of GaN/C samples prepared at 500 - 650 °C. Also Fig. 5.5 shows the TGA profiles run in air of this material using a lower flow rate (50 mL/ min) at 600 °C for 1 and 2 h. It was observed that at 600 ºC there is ~ 9.5% weight loss of carbon while at 500, 550 and 650 ºC it is ~ 1.5, 4.5 and 5.5% respectively. This means that there was more carbon deposited on GaN/C sample prepared at 600 ºC when compared to other reaction temperatures. The data suggest that the carbon deposited at lower temperatures is amorphours and at 650 °C is graphitic. It was observed that when the flow rate was decreased from 100 ml/min to 50 ml/min the carbon deposited on the surface changed to ~17.5% and 10% after 1 h and 2 h respectively. This means that the lower flow rate deposited more carbon than the higher flow rate.

The differential TGA curves (Fig. 5.4) indicates that the carbon deposited at different temperatures is similar. The peak for GaN/C synthesized at 600 °C shifts slightly to the right. The deposition time, by contrast does indicate an effect on the TGA profiles (Fig. 5.5). The data suggest that carbon is less graphite after deposition after the longer reaction time (t = 2h).

Another feature noted from the TGA data is the increase in mass at T > 700 °C. This is due to the oxidation of the GaN as it converts to Ga_2O_3. There is no obvious correlation of the temperature at which this occurs and the amount of carbon deposited.

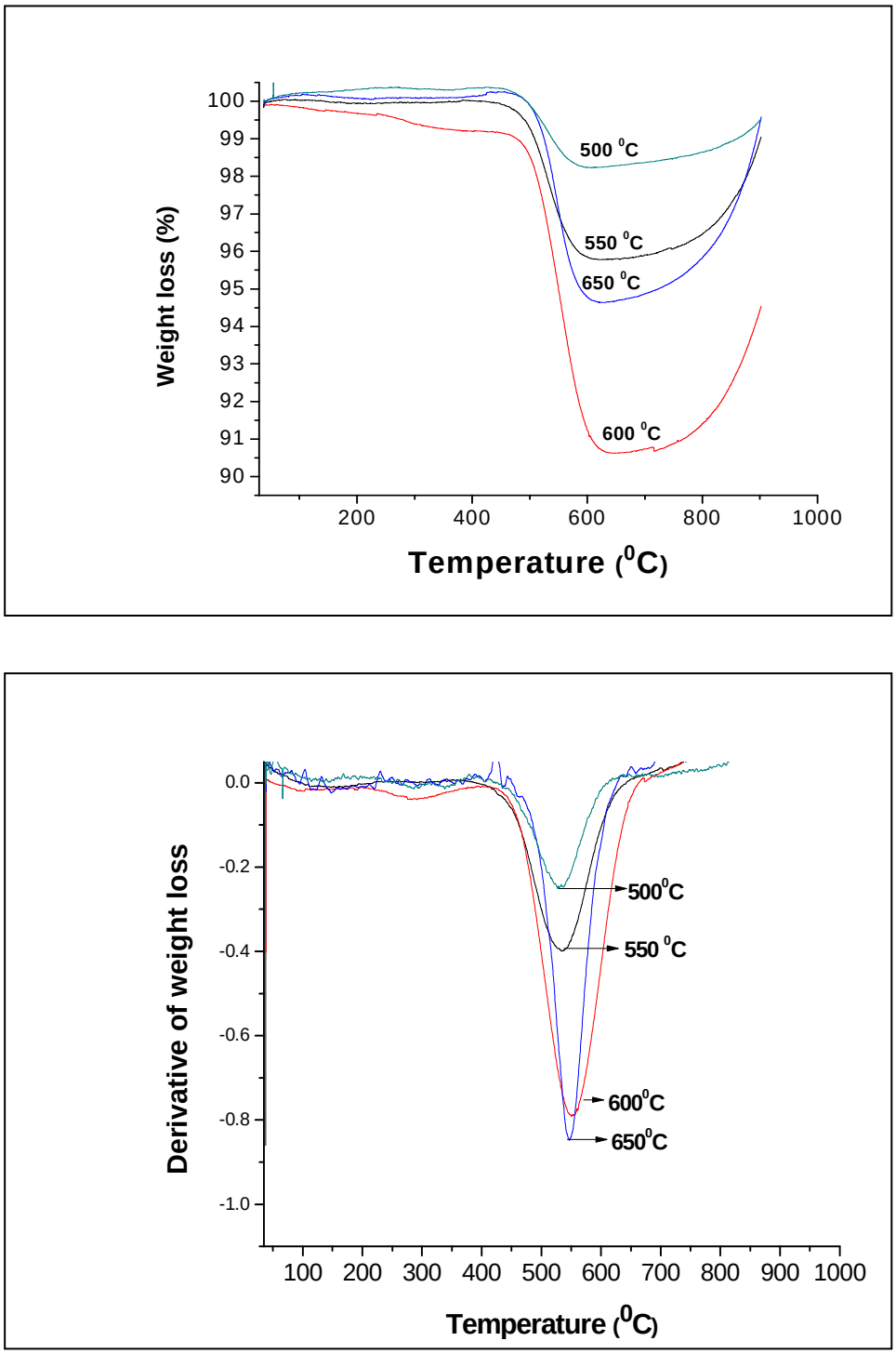


Fig. 5.4: TGA profile and derivative of GaN/C synthesized at different temperatures.

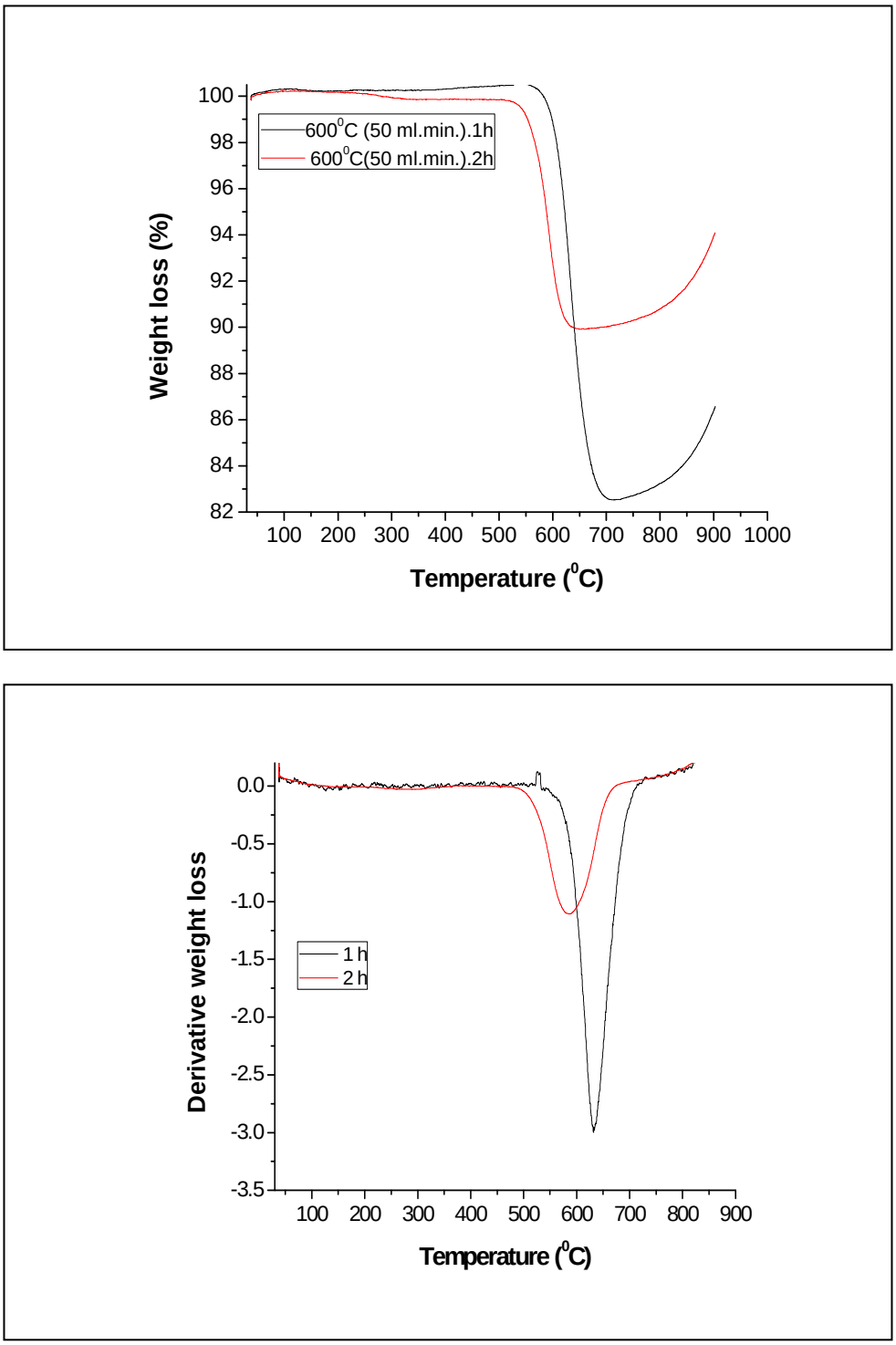


Fig. 5.5: (a) TGA profile and (b) the derivative of GaN/C as a function of time. (T = 600 °C, flow rate = 50 mL/min).

Fig. 5.6 shows the TGA profile run in air of GaN/C and fGaN/C (30% and 55% HNO_3) synthesised at 600 °C using a flow rate of 50 mL/min. It was observed that the thermal stability of the functionalised material decreased relative to GaN with the decomposition temperature decreasing from 633 °C to 531 °C. The weight loss for as synthesized sample was observed to be ~ 17% and for the 30% and 55% functionalised sample was shown to be about 8% and 6% respectively. A number of other features can be noted in the TGA data (i) less carbon on functionalized GaN/C and (ii) GaN coverted to Ga_2O_3.

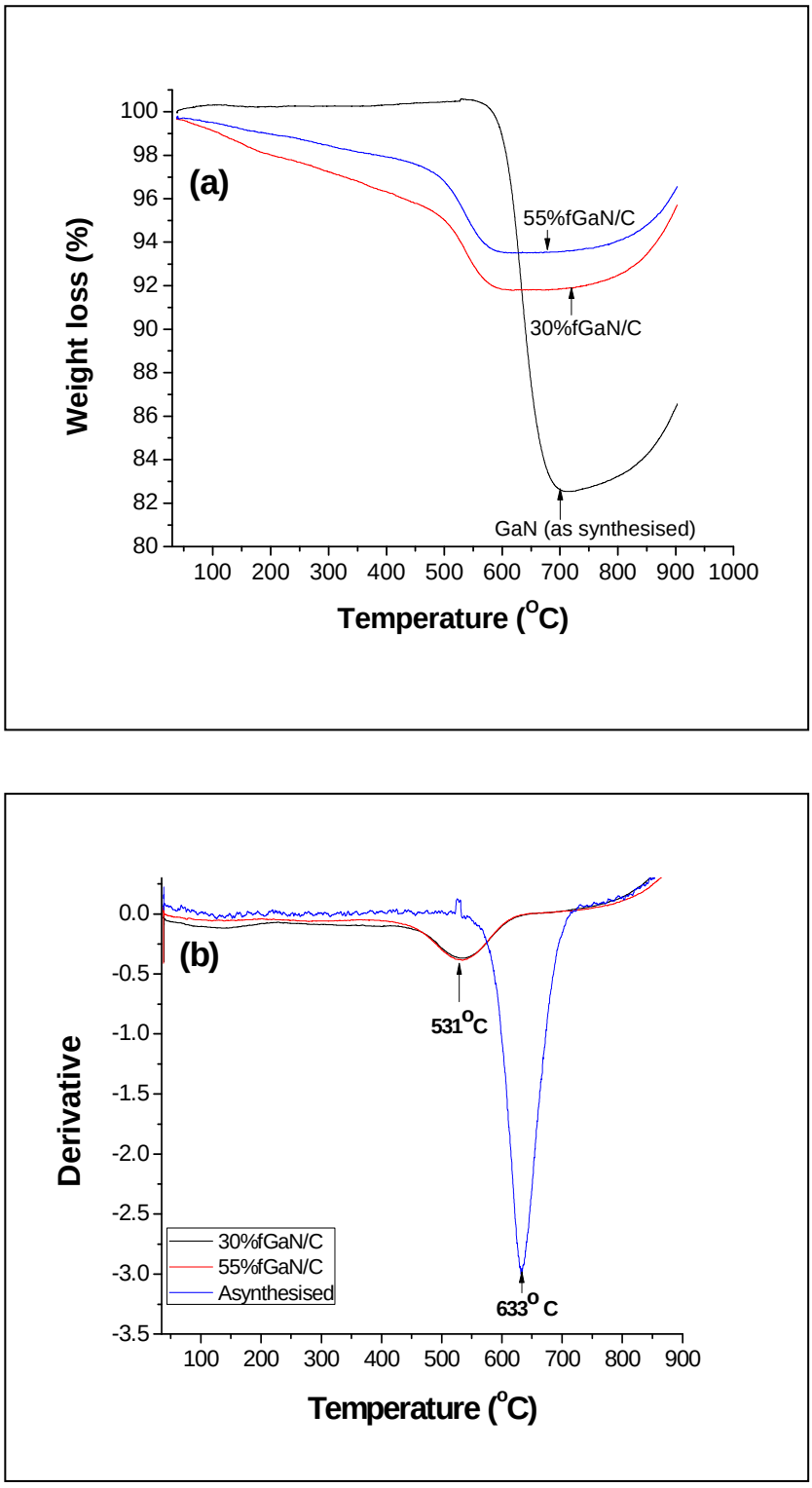


Fig. 5.6: TGA profile of (a) the functionalized samples and as synthesized GaN/C and (b) their derivative curves.

5.3.5 BET surface area analysis

Table 5.1 shows the surface area and the pore volume of the unfunctionalized and functionalized GaN/C materials after treatment with different concentrations of nitric acid. An increase of the surface area of the functionalized materials was observed while the change between the two samples treated with acid was nominal.

Table 5.1: BET surface area of carbon coated GaN and functionalised GaN/C.

Sample name	Surface area (m^2/g)	Pore volume (cm^3/g)
GaN/C	15.2	0.11
30%fGaN/C	19.3	0.14
55%fGaN/C	20.1	0.12

5.3.6 Raman analysis

Raman analysis has been used to study the vibrational properties of the GaN and fGaN materials. Fig. 5.7 shows four broad peaks for the as synthesized material and six peaks for the 30% and 55% acid functionalised materials. The peaks at 565 and 724 cm^{-1} were assigned to E_2(high) and A_1(LO) phonons respectively and the peaks at 1455 and 2186 cm^{-1} were assigned to the second and third phonon modes of A_1(LO). The intensity of the A_1(LO) mode peak in the functionalised material is sharper and higher than the E_2(high) mode and this shows that the material has a high electronic quality. The peaks at 1328 and 1590 cm^{-1} were assigned to disorder (D band) and ordered graphite (G band) peaks associated with the carbon on the GaN. The broad peak of a D band suggests that the carbon on GaN is disordered.

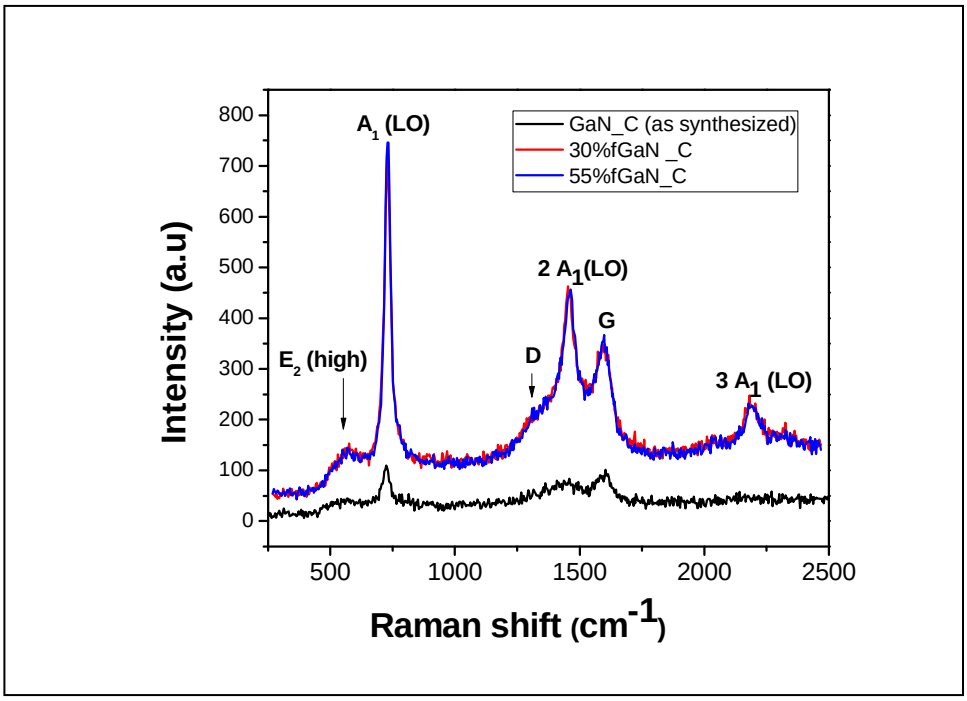


Fig. 5.7: Raman spectra for as synthesized and fGaN/C samples.

5.3.7 Photoluminescence (PL) analysis

The optical properties of GaN/C synthesised at 600 °C for 1 h were measured by PL using 325 nm excitation from a He-Cd laser. Fig. 5.8 shows the peaks in the 1.8-2.3 eV region that are associated with a yellow luminescence band. The yellow luminescence in GaN is associated with a broad luminescence band around 2.2-2.3 eV [12]. It has been reported that the carbon incorporated into GaN produces yellow luminescence around 2.2 eV [13]. Ogino and Aoki also reported that the peak around 2.2 eV is due to the transition between a shallow donor and a deep acceptor. They explained that the deep acceptor consists of a gallium vacancy and a carbon atom substituted next to the gallium sites [14]. Carbon in GaN acts as an acceptor and occupies an anion site [13]. The UV emission band at 3.3 eV is associated with the near band-edge transition of GaN [15]. Fig. 5.9 shows the higher magnified PL spectrum between 2.2 and 2.4 eV.

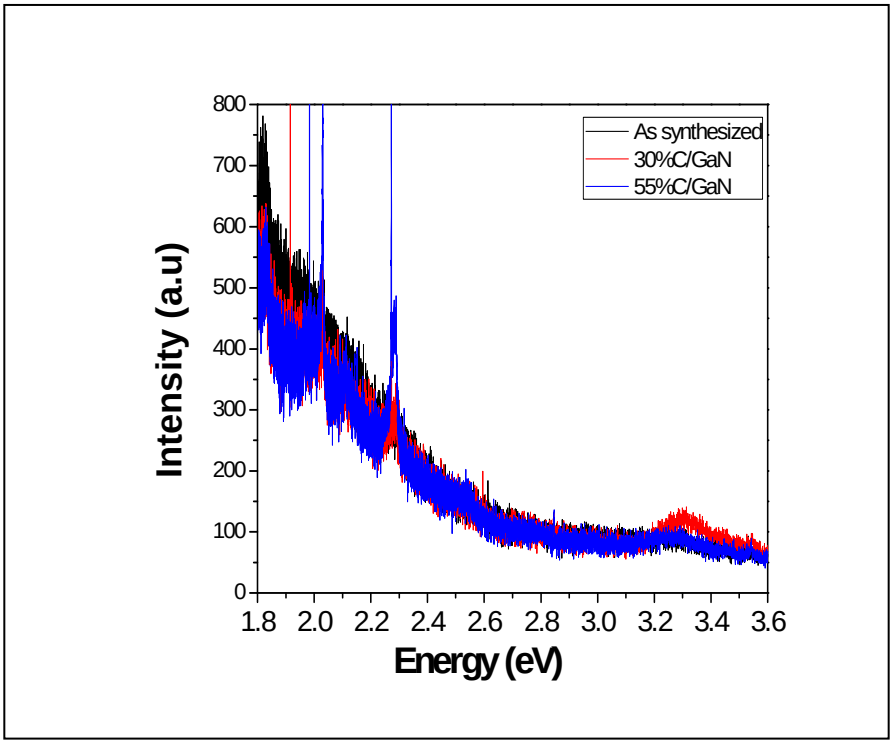


Fig. 5.8: Room temperature PL spectra for GaN/C and fGaN/C.

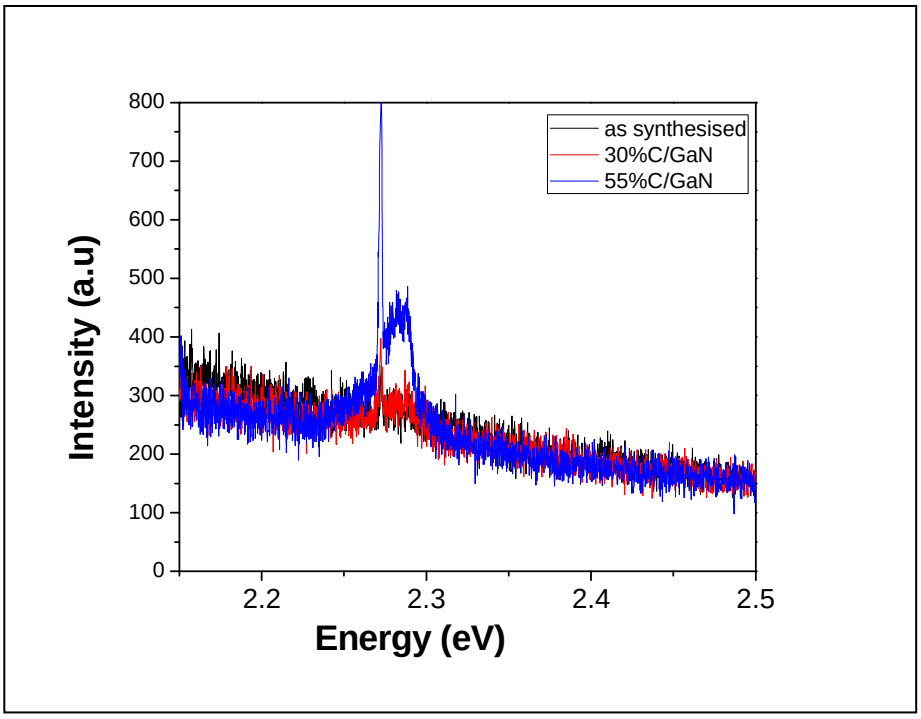


Fig. 5.9: Room temperature PL spectra (zoom) for GaN/C and functionalized GaN/C.

5.4 Conclusions

The study showed that GaN NS can be partially covered with carbon at CVD temperatures between 500 °C – 600 °C when acetylene is deposited over GaN. The morphology of the nanostructures did not change when carbon was deposited on the surface of the GaN. Selected area electron diffraction (SAED) patterns of the functionalized GaN/C nanostructures show clearly visible diffraction spots. The thermal stability of functionalized GaN/C decreased with decomposition temperature. The increase in mass at T > 700 °C was due to the oxidation of the GaN as it converts to Ga_2O_3. An increase in surface area of the functionalised materials and a high electronic quality on the functionalised GaN/C materials was observed. A yellow luminescence band and the near band – edge transition on as synthesised GaN/C and fGaN/C was observed.

5.5 References

1. H. W. Seo, S. Y. Bae, J. Park, H. Yang, K. S. Park, S. J. Kim, J. Phys. Chem. 107 (2003) 6379.
2. A. F. Wright, J. Appl. Phys. 92 (2002) 2575.
3. C. H. Seager , A. F. Wright, J. Yu, W. Gotz, J. Appl. Phys. 92 (2002) 6553.
4. T. Kimura, S. Ootomo, T. Nomura, S. Yoshida, T. Hashizume, Jpn. J. Appl. Phys. 46 (2007) L224.
5. P. B. Klein, S. C. Binari, K. Ikossi, A. E, Wickenden, D. D. Koleske, R. L. Henry, Appl. Phys. Lett.79 (2001) 3527.
6. W. Han, P. Redlich, F. Ernst, M. Ruhle, Appl. Phys. Lett., 76 (2000) 652.
7. W. Han, S. Fan, Q. Li, Y. Hu, Science, 277 (1997) 1287.
8. W. Han, A. Zettl, AdV. Mater. 14 (2002) 1560.
9. E. Sutter, P. Sutter, R. Calarco, T. Stoica, R. Meijers, Appl. Phys. Lett. 90 (2007) 093118.
10. G. Popovici, H. Morkoc, S. N. Mohammad, in Group III Nitride Semiconductor Compounds (Ed: B. Gil), Clarendon Press, Oxford 1998, Ch.2.
11. L. Yang, C. Xu, C. Wang, H. Li, Nanotechnol. 14 (2003) 50.
12. J. Neugebauer and C. G. Van de Walle, Appl. Phys. Lett. 69 (1996) 503.
13. R. Zhang, T. F. Kuech, Appl. Phys. 72 (1998) 1611.
15. T. Ogino, M. Aoki, Jpn. J. Appl. Phys. 19 (1980) 2395.
16. S. C. Lyu, O. H. Cha, E. K. Suh, H. Ruh, H. J. Lee, Chem. Phys. Lett. 367 (2003) 136.

Chapter 6

Synthesis and functionalization of GaN/C nanostructured composites for hydrogen gas sensing

6.1 Introduction

Wide band gap semiconductors such as GaN, SnO_2, TiO_2 and ZnO have excellent potential for H_2 gas sensing because of their sensitivity to surface charge and their ability to operate over large temperature ranges [1-5]. Hydrogen gas sensors based on oxides such as, ZnO nanorods, SnO_2 nanowires, and In_2O_3 nanowires have been reported and they show excellent response and recovery characteristics [1, 3, 6] due to their high surface area to volume ratios [7]. However few reports on H_2 gas sensors based on GaN nanowires which can offer environment stability have been reported [8].

Highly sensitive and selective hydrogen gas sensors are needed in many industries for the detection of H_2 leakage [9]. Pd and Pt are commonly used catalysts to improve the sensitivity and selectivity of GaN [8, 10]. The metal leads to catalytic dissociation of H_2 to atomic hydrogen, which generates a sensor response through binding to surface atoms and altering the surface potential [11]. The mechanism of a metal deposited on a functional layer for H_2 sensing is well understood and is used as a matter of choice. Both Pt and Pd have been used as the metals of choice to make functional layers on oxide and nitride based sensors. There have been a few studies that have compared Pt and Pd metal functionalities in the above reactions [10, 12, 13].

In this study we report the synthesis and characterization of GaN/C nanostructures (NSs) for hydrogen gas sensing. The GaN/C NSs were synthesised by a CVD method at high temperature (1100 °C) by using a mixture of gallium oxide and activated carbon. The activated carbon was used to reduce the synthesis temperature and the reaction time. The range of Ga_2O_3 to carbon ratios used were 1:0.5, 1:1, 1:2, 1:3, 1:4, and 1:5. These materials were then functionalised with a piranha solution. The functionalised materials were loaded with 3% Pd metal and characterized by different techniques and hydrogen gas sensing was performed on the metal loaded GaN NSs at room temperature.

6.2 Experimental

6.2.1 Synthesis and functionalization of GaN/C NSs

The GaN/C NSs were synthesized by a CVD method using Ga_2O_3 and activated carbon as precursors. Commercial gallium oxide (Ga_2O_3) (Sigma Aldrich) was used as a source of Ga, Norit activated carbon (C) as a reducing agent, and ammonia (NH_3) (Afrox) gas was used as the nitrogen source. Different ratios of Ga_2O_3 to activated carbon (1:0.5, 1:1, 1:2, 1:3, 1:4, 1:5) were mixed together and placed in a crucible in the centre of a quartz tube in a horizontal furnace. First, pure N_2 was allowed to flow through the quartz tube at a flow rate of 12 mL/min and then the Ga_2O_3 was heated to 1100 °C at 10 °C/min under the N_2 flow. Pure NH_3 at a flow rate of 12 mL/min was introduced when the temperature reached the desired value (1100 °C) while N_2 was continuously flowed with the same flow rate. The reaction was allowed to take place for 30 min, 45 min, 1 h and 1.5 h respectively. The furnace was then cooled to room temperature while N_2 was passed through the reactor. The crucible was then removed from the reactor and weighed to establish the amount of GaN product formed. Yellow, grey and black powders were obtained depending on the amount of carbon used. The colour of GaN with different ratios is yellow (1:0.5-1:1), grey (1:2 -1:3) and black (1:4-1:5). The carbon with the ratios of 1:05 and 1:1 made pure GaN.

The GaN made with gallium oxide and activated carbon ratios (1:0.5, 1:2 and 1:5) was used in further studies. A piranha solution (i.e. mixture of 0.52 M HNO_3 + 0.12 M H_2SO_4) was used to functionalise the GaN NSs material. GaN was immersed and stirred in the piranha solution for 1 hour at room temperature. The functionalised materials were washed with distilled water until the filtrate had a pH ~ 7 (neutral). The product was then dried in an oven at 110 °C overnight.

6.2.2 Preparation of Pd (3 wt %) loading on GaN/C support.

The functionalised material was used to prepare a Pd/GaN catalyst. These catalysts were prepared using the liquid phase reduction method in an ethylene glycol solution. The support (200 mg) was placed into a 250 mL round bottomed flask and ethylene glycol (60 mL) was added to the flask. The flask contents were sonicated for 15 min followed by magnetic stirring for 30 min. The metal precursor solution (0.05 M palladium acetate) was then added drop-wise to the mixture of GaN support and ethylene glycol (60 mL). The concentrations of the precursor solutions in the ethylene glycol solutions were calculated in order to prepare catalysts with metal loadings of 3 wt %. The resultant solution was vigorously stirred with a magnetic stirrer for a further 3 h at room temperature and then refluxed at 195 ^{o}C in an oil bath for 3 h. The solution was then cooled to room temperature. The resultant solution was filtered and thoroughly washed with 20 mL of acetone followed by excess distilled water. The resulting supported metal catalysts were dried in air for 8 h at 80 ^{o}C.

6.3 Characterization of GaN NSs

The morphology and structure of the GaN NSs were ascertained by scanning electron microscopy (SEM; JEOL 7500F SEM) and transmission electron microscopy (TEM; FEI Tecnai G^2 Spirit electron microscope at 120 kV), respectively. Powder X-ray diffraction (PXRD; Bruker D2 Phaser) was used to study the crystallinity of the materials. A Brunauer-Emmett-Teller (BET) TRISTAR 3000 analyzer was used to measure the surface area and porosity. Raman spectroscopy (Jobin-Yvon LabRAM) with the 514.5 nm line of an argon ion laser, a 600 gr/mm grating and a liquid cooled CCD detector was used to investigate the vibrational properties. Resonance Raman and photoluminescence (PL) spectroscopic studies was performed in the backscattering configuration using a micro-Raman setup (InVia, Renishaw) with 325 nm excitation from a He-Cd laser, 2400 gr/mm grating and a thermoelectrically cooled CCD detector.

6.4 Results and discussion

6.4.1 PXRD analysis

In an attempt to lower the synthesis temperature and reaction time, activated carbon was mixed with Ga_2O_3. The role of activated carbon was to reduce the Ga_2O_3. When a range of Ga_2O_3 to activated carbon ratios were used (1:0.5, 1:1, 1:2, 1:3, 1:4, and 1:5) at 1100 °C, GaN was produced. However, GaN was not obtained at temperatures below 1100 °C in a single stage oven. Fig. 6.1 shows that a reaction time of 30 – 45 min at 1100 °C was sufficient to yield GaN and no Ga_2O_3 was observed. It was observed (Fig. 6.2) that a ratio of Ga_2O_3:C of 1:0.5 (w/w) was sufficient to form GaN in 45 min at 1100 °C.

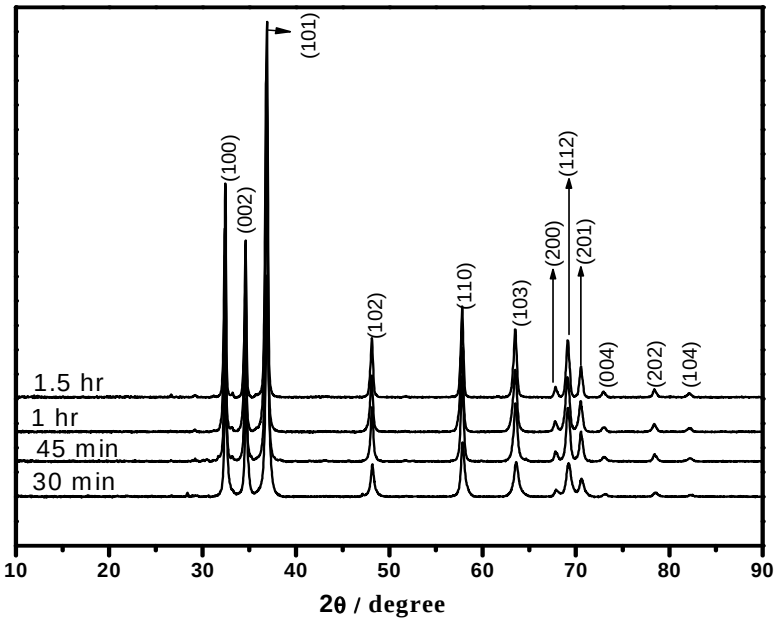


Fig. 6.1: PXRD patterns showing the effect of synthesis time on GaN synthesis using a Ga_2O_3/C ratio (1:3) in NH_3 at 1100 °C.

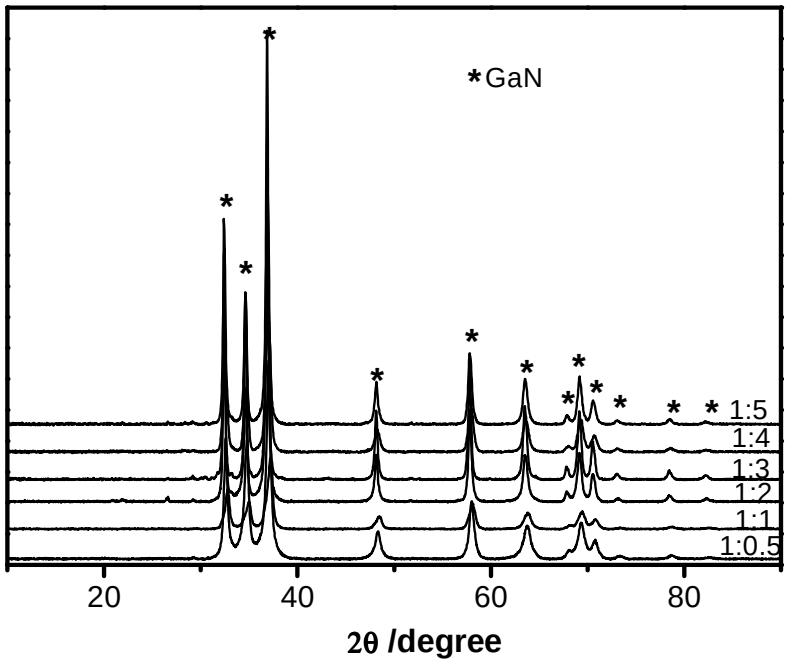


Fig. 6.2: PXRD patterns showing the effect of Ga_2O_3/C ratio on the synthesis of GaN NSs. Synthesis was carried out at 1100 °C for 45min.

6.4.2 Morphological studies.

When activated carbon was used in the synthesis reaction, the obtained GaN NSs had small sizes and most of them were cylindrical in shape (Fig. 6.3). As the activated carbon ratio varied so did the morphology change from a rectangular (Fig 6.3b) to a rod (Fig 6.3f) like structure. Amorphous carbon was observed in SEM results when the ratio of Ga_2O_3: C was greater than 1:1. When the ratio of Ga_2O_3: C was less than 1:3 the GaN NSs appeared as nanoparticles that were agglomerated and rod-like with a rough surface. It was observed that when the ratio of Ga_2O_3: C was greater than 1:2 the surface of GaN NSs became smoother, the diameter was reduced and the rods became straighter and longer.

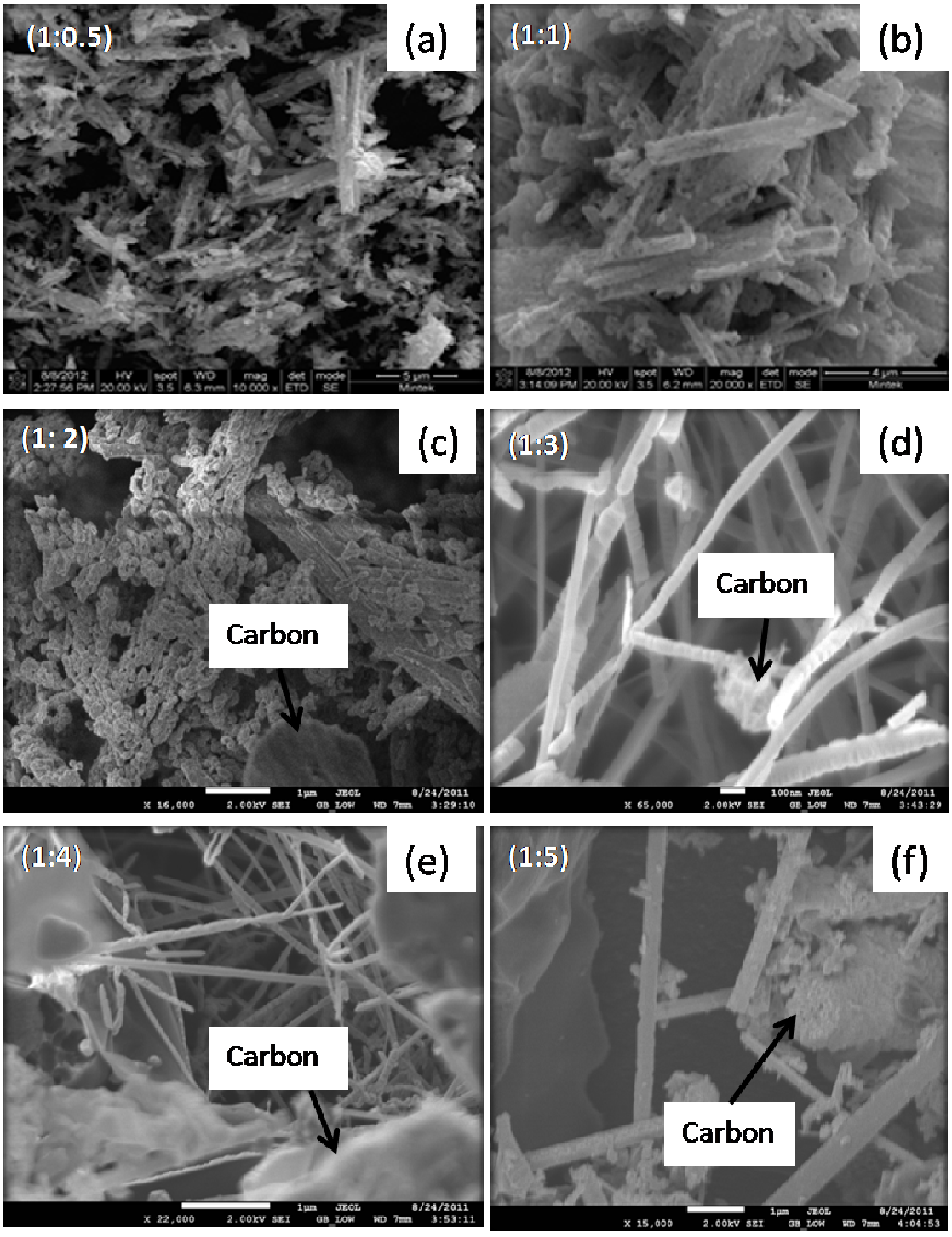


Fig. 6.3 SEM images of GaN synthesised with different ratios of Ga_2O_3 to activated carbon (a) 1:0.5 (b) 1:1 (c) 1.:2 (d) 1:3 (e) 1: 4 (f) 1: 5

6.4.3 BET Analysis

Table 6.1 shows the surface area and pore volumes of the products synthesized at 1100 °C. The activated carbon used was highly porous in nature and had a surface area of 1110 m^2/g. The commercial Ga_2O_3 used had a surface area of 10.0 m^2/g. The surface area of GaN synthesized with activated carbon showed an increase in surface area as the amount of activated carbon was increased. This is due to the high surface area of the activated carbon that was left in the GaN sample. However the surface areas of GaN synthesized using Ga_2O_3/C precursors with (1:0.5) and (1:1) ratios were less than the pure GaN product formed without activated carbon. This suggests that all the activated carbon was used up during the reaction.

Table 6.1: BET surface areas showing the variation of surface area with and without carbon (synthesis time = 45 min, temperature = 1100 °C). The ratio refers to the Ga_2O_3: C mass ratio.

Reaction precursors	**Surface area (m^2/g) of GaN materials**	**Pore volume (cm^3/g)**
$Ga_2O_3 + NH_3$	10.8	0.06
Ga_2O_3/C (1:0.5)	8.1	0.02
Ga_2O_3/C (1:1)	8.6	0.04
Ga_2O_3/C (1:2)	49.3	0.06
Ga_2O_3/C (1:3)	568	0.39
Ga_2O_3/C (1:4)	935	0.61
Ga_2O_3/C (1:5)	1093	0.72

6.4.4 TGA analysis

Fig. 6.4 and Fig. 6.5 show the TGA profiles and the derivative plots of the GaN materials synthesized in the presence of activated carbon. The carbon content of the different materials can be associated with the weight loss when carbon is oxidized in air. The materials synthesized by passing NH_3 over Ga_2O_3 alone as well as passing NH_3 over samples with Ga_2O_3: C (1:0.5) and Ga_2O_3: C (1:1) ratios were thermally stable up to 950 °C. No carbon was observed suggesting that the carbon was used up in the reaction. When the Ga_2O_3: C ratios were greater than 1:2 and 1:3, the decomposition of carbon occurred between 600 and 650 °C. No gallium oxide being formed (see TGA in Chapter 5). The peak positions of the GaN materials in Fig. 6.5 were shifted to the right compared to the peak of the activated carbon. This indicates that the GaN composites are thermally stable up to ~ 650 °C unlike the activated carbon (< 600 °C). The weight loss increased with the Ga_2O_3: C ratio (see Fig. 6.5). The results suggest that the optimum condition to make good quality GaN NSs is to use 1:0.5 – 1:1 ratios of Ga_2O_3 and C to ensure all the C is reacted.

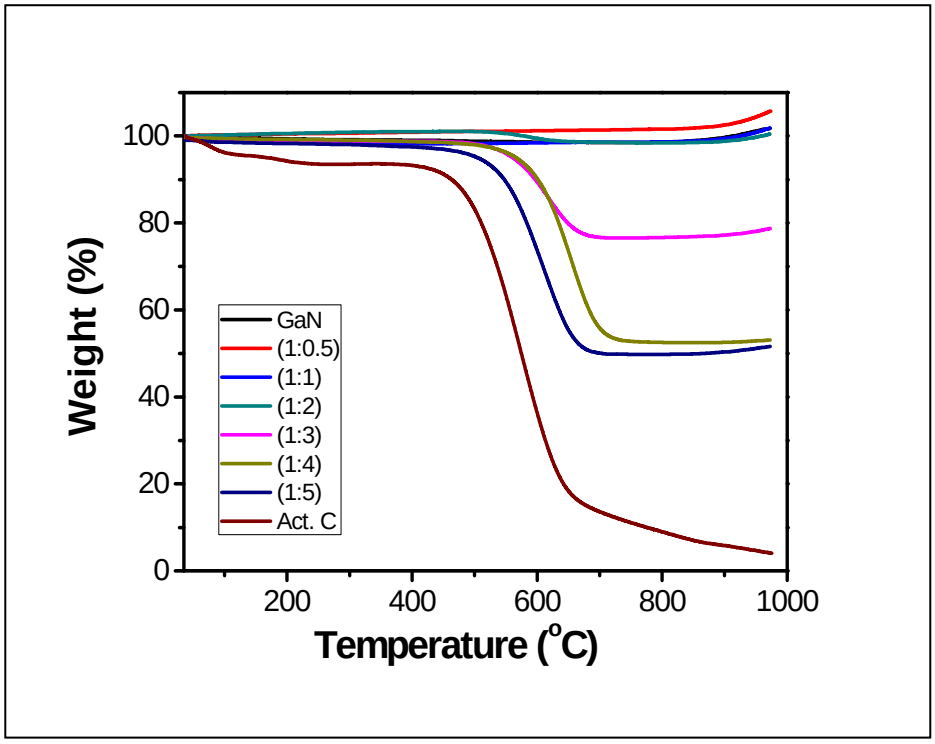


Fig. 6.4: TGA profiles of GaN NSs synthesized with and without activated carbon at 1100 °C.

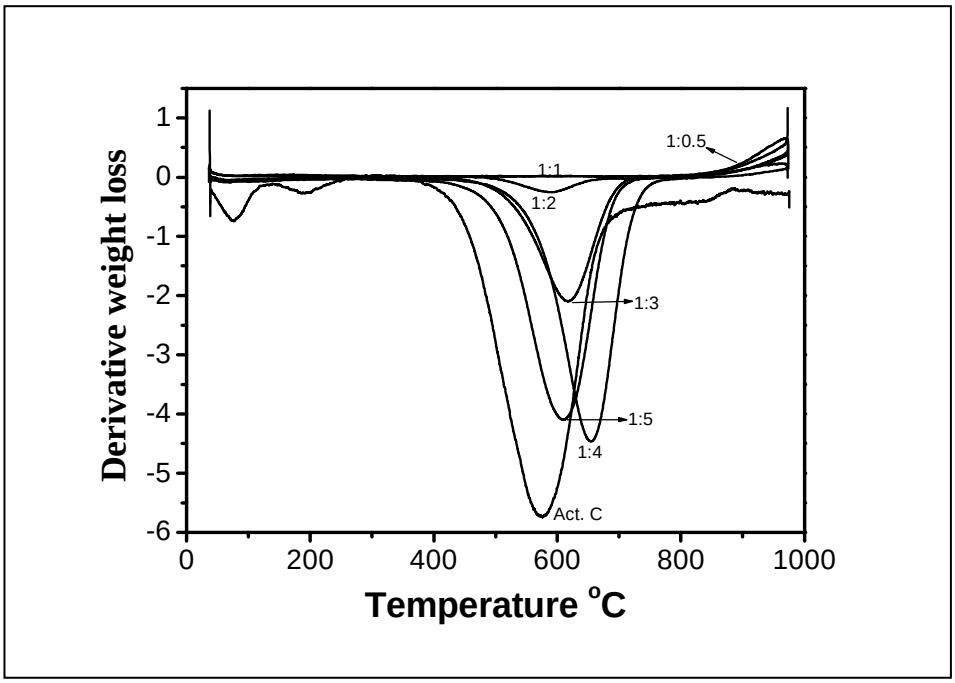


Fig. 6.5: Derivative plots of GaN-NSs synthesized with and without activated carbon at 1100 °C.

6.4.5 Raman spectroscopic analysis

The vibrational properties of the GaN NSs were investigated by Raman spectroscopy. The technique has been established to be a valuable tool for probing phonon excitations in semiconductors [14] and for the investigation of material properties such as doping concentration, lattice defect identification, or crystal orientation [15]. Fig. 6.6 (a) shows six phonon bands in the Raman spectrum of GaN for the GaN synthesized with Ga_2O_3:C ratios of 1:0.5 - 1:5. The peaks at 720 cm^{-1} and 562 cm^{-1} are associated with the A_1(LO) mode and E_2(high) mode respectively. The peaks at 412 cm^{-1} and 250 cm^{-1} are assigned to a zone boundary (ZB) phonon in the finite sized NSs. The peaks at 307 and 353 cm^{-1} marked as (*) are of unknown origin.

Fig. 6.6 (b) show the resonance Raman spectrum with a strong A_1(LO) phonon mode at 731cm^{-1} along with an E_2(high) mode at 564 cm^{-1}. These modes deviate slightly from the phonon modes reported in the non-resonant condition. It has been reported that when the excitation energy is greater than the band gap of GaN the electrons in the conduction band couple with LO phonons to make Frolich interactions, which are responsible for the observation of a strong A_1(LO) mode intensity along with a possible shift of Raman peak positions [16]. The peaks at 1305 and 1608 cm^{-1} were assigned to disorder (D band) and ordered graphite (G band) peaks associated with the carbon on the GaN and the peaks at 1456 and 2190 cm^{-1} may be assigned to 2^{nd} and 3^{rd} order modes of A_1(LO).

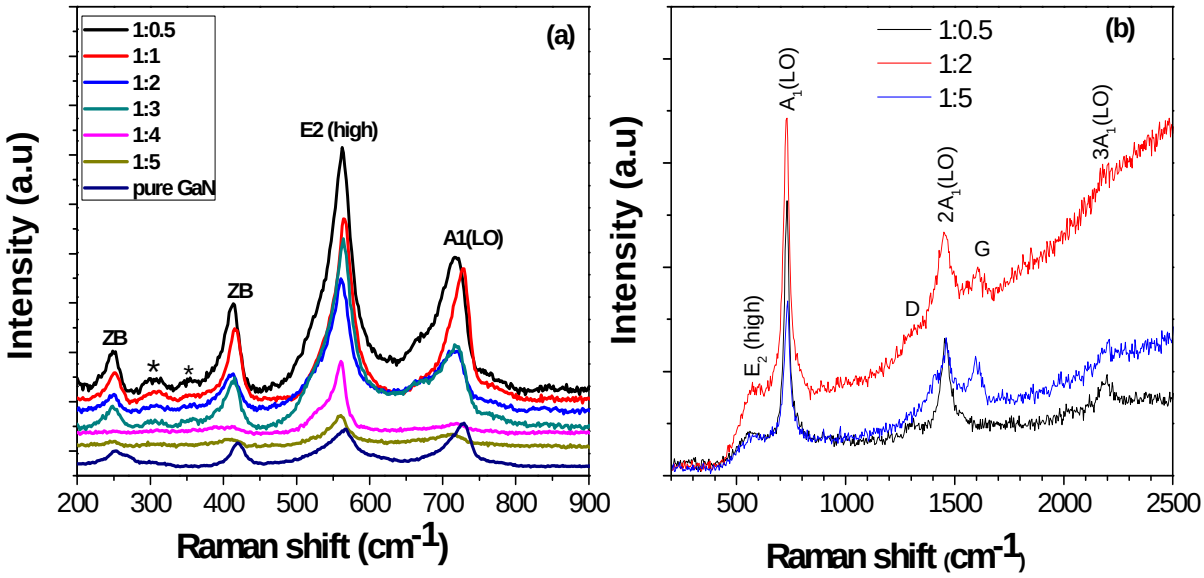


Fig. 6.6: (a) Raman spectra of GaN nanostructures with different ratios of Ga_2O_3/C using the 514.5 nm excitation. (b) Resonance Raman spectra of GaN nanostructures with different ratios of Ga_2O_3/C using 325 nm excitation.

6.4.6 Photoluminescence (PL) analysis

Fig. 6.7 shows the room temperature PL spectra for GaN nanostructures doped with different ratios of Ga_2O_3 to activated carbon using the 325 nm excitation. When the ratios of 1:0.5, 1:2, 1:5 of Ga_2O_3 to activated carbon was used, peaks at 3.27, 3.28 and 3.31eV were observed and associated with free-to-bound (FB) recombination related emission [17]. Ga vacancies favour the creation of a deep level acceptor state [18], which may radiatively recombine with the free electron to give the FB band emission. A strong depletion in N is expected in the growth process at high temperature (1100 °C). It is reported in the literature that the NH_3 starts to dissociates to species at a temperature as low as 430 ^oC [19]. The other peaks between 3.6 - 3.8 eV are Raman peaks.

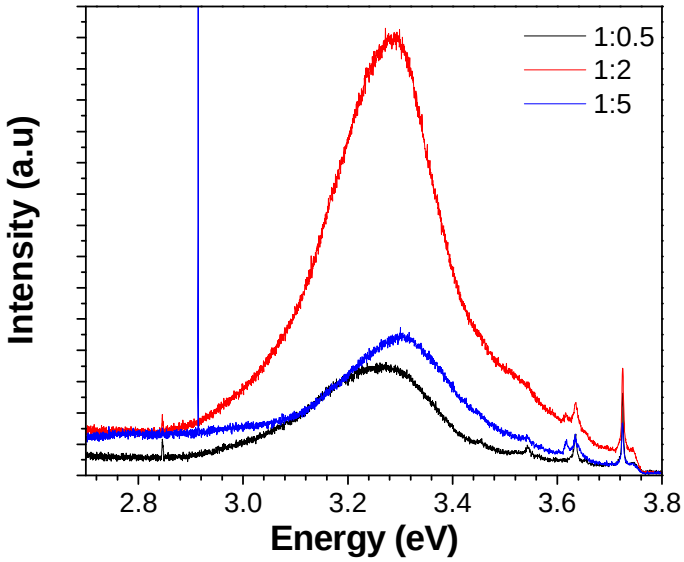


Fig. 6.7: Room temperature PL spectra of the GaN nanostructures with different ratios of Ga_2O_3/C using the 325 nm excitation.

6.4.9 Morphological studies and elemental analysis after 3%Pd loaded on GaN NSs.

Fig. 6.8 shows the high magnification TEM images of 3%Pd loaded on GaN NSs synthesized using a 1:2 ratio of Ga_2O_3 to activated carbon. It was observed that the small Pd metal particles (the circled dark spots) were dispersed on the surface of GaN NSs. The EDX spectrum (Fig. 6.9) also confirmed the presence of Pd metal on the surface and the quantitative results with weight % (inset) of each element detected in the material are shown. The Cu is from the grid that was used to prepare the sample for the analysis. The P, Fe and Co elements are impurities. These are present in very small amounts < 1 %.

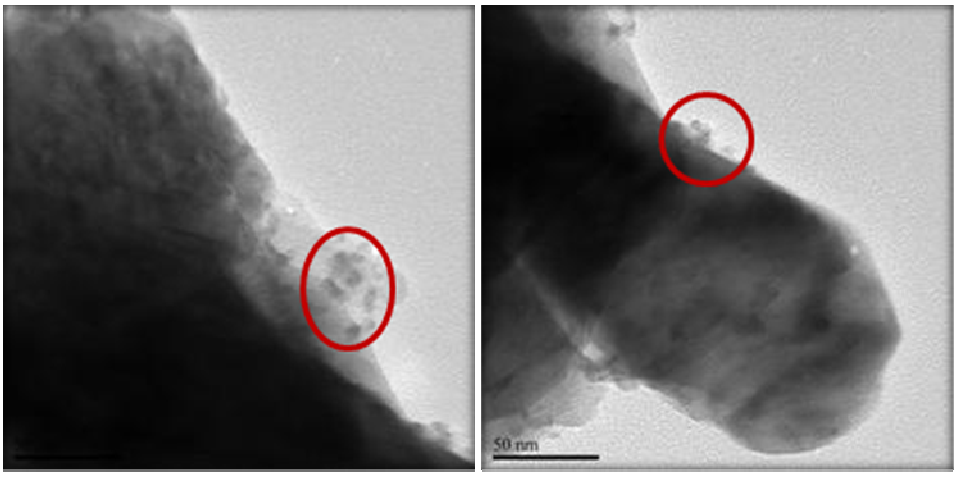


Fig. 6.8: TEM images of 3%Pd /GaN/C (1:2) synthesized at 1100 °C.

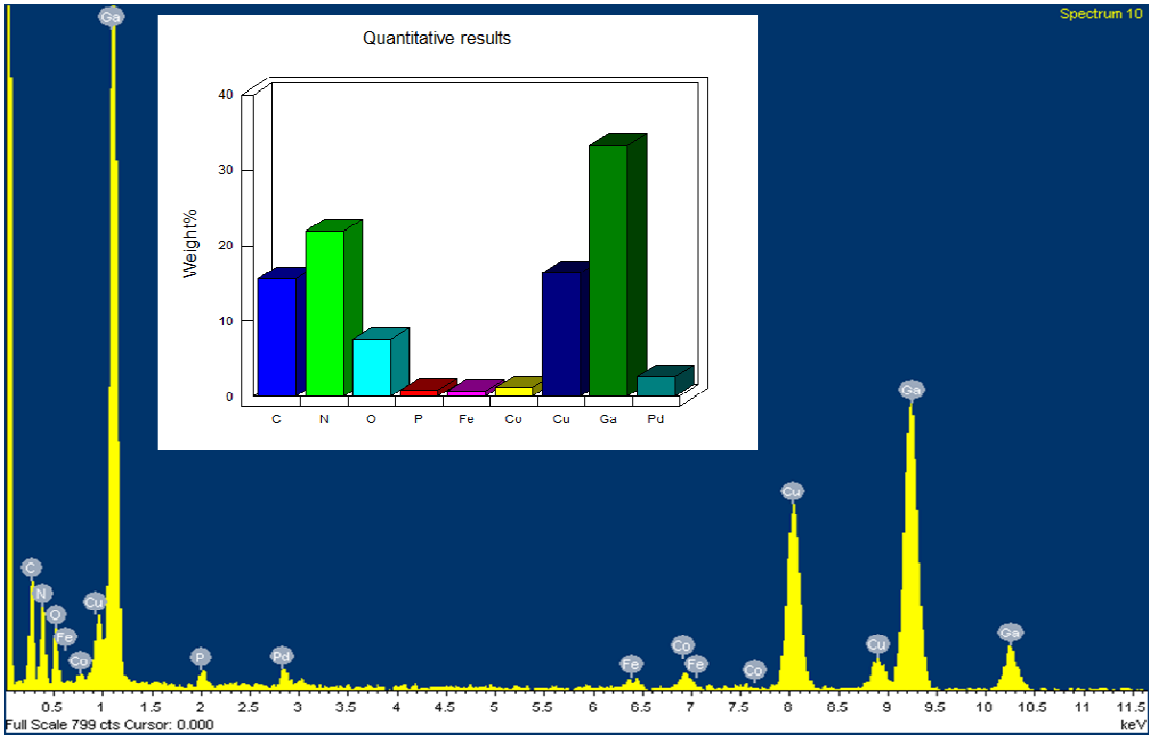


Fig. 6.9: EDS spectrum of 3%Pd/ GaN /C (1:2) synthesized at 1100 °C.

6.5 Hydrogen gas sensing

A H_2 gas sensing study was initiated on Pd loaded GaN NSs made with a Ga_2O_3/C ratio of 1:2. The response from using different concentrations of H_2 (200 – 500 ppm) was recorded at 200 °C. H_2 gas was not sensed at lower temperatures i.e. (room temperature, 50 °C, 100 °C, and 150 °C). At 200 °C H_2 sensing by GaN/C commenced. H_2 gas of increasing concentration was passed over the GaN/C materials at 200 °C. This was done by allowing H_2 in an H_2/Ar mixture to pass over the material for 2 min and then the H_2 flow was stopped but the argon flow continued for 2 min to flush the system after exposing to H_2 gas. This is to regenerate the surface for the next exposure. The typical delay times was for 40 - 45 secs and allowed the sample to recover until it reached the original resistance. The recovery occured during the same time. At the end of this time the H_2 gas flow was continued but at a higher concentration and the process repeated. When the gas was introduced into the system the resistance decreased and when the H_2 gas was switched off the resistance changed. A good sensor should have a quick response and recovery time i.e. should respond and recover immediately to a gas that is to be detected. Fig. 6.10 shows the resistance as a function of time and the response corresponding to different H_2 concentrations (inset). It was observed that with increase in gas concentration the resistance decreased and the response also increased up to 400 ppm. This shows that the Pd surface was gradually saturated with H_2 due to complete coverage by atomic hydrogen at the Pd/ nanostructures interface [8]. A maximum response value of ~ 3.8% for 400 ppm H_2 gas was detected. A change in the reference value of the resistance with the variation of H_2 concentration was observed and this was due to the value of resistance which had not recovered completely in the sequential measurement period [20].

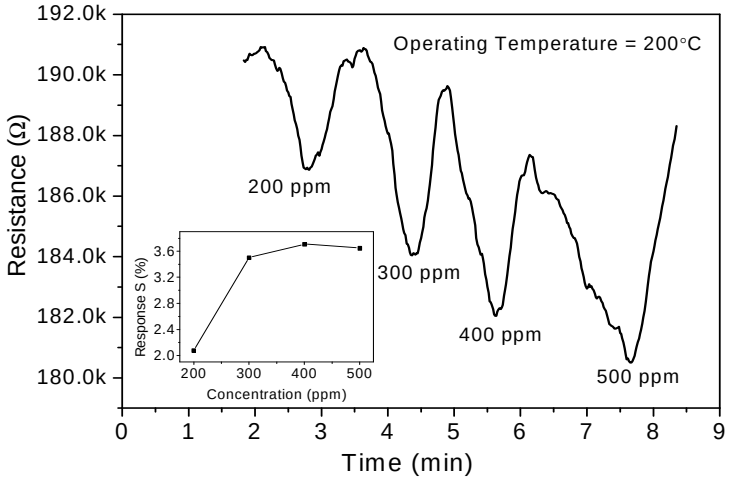


Fig. 6.10: Resistance and response curve (inset) of the GaN/C to different H_2 concentrations at 200°C.

Note: The sensing data was collected in India and so far only one sample has been tested because there was a problem with the testing equipment. Further data will be collected at a later date. However, the preliminary data do suggest that these Pd/GaN/C materials made with activated carbon do not look especially promising for H_2 sensing.

6.6. Conclusions

The synthesis of GaN/C NSs with different morphologies was made using different ratios of activated carbon to Ga_2O_3. It was observed that different Ga_2O_3/C ratios affected the morphology of the GaN NSs. The synthesis using carbon required high temperatures to obtain the GaN NSs. It was observed that a ratio of Ga_2O_3: C of 1:0.5 (w/w) was sufficient to form GaN. The surface area of the material increased with increase in the amount of the activated carbon. The resonance Raman spectrum showed the high electronic quality of the material. The presence of metal (Pd) loaded on a Ga_2O_3:C 1:2 sample was confirmed by EDX and TEM. A maximum response value of ~3.8 % for 400 ppm H_2 gas was

detected at 200 °C. The change in the reference value of resistance with the variation of H_2 concentration makes this material a poor gas sensing material.

6.7. References

1. O. Lupan, G. Chai, L. Chow, Microelectron. J. 38 (2007) 1211.
2. H. T. Wang, B. S. Kang, F. Ren, L. C. Tien, P.W. Sadik, D. P. Norton, S. J. Pearton, J. Lin, Appl. Phys. Lett. 86 (2005), 243503-1-3.
3. Y. H. Choi, S. H. Hong, Sens. Actuators B 125 (2007) 504.
4. H. Miyazaki, T. Hyodo, Y. Shimizu, M. Egashira, Sens. Actuators B 108 (2005) 467.
5. H. Wang, T. J. Anderson, F. Ren, C. Li, Z. Low, J. Lin, B. P. Gila, S. J. Pearton, A. Osinsky, A. Dabiran, Appl. Phys. Lett. 89 (2006), 242111-1-3.
6. M. Suchea, N. Katsarakis, S. Christoulakis, S. Nikolopoulou, G. Kiriakidis, Sensors and Actuators B 118 (2006) 135.
7. G. Shen, P-C. Chen, K. Ryu, C. Zhou, J. Mater. Chem, 19 (2009) 828.
8. W. Lim, J. S. Wright, B. P. Gila, J. L. Johnson, A. Ural, T. Anderson, F. Ren, S. J. Pearton , Appl. Phys. Lett. 93 (2008) 072109.
9. K. Zdansky, Nanoscale Res. Lett. 6 (2011) 490.
10. J. S.Wright,W. Lim, B.P. Gila, S. J. Pearton, J. L. Johnson, A. Ural, F. Ren, Sensors and Actuators B 140 (2009) 196.
11. L. C. Tien, H. T. Wang, B. S. Kang, F. Ren, P. W. Sadik, D. P. Norton, S. J. Pearton, J. Lin, Electrochem. Solid-State Lett. 8 (2005) G230.
12. W. Lim, J. S. Wright, B. P. Gila, J. L. Johnson, A. Ural, T. Anderson, F. Ren, S. J. Pearton, Appl. Phys. Lett. 93 (2008) 072109.
13. M. Epifani, T. Andreu, R. Zamani, J. Arbiol, E. Comini, P. Siciliano, G. Faglia, J. R. Morante, CrystEngComm, 14 (2012) 3882.
14. F. Xu, Y. Xie, X. Zhang, S.Y. Zhang, X.M. Liu, W. Xi, X.B. Tian, Adv. Funct. Mater. 14 (2004) 464.
15. J. Zhang, L. Zhang, J. Phys. D: Appl. Phys. 3 (2002) 1481.
16. S. Dhara, S. Chandra, G. Mangamma, S. Kalavathi, P. Shankar, K. G. M. Nair, A. K. Tyagi, C. W. Hsu, C. C. Kuo, L. C. Chen, K. H. Chen, K. K. Sriram, Appl. Phys. Lett. 90 (2007) 213104.

17. P. Sahoo, S. Dhara, S. Amirthapandian, M. Kamruddin, S. Dash, B. K. Panigrahi, A. K Tyagi, Cryst. Growth Des. 12 (2012) 2375.
18. P. Boguslawski, E. L. Briggs, J. Bernholc, Phys. Rev. B 51 (1995) 17255.
19. V. Hacker, K. Kordesch, in: W. Vielstich, A. Lamm, H.A Gasteiger (Eds.) Fundamentals, Technology and Application, Chichester, 2003, pp. 121-127.
20. P. Sahoo, S. Dhara , S. Dash, S. Amirthapandian, A. K. Prasad, A. K. Tyagi, Int. J Hydrogen Energ, 38 (2013) 3513.

Chapter 7

Application of GaN nanostructures and nitrogen doped carbon spheres as supports for the hydrogenation of cinnamaldehyde

7.1 Introduction

The selective hydrogenation of α,β-unsaturated aldehydes is of interest due to the wide [1]industrial applications of their corresponding hydrogenation products in the fine chemicals and pharmaceuticals industries [1]. The hydrogenation of α,β-unsaturated aldehydes to generate α,β-unsaturated alcohols and saturated alcohols depends on the method used to prepare the catalysts, the amount of catalyst used, the type of support, the catalyst precursors, solvents, additives (or promoters) and the reaction conditions employed e.g. temperature [2]. A standard reaction used to evaluate catalysts and supports is the hydrogenation of cinnamaldehyde (CALD) (Fig 7.1). CALD hydrogenation can yield hydrocinnamaldehyde (HCALD), cinnamyl alcohol (CALC) and 3-phenyl-1-propan-1-ol (3P1P) and thus provides a range of easily identifiable (and important) chemicals to evaluate catalyst behaviour [3].

HCALD is of interest because it has been found to be an important intermediate for the preparation of chemicals used in the treatment of the HIV. It is also commonly used as an additive in the food industry as a flavouring agent [3]. CALC is also an important chemical but the production of CALC via selective hydrogenation is a difficult task because the formation of the saturated aldehyde is thermodynamically favoured over that of the unsaturated alcohol [4].

[1] T. Kente et al. J. Nanosci Nanotechno. Vol. 13, No 7, 2013, pp. 4990- 4995(6).

Considerable efforts have been made to search for a catalytic system that is able to actively and selectively carry out the preferential hydrogenation of the C=O bond in the presence of a conjugate C=C bond [5]. Selectivity towards the unsaturated alcohol can be improved significantly using designed heterogeneous catalysts [4]. Previous studies have shown that it is much easier to hydrogenate the unsubstituted isolated C=C bond than to hydrogenate the isolated C=O aldehydic or ketonic group [6]. The hydrogenation of CALD in polar solvents is known to favour the transformation of the C=O bond, while hydrogenation in non-polar solvents favours transformation of the C=C bond [7].

Further hydrogenation of CALC and HCALD produces 3-phenyl-1-propan-1-ol (Fig. 7.1). While also a useful chemical the products HCALD and CALC are the target compounds in this reaction.

Many catalysts (e.g. Pd on carbon nanotubes) have been reported for the hydrogenation of CALD but selectivity to the final required products remains a challenge [3, 8 – 11]. Indeed, carbon supported Pd catalysts are known to be one of the most effective catalysts for the selective hydrogenation of the C=C bond [3]. Thus, carbon supported Pd catalysts provide a measure of the catalyst selectivity of other Pd supported catalysts.

We have recently commenced a study to investigate the use of classical semiconductors as supports in heterogeneous catalysis. It is believed that the semi-conducting power of a support will affect the metal-support interaction and hence influence the activity and selectivity of a metal catalyst. The new synthetic strategies that allow for the synthesis of nano shaped/sized semi-conductors thus opens up the use of these materials as catalyst supports. These studies will thus complement the typical studies of semiconductors as sensors etc.

In the first of these studies we have explored the synthesis and use of nano GaN as catalyst support for hydrogenation reactions. GaN is stable material at high temperatures and it is not easily oxidized to gallium oxide or reduced to Ga metal by oxidizing or reducing atmospheres. The ability to make nanoscale GaN, as seen with other nanomaterials, gives high surface area GaN with tunable electrical

and optical properties, making it a good candidate for various applications including catalysis; hence our choice to exploit its ability to act as a support material for Pd catalysts.

As mentioned earlier, Pd/C catalysts provide a good model for comparing with other catalyst/support combinations. In earlier studies we have shown that nitrogen (N) doping of carbon structures leads to better catalyst stability/activity than when undoped carbon structures are used. We have thus chosen to use N doped carbon spheres (NCSs) as our model system. These are easy to prepare and are easy to study by electron microscopy techniques. In this work we have thus compared Pd/GaN NSs and Pd/NCSs (1 wt% and 3 wt% Pd loadings) for the preferential selective hydrogenation of CALD to the corresponding saturated aldehyde (HCALD) at different temperatures under atmospheric pressure.

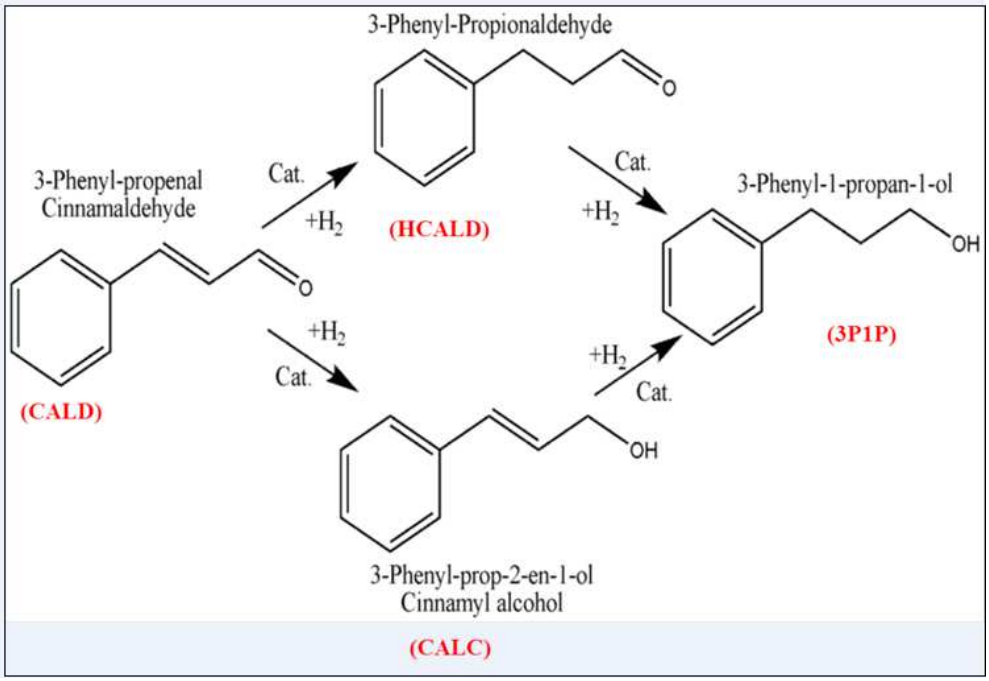


Fig. 7.1: Reaction scheme proposed for the selective hydrogenation of cinnamaldehyde [12].

7.2 Experimental

7.2.1. Synthesis and Functionalization of GaN Nanostructures

GaN nanorods were synthesized in a quartz tube placed in a two-stage furnace. The first zone (zone 1) of the double stage furnace was heated to 1100 °C to preheat the NH_3 and cause its dissociation into NH_2, NH, and N reactive species. The second reactor zone (zone 2), was heated to 750 °C. Ga_2O_3 powder was placed in a quartz crucible placed in the center of the quartz tube in zone 2. N_2 was allowed to flow through the quartz tube (to remove air) at a flow rate of 12 ml/min while the two zones of the reactor reached their respective reaction temperatures. When the desired temperatures were reached NH_3, at different flow rates, was introduced. The NH_3 and decomposed NH_3 species reacted with Ga_2O_3 in zone 2 to convert the reactant to GaN NSs. The NH_3 flow rate was varied from 12 – 210 ml/min while N_2 was kept at the same flow rate. The optimized flow rate used in this study was 210 ml/min. After 2 h, the furnace was cooled to room temperature while N_2 was passed through the reactor. The crucible was then removed from the reactor and weighed to establish the amount of GaN product formed. A piranha solution (i.e. mixture of 0.52 M HNO_3 + 0.12 M H_2SO_4) was used to create functional groups on the GaN NS support prior to catalyst synthesis stage [13].

7.2.2. Synthesis and Functionalization of NCSs

The synthesis method for producing NCSs was adopted from Deshmukh et al. with minor modifications [14]. NCSs were synthesized using a non-catalytic CVD method from acetylene (C_2H_2) as a carbon source and acetonitrile (CH_3CN) as the N (and C) source. N_2 was first flowed through the quartz tube (to remove air) at 100 ml/min while the furnace was heated from room temperature to 950 ^oC at a heating rate of 10 ^oC/min. Once the desired temperature was attained the N_2 flow was switched off and C_2H_2 was bubbled through the CH_3CN solution (80 ^oC) at a flow rate of 100 ml/min for 90 minutes. After the required carbonization time, the C_2H_2 was switched off and N_2 was flowed through the system at 100 ml/min until

the furnace had cooled down to room temperature. NCSs were then collected from the walls of the quartz tube and weighed. Functionalization of the NCSs was carried out by treatment with 55% nitric acid (HNO_3) for 24 h at 40 ^oC. The functionalized NCSs were then filtered and washed with deionized water until the pH of the filtrate was neutral. The NCSs were then dried in an oven for 12 h at 80 ^oC.

7.2.3 Preparation of Pd/GaN and Pd/NCS Catalysts

The catalysts were prepared using the liquid phase reduction method in an ethylene glycol solution. The supports (500 mg) were placed into a 500 ml round bottomed flask and ethylene glycol (150 ml) was added to the flask. The flask contents were sonicated for 15 min followed by magnetic stirring for 30 min. The metal precursor solution (0.05 M palladium acetate) was then added drop-wise to the mixture of carbon support and ethylene glycol. The concentrations of the precursor solutions in the ethylene glycol solutions were calculated in order to prepare catalysts with metal loadings of 1 and 3 wt %. The resultant solution was magnetically stirred vigorously for a further 3 h at room temperature and then refluxed at 195 ^oC in an oil bath for 3 h. The solution was then cooled to room temperature. The resultant solution was filtered and thoroughly washed with 20 ml of acetone followed by excess distilled water. The supported metal catalysts were dried in air for 8 h at 80 ^oC and then ground in a mortar to form a powder.

7.2.4 Characterization of the Supports and Catalysts

The structural morphology of the support materials and catalysts was ascertained by transmission electron microscopy (FEI Tecnai G^2 Spirit electron microscope at 120 kV). Powder X-ray diffraction (Bruker D2 Phaser) was used to study the chemical composition and crystallinity of the materials. A Brunauer-Emmett-Teller (BET) TRISTAR 3000 analyzer was used to measure the surface area and porosity of the catalysts.

7.2.5 Hydrogenation of Cinnamaldehyde

Hydrogenation of CALD was carried out in a three necked round bottomed flask. The catalyst (0.01 g) and a 0.01 M CALD (dissolved in solvent) were added into the reaction flask. The air inside the system was expelled by passing N_2 through the flask for 30 min while the contents were heated to the required temperature. After this, hydrogen gas (50 ml/min) was bubbled through the system while the flask contents were stirred. The course of the reaction was monitored by withdrawing liquid samples from the flask every hour for 6 h. The products were analyzed on a gas chromatogram equipped with an FID detector. The column used was a ZB-1 capillary column (30 m × 0.53 mm × 1.5 μm). Reaction products were identified by comparison with authentic GC standards of CALD, HCALD, 3P1P, and CALC.

7.3 Results and Discussion

7.3.1 XRD and TEM analysis

Powder XRD was used to study the chemical composition and purity of the GaN NSs and NCSs. Fig. 7.2 shows that the as-synthesized materials were the required materials. The peaks observed in Fig. 7.2(a) were indexed and found to correspond to crystalline hexagonal lattice planes of the wurzite structure of GaN. In Fig. 7.2(b), the two diffraction peaks at 25.5° and 43.3° correspond to the (002) and (101) hexagonal lattice planes of graphitic carbon respectively [14].

Since the materials were relatively free of impurities no purification process was required. However, it was necessary to modify the surface of the materials through acid treatments to make them dispersible in solution and to allow uniform dispersion of Pd catalysts on the supports. This step impacted on the Pd-support interaction and hence the dispersion and activity of the Pd. We have shown in our

previous studies on carbon nanotubes that the degree of functionalization of the support materials affects the activity of the catalyst [15].

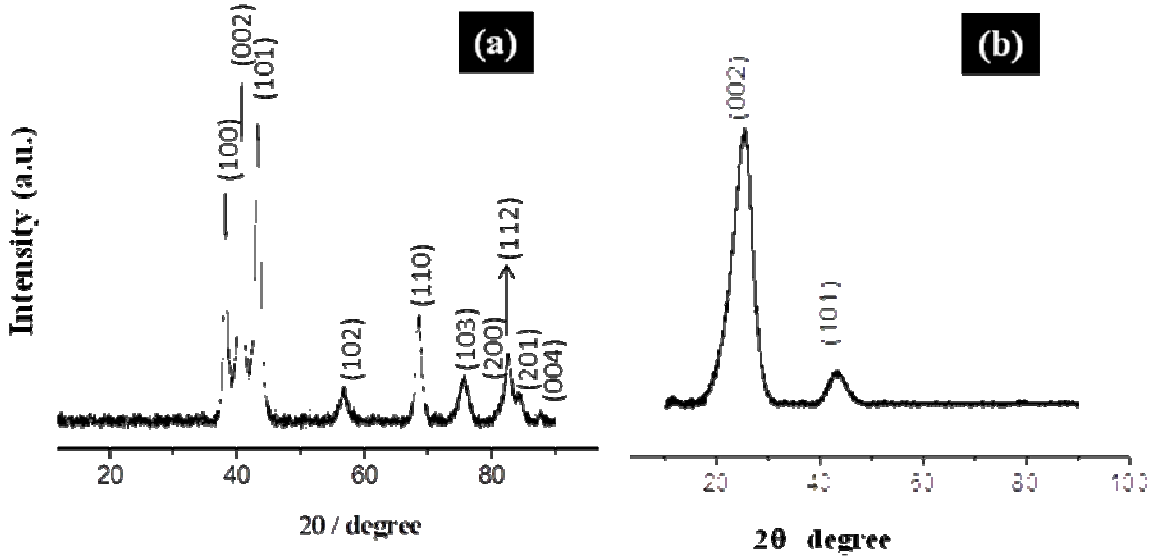


Fig.7.2: PXRD patterns of (a) as-synthesized GaN NSs (synthesis temp = 750 °C) and (b) as-synthesized NCSs.

The TEM images of the GaN and NCS supports revealed the rod like structure of the GaN (comprised of smaller particles) and the spherical shape of NCSs (not shown here). The TEM images of the four Pd supported samples studied (1%Pd/GaN; 3%Pd/GaN; 1%Pd/NCSs and 3%Pd/NCSs) are shown in Fig. 7.3. The Pd loaded on the NCSs can readily be seen while the Pd loaded on the GaN is more difficult to observe due to (i) the small Pd particle size (ii) the distribution of Pd on the rough surface and (iii) the colour contrast of Pd and GaN. The Pd nanoparticles were found to be well dispersed on the surface of the nanostructures with an average size range of between 4 – 15 nm. The Pd particle sizes were smaller on the GaN than on the NCSs (Fig. 7.4). For example 3% Pd/GaN gave Pd particles with an average diameter of 10 nm, while the diameters of the Pd on the 3% Pd/NCSs were 15 nm (Fig. 7.4). The 1 % Pd/NCS catalysts had Pd average particle sizes of 4.7 nm; the Pd on the 1%Pd/GaN was difficult to see and thus a meaningful particle size analysis could not be achieved. As the loading of

Pd was increased, agglomeration occurred and larger particles formed, and the average particle size increased [16].

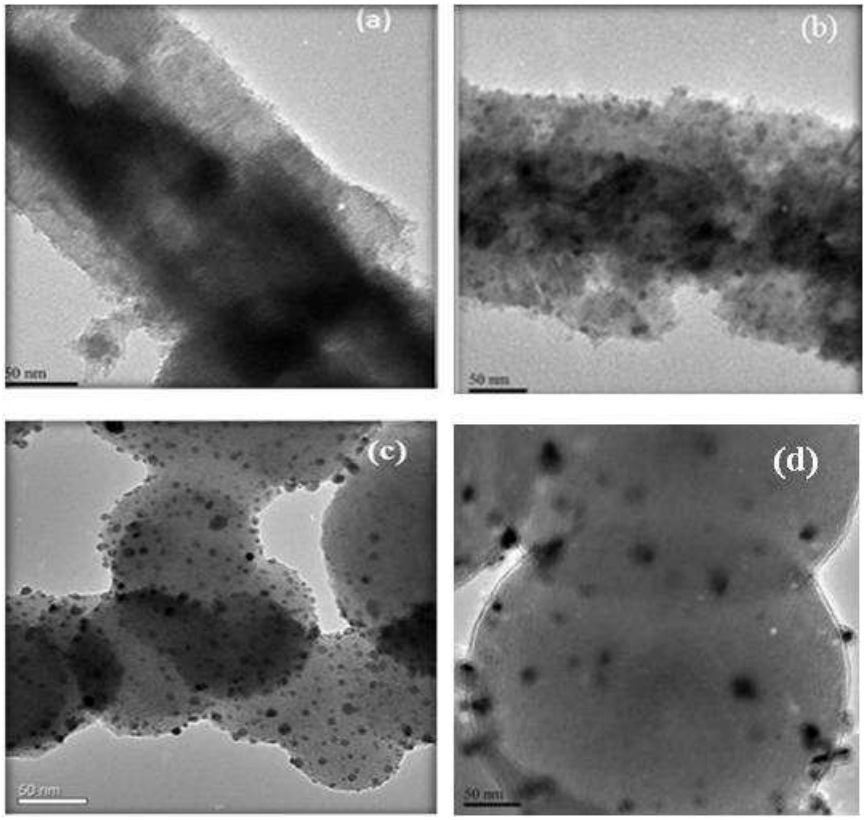


Fig.7.3: TEM images of (a) 1%Pd/GaN, (b) 3%Pd/GaN, (c) 1%Pd/NCSs and (d) 3%Pd/NCSs. The dark spots are Pd nanoparticles.

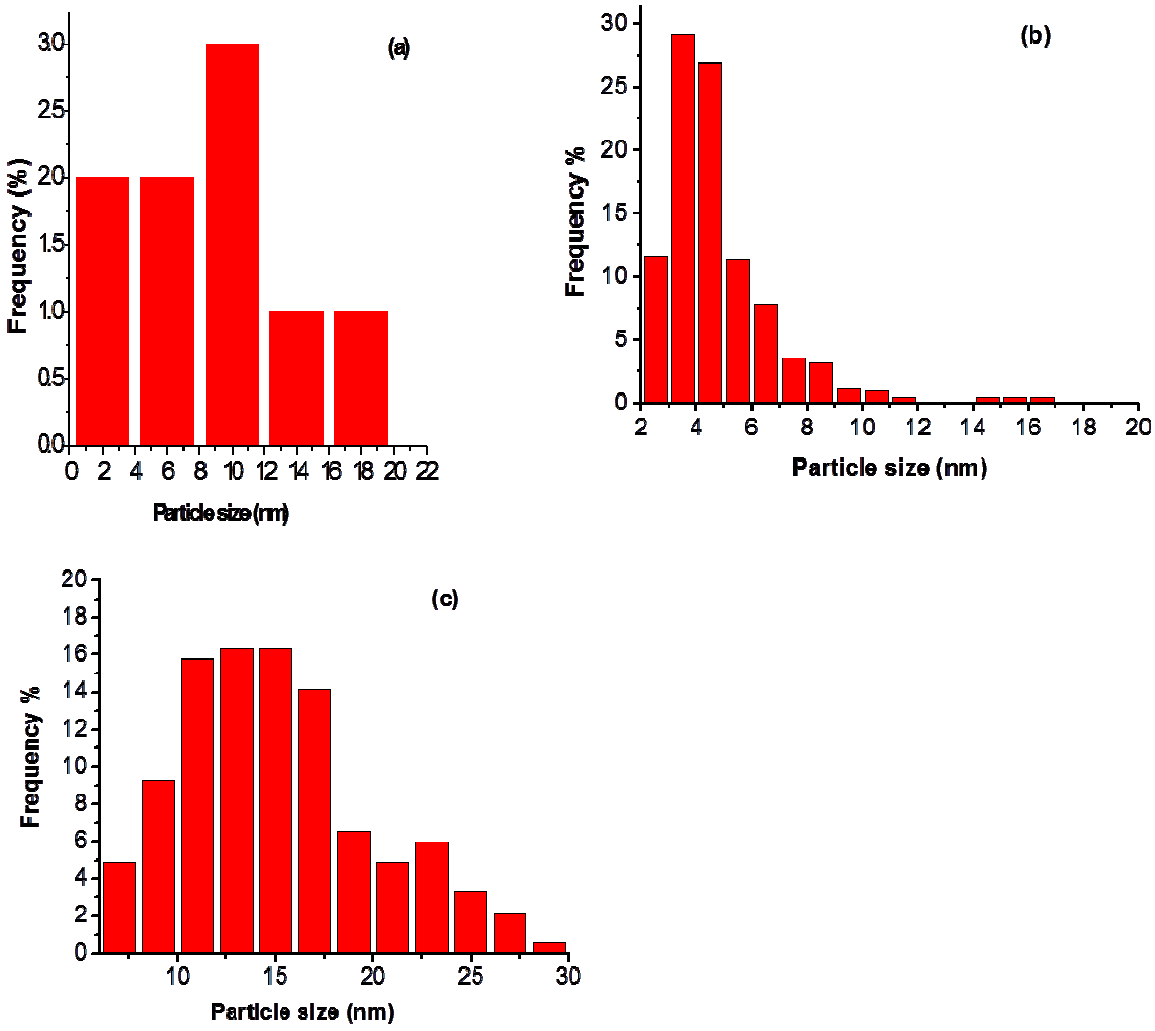


Fig. 7.4: Particle size distribution graphs of (a) 3 % Pd/GaN, (b) 1 % Pd/NCSs and (c) 3 % Pd/NCSs.

7.3.2 BET Surface Area Analysis

Table 7.1 shows the surface areas and pore volumes of the supports and catalysts. Comparison of the surface areas of the supports revealed that the GaN NS had a higher surface area (~ 20 m^2/g) than the NCSs (~ 1 m^2/g). The surface area increased when the Pd was added to the support materials. The highest surface area (i.e. 63.5 m^2/g) was observed with the 3%Pd/GaN catalyst. This suggests that most of Pd nanoparticles that were deposited on the surface did not block any

of the mesopores [17]. The higher surface area for GaN would suggest a better dispersion of Pd particles (as seen for the 3% loaded sample).

Table 7.1: BET surface areas and pore volumes of the supports and catalysts.

Sample	**BET surface area (m^2/g)**	**Pore volume (cm^3/g)**
GaN	19.6	0.01
NCSs	1.5	0.003
1%Pd/GaN	23.9	0.1
1%Pd/NCSs	3.8	0.02
3%Pd/GaN	63.5	0.2
3%Pd/NCSs	4.2	0.02

7.3.3 Comparison of Catalyst Activity: Cinnamaldehyde Hydrogenation

Fig. 7.5 and Table 7.2 shows the CALD hydrogenation results using a 1% wt loading of Pd on the GaN and NCS supports carried out at reaction temperatures of 40 and 60 ^{o}C. The 1%Pd/GaN catalyst gave lower conversions at both temperatures when compared to the 1%Pd/NCSs catalyst. This was unexpected as the Pd particles are smaller on the GaN and hence the dispersion and turnover number would be expected to be larger on the GaN. This suggests a strong Pd-GaN interaction (relative to the Pd-NCS interaction) that modifies the catalyst behaviour. This was also suggested by the selectivity data – the Pd/GaN does not over hydrogenate the HCALD to 3PIP.

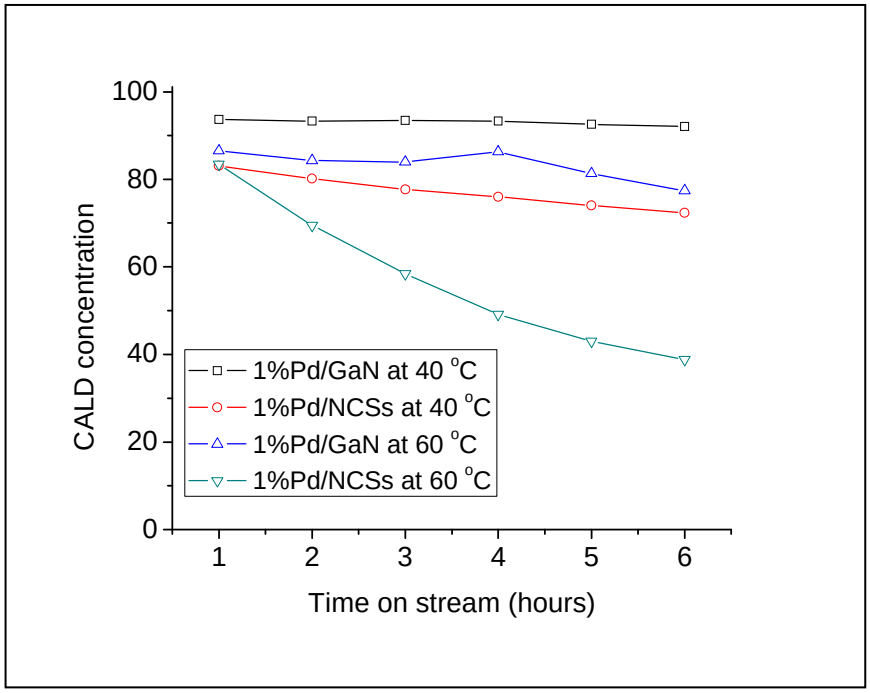


Fig. 7.5: Graphs showing CALD remaining as a function of time on stream at 40 and 60°C for 1% Pd/GaN and 1% Pd/NCSs catalysts.

In an attempt to increase the catalyst activity 3%Pd loaded catalysts were studied (Fig. 7.6, Table 7.2). The 3% loaded catalysts show superior activity as expected but a reduced selectivity to the HCALD. At 60 °C the 3%Pd/GaN has a slightly higher activity than the 3%Pd/NCS catalyst, but the reason for this is not obvious. Fig. 7.6(b) indicates that this is true throughout the full reaction timeframe.The selectivity data suggest that there is little difference between the two catalysts. It appears that the HCALD/3PIP ratio did not vary with time on stream (or conversion), perhaps suggesting that the secondary hydrogenation step only occurs when the CALD is bound to the Pd.

The data thus suggest the following. The Pd binds to the CALD and provided the interaction is strong enough conversion to HCALD occurs. Not unexpectedly any C=O–Pd interactions must be weak as no CALC was formed in the reaction. Once the C=C bond has been hydrogenated the HCALD-Pd intereaction must be weak and the product will dissociate from the Pd. At the higher temperatures 3PIP is formed. Thus the size of the Pd particle and the Pd-support interaction detemine

the course of the reaction. In future studies the stability of the catalyst will be evaluated under the reaction conditions.

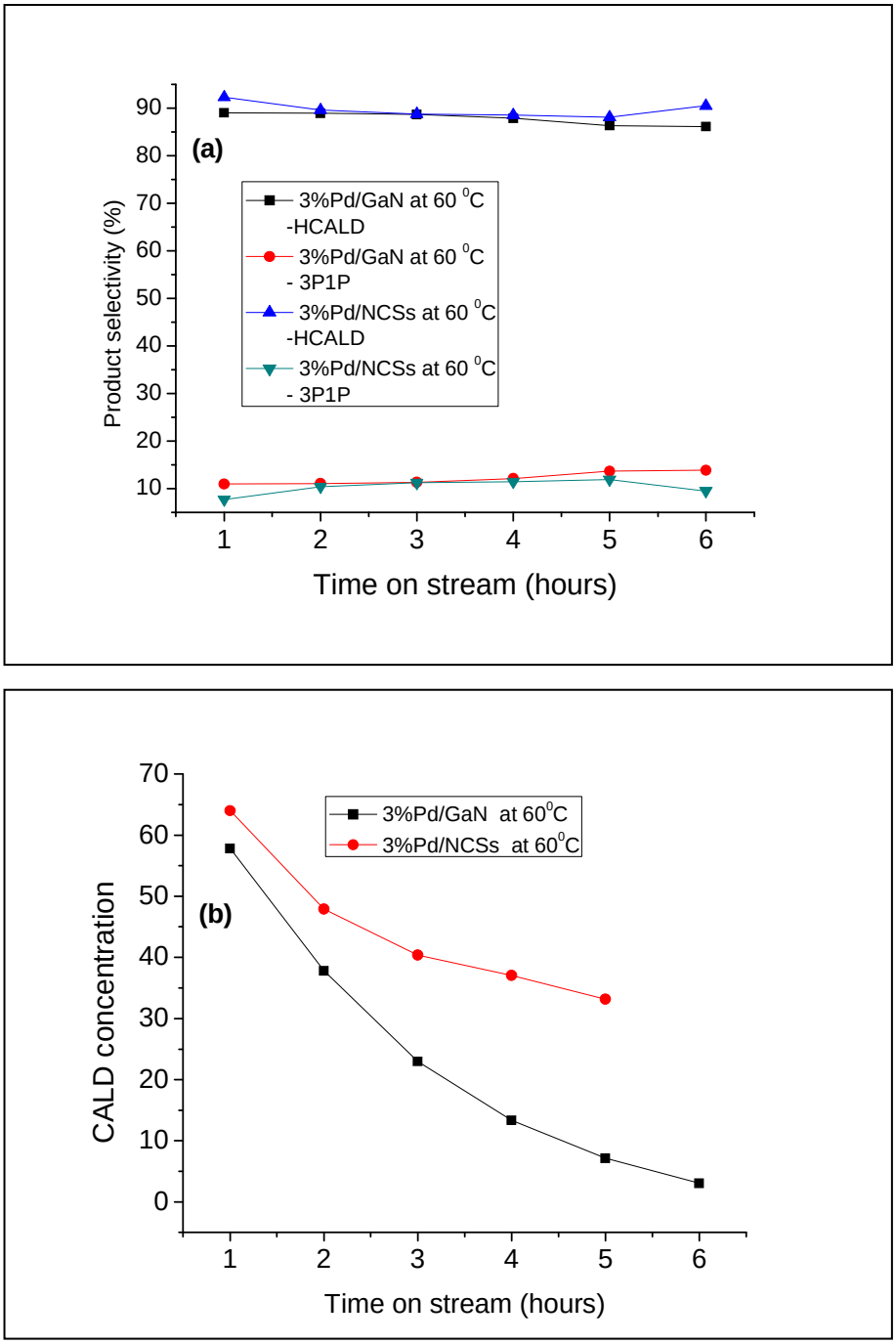


Fig. 7.6: Graphs showing (a) the product selectivity to HCALD and 3P1P (b) CALD remaining as a function of time on stream at 60°C for 3%Pd/GaN and 3% Pd/NCSs catalysts.

Table 7.2: A summary of the % CALD conversions and selectivities of the Pd/GaN and Pd/NCSs catalysts using different Pd loadings and reaction temperatures.

Catalyst	**Temperature (^oC)**	**CALD conversion (%)**	**Product Selectivity (%)[a]**	
			HCALD	**3P1P**
1%Pd/GaN	40	8	100	0.00
	60	23	100	0.00
1%Pd/NCSs	40	27	86	14
	60	61	94	5.6
3%Pd/GaN	60	97	86	13.9
3%Pd/NCSs	60	60	90	9.5

[a] No CALC observed.

7.4 Conclusions

This study has shown for the first time that GaN NSs can be used as support materials for Pd nanoparticles for the hydrogenation of CALD. The data reveal that the GaN inhibits the hydrogenation relative to NCSs and in doing so gives catalyst with better selectivity to HCALD. Higher conversions of CALD and poorer selectivity towards HCALD were obtained using the 3%Pd/GaN and 3%Pd/NCSs catalysts. TEM images showed that the Pd metal nanoparticles are well dispersed on the surface of the support materials and that small Pd particles give lower conversions but higher selectivities. The uniform dispersion of the Pd

nanoparticles was achieved by support functionalization using different acid treatments. The GaN NSs can thus be used as supports for catalytic reactions in solution (and presumably in the gas phase). This study suggests that the use of GaN NSs may not only be used in electronic applications but can also be exploited in heterogeneously catalysed reactions such as this one. The interaction between the Pd nanoparticles and the GaN NSs is yet to be established.

7.5 References

1. L. Zhang, M. Winterbotton, A. P. Boyes and S. Raymahasay, J. Chem. Tech. Biotechnol. 72, 264 (1998).
2. U. K. Singh, M .A. Vannice, Appl. Catal. A: General 213, 1(2001).
3. C. Ge, Y. Li, J. Zhao, R. Zhou, Ind. J.Chem, 49A, 281 (2010).
4. A. B. Merlo, B. F. Machado, V. Vetere, J. L. Faria, M. L. Casella, Appl. Catal. A: General 383, 43 (2010).
5. M. Lashdaf, A.O.I. Krause, M. Lindblad, M. Tiitta, T. Venalainen, Appl. Catal. A: General 241, 65 (2003).
6. H. Chen, X. Li, M. Wang, Y. Xu., Appl. Catal. A 225, 117(2002).
7. H. Yamada, S. Goto, J. Chem. Eng. Japan 36,586 (2003).
8. H. Vu, F. Goncalves, R. Philippe, E. Lamouroux, M. Corrias, Y. Kihn, D. Plee, P. Kalck, P. Sero, J. Catal. 240, 18 (2006).
9. Y. Li, G.H. Lai, R. X. Zhou, Appl. Surf. Sci, 253, 4987 (2007).
10. H. X. Ma, L. C. Wang, L.Y. Chen, C. Dong, W. C. Yu, T. Huang, T. Y. Qian, Catal. Commun. 8,452(2007).
11. A. Corna, H. Garcia, A. Leyva, J. Mol. Catal. A: Chem. 230, 97 (2005).
12. K-Y. Jao, K-W. Liu, Y-W.Yang, A-N. Ko, J. Chin. Chem. Soc. 56, 885 (2009).
13. C. W. Hsu, C. P. Chen, C. C. Kuo, P. P. Paskov, P. O. Holtz, L. C. Chen, K. H. Chen, J. Appl. Phys. 109, 053523 (2011).
14. A. A. Deshmukh, R. Ul. Islam, M. J. Witcomb, W. A. L. van Otterlo, N. J. Coville, ChemCatChem. 2, 51 (2010).
15. M.A.M. Motchelaho, H. Xiong, M. Moyo, L.L. Jewell, N.J. Coville, J. Mol. Catal. A: Chemical 335, 189 (2011).
16. Y. Liao, L. Gao, X. Zhang and J. Chen, Mater. Res. Bulletin 47, 1625 (2012).
17. M. Moyo, M. A. M. Motchelaho, H. Xiong, L. L. Jewell, N. J. Coville, Appl. Catal. A: General 413, 223 (2012).

Chapter 8

Conclusions and Recommendations

8.1 Conclusions

The study has shown that small particles of GaN with diameters in the range 12 - 16 nm can be synthesized in a double stage furnace at temperatures as low as 750 °C. Synthesis of the GaN NSs using a double stage furnace gave several advantages over GaN produced by other methods. It was found that by preheating NH_3, the GaN NSs could be synthesized at the lower temperatures (750 °C) for the first time. GaN NSs synthesized in a double stage furnace possessed surface areas of 20 m^2/g. Growth parameters such as reaction temperature, time, and flow rate and precursors impacted on the synthesis of GaN and have been optimized in this study. The NH_3 decomposition reaction plays an important role in the formation of GaN.

Carbon coated GaN nanostructures were synthesized by CVD. The GaN/C materials were partially covered with amorphous carbon. The morphology of the nanostructures did not change when carbon was deposited on the surface and also an acid functionalization step did not affect the morphology. The visible diffraction spots on functionalized nanostructures were indexed to the reflections of hexagonal GaN. The thermal stability of functionalised materials decreased with decomposition temperature. The increase in mass at T > 700 °C was due to the oxidation of the GaN as it converts to Ga_2O_3. An increase in surface area of the functionalised materials and high electronic quality of the functionalized materials was observed. A yellow luminescence band and a near band – edge transition for the synthesised GaN/C and fGaN/C was observed.

The synthesis of GaN NSs using different ratios of reducing agent (activated carbon) to Ga_2O_3 was studied. It was observed that different Ga_2O_3/C ratios affected the morphology of the GaN NSs. However, the synthesis using carbon

still required high temperatures (1100 °C) to obtain the GaN NSs. It was observed that a ratio of Ga_2O_3: C of 1:0.5 (w/w) was sufficient to form GaN. The surface area of the material increased with increase in the amount of the activated carbon used. The resonance Raman spectrum showed the high electronic quality of the material. The presence of metal (Pd) loaded on a Ga_2O_3/C 1:2 sample was confirmed by EDX and TEM. A maximum response value of ~3.8 % for 400 ppm H_2 gas was obtained at 200 °C. The change in the reference value of resistance with the variation of H_2 concentration makes this material a poor gas sensing material.

This study has also shown that GaN NSs can be used as support materials for Pd nanoparticles for the hydrogenation of cinamaldehyde (CALD). The data reveal that the GaN inhibits the hydrogenation relative to NCSs and in doing so gives a catalyst with better selectivity to HCALD. Higher conversions of CALD and poorer selectivity towards HCALD were obtained using the 3%Pd/GaN and 3%Pd/NCSs catalysts. The uniform dispersion of the Pd nanoparticles was achieved by support functionalization using different acid treatments. TEM images showed that the Pd metal nanoparticles are well dispersed on the surface of the support materials and that small Pd particles give lower conversions but higher selectivities. The GaN NSs can thus be used as supports for catalytic reactions in solution (and presumably in the gas phase). This study suggests that the use of GaN NSs may not only be used in electronic applications but can also be exploited in heterogeneously catalysed reactions such as this one. The interaction between the Pd nanoparticles and the GaN NSs is yet to be established.

8.2 Recommendations

The morphology of the GaN NSs needs to be improved. The role of carbon incorporated on GaN NSs for gas sensing also needs to be investigated in detail. The interaction between the Pd nanoparticles and the GaN NSs is not yet established. These materials also need to be tested for sensing other gases e.g. CH_4, N_2O_2, NH_3 etc.